RECEIVED
LAWRENCE
RADIATION LABORATORY

JUL 17 1970

LIBRARY AND
DOCUMENTS SECTION

UCRL-19867
c.2

THE ACTIVE CENTER OF THE PLANT-TYPE FERREDOXINS: STUDIES BY MOSSBAUER SPECTROSCOPY

William Richard Dunham
(Ph.D. Thesis)

June 1970

AEC Contract No. W-7405-eng-48

TWO-WEEK LOAN COPY

This is a Library Circulating Copy which may be borrowed for two weeks. For a personal retention copy, call Tech. Info. Division, Ext. 5545

UCRL-19867

LAWRENCE RADIATION LABORATORY
UNIVERSITY of CALIFORNIA BERKELEY

DISCLAIMER

This document was prepared as an account of work sponsored by the United States Government. While this document is believed to contain correct information, neither the United States Government nor any agency thereof, nor the Regents of the University of California, nor any of their employees, makes any warranty, express or implied, or assumes any legal responsibility for the accuracy, completeness, or usefulness of any information, apparatus, product, or process disclosed, or represents that its use would not infringe privately owned rights. Reference herein to any specific commercial product, process, or service by its trade name, trademark, manufacturer, or otherwise, does not necessarily constitute or imply its endorsement, recommendation, or favoring by the United States Government or any agency thereof, or the Regents of the University of California. The views and opinions of authors expressed herein do not necessarily state or reflect those of the United States Government or any agency thereof or the Regents of the University of California.

to Stephanie

TABLE OF CONTENTS

	Page
List of Figures	vi
List of Tables	viii
Acknowledgements	ix
Vita and Fields of Study	xi
Abstract of the Dissertation	xii
I. Plant-Type Ferredoxins	1
A. Introduction	1
B. Function of the Plant-Type Ferredoxins	7
C. Physical Properties of the Plant-Type Ferredoxins	11
D. Why Mossbauer Spectroscopy?	22
II. ^{57}Fe Mossbauer Spectroscopy	24
A. The Mossbauer Effect	24
B. Isomer Shift	29
C. Nuclear Quadrupole Interaction	33
D. Magnetic Effects	42
E. Paramagnets in Applied Magnetic Field	50
F. Magnetic Hyperfine Interactions in ^{57}Fe Ions	53
G. Exchange Coupling	58
III. Experimental Procedure	62
A. Mossbauer Spectrometer	62
B. Preparation of Biological Samples for Mossbauer Spectroscopy	75
C. Impurity Signals	76
D. Materials and Methods	78

Figure		Page
18.	High-Temperature Mossbauer Spectra For Reduced Spinach Ferredoxin With Computer Fits	103
19.	Variable-Temperature, Low Applied Magnetic Field Mossbauer Spectra For Reduced Spinach Ferredoxin	107
20.	Low-Temperature, Low Applied Magnetic Field Mossbauer Spectra For Reduced Plant-Type Ferredoxins	110
21.	Low-Temperature, High Applied Magnetic Field Mossbauer Spectra For Reduced Plant-Type Ferredoxins	112
22.	Low-Temperature Mossbauer Spectra for Reduced Spinach Ferredoxin With Computer Fits	114
23.	Low-Temperature, Zero Applied Magnetic Field Mossbauer Spectra For Reduced Plant-Type Ferredoxins	118
24.	Structure of Oxy-Bridged Fe^{+++} Schiff-Base Complexes	119
25.	Diagram For "Spin-Coupled" Model	120
26.	Electronic Energy Levels For Ferrous Site of "Spin-Coupled" Models	121
27.	The Measured Magnetic Field at the Nucleus Vs. the Applied Magnetic Field For the Oxidized Protein Mossbauer Spectra	126
28.	Persulfide Structures For Active Site of Plant-Type Ferredoxins	130
29.	Proposed Model For the Active Center of the Plant-Type Ferredoxins	132

LIST OF TABLES

Table		Page
1.	Properties of the Plant-Type Ferredoxins Investigated	12
2.	Orbital Contributions to EFG	42
3.	Calculated Contact Terms	55
4.	Matrix Elements For the Magnetic Hyperfine Interaction	56
5.	Mossbauer Parameters For the Oxidized Proteins	99
6.	Mossbauer Parameters For the High-Temperature Reduced PPNR Spectra	104
7.	Mossbauer Parameters For the Low-Temperature Reduced PPNR Spectra	115
8.	A-Values For Ferrous Iron	124

ACKNOWLEDGEMENTS

I am deeply grateful to my research adviser, Prof. Alan J. Bearden for providing the basic elements of this research, namely the Mossbauer spectrometer and laboratory facilities, collaborations with other research groups, and the original idea for the research project. I am most indebted, however, for his patient instruction which leaves me with many sound principles on which to critically decide between varying approaches to a research problem.

The protein samples were kindly provided by: Profs. H. Beinert and W.H. Orme-Johnson at the University of Wisconsin, Madison, Wisconsin; Prof. G. Palmer at the University of Michigan, Ann Arbor, Michigan; and Prof. I.C. Gunsalus and Dr. J.C.M. Tsibris at the University of Illinois, Urbana, Illinois. I am particularly thankful to Prof. R.H. Sands and Dr. I. Salmeen for helping me to overcome many calculational problems during the course of the work. I also thank my classmate, Mr. John Sharp, and Prof. W.H. Orme-Johnson for their tips on laboratory techniques for proteins. The fine technical skill of Mr. C.N. Bartlett was of central importance to this effort and is gratefully acknowledged.

The Computer Centers at the University of California at San Diego and at the University of California Lawrence Radiation Laboratory, Berkeley, provided the facilities and consultants who enabled me to do the computational portion of this research effort.

This work was supported by USPHS pre-doctoral traineeship, #2-T01-GM-01045-06, by NSF grants GB 5458 and GB 13585, and by the

Atomic Energy Commission through Donner Laboratory, University of California Lawrence Radiation Laboratory, Berkeley.

VITA

June 15, 1943 - Born - Monterey, California

1964 - 1965 - Active Duty, United States Marine Corps

1966 - A.B., University of California, Berkeley

FIELDS OF STUDY

Major Field: Physical Chemistry
Studies in Physical Biochemistry
Professor Alan J. Bearden, University of California Radiation Laboratory, Berkeley, California

Studies in Dye-Binding on Nucleic Acids
Professor C. T. O'Konski, University of California at Berkeley

Studies in Radioactive Dating of Woods and Seawater
Professor Hans E. Suess, University of California at San Diego

ABSTRACT OF THE DISSERTATION

The Active Center of the Plant-Type Ferredoxins:

Studies by Mossbauer Spectroscopy

by

William Richard Dunham

Doctor of Philosophy in Chemistry

University of California, San Diego, 1970

Professor Alan J. Bearden, Chairman

Professor Martin D. Kamen, Co-Chairman

The plant-type ferredoxins from spinach, parsley, Pseudomonas putida, Azotobacter vinelandii, Clostridium pasteurianum and pig adrenal cortex were investigated by Mossbauer spectroscopic experiments at varying temperatures (4.2 to 256°K) and applied magnetic field up to 46 kGauss. The results of these experiments, when correlated with other data on these proteins, have led to a structural model for the active center of the plant-type ferredoxins. The following properties of the active center are well-substantiated experimentally by the present study. 1) The active center of the oxidized plant-type

ferredoxins contain two iron atoms with identical electronic environments at the nuclei. These iron atoms are high-spin ferric ($S = 5/2$), spin-coupled to give a resultant diamagnetism for the complex. 2) In the reduced state, the active center contains one high-spin ferric state spin-coupled to one high ferrous state ($S = 2$) to give a resultant $S = 1/2$ complex. 3) The ligand symmetry around both iron atoms is tetrahedral, but with both axial and rhombic distortions. This basic symmetry is not affected by reduction of the proteins. 4) The active center of the plant-type ferredoxins is nearly identical in every protein studied. The only differences in this active center are the presence and magnitude of the rhombic distortion of the symmetry for the ferrous iron in the reduced proteins.

The reduction potentials of the plant-type ferredoxins are attributed to an electron repulsion term between the d_{z^2} orbitals of the two iron atoms. The two labile sulfur atoms of the active center form bridging ligands to the two iron atoms, each of which is further tetrahedrally ligated to two cysteine sulfur atoms.

I. PLANT-TYPE FERREDOXINS

A. INTRODUCTION

Metalloproteins form an interesting subclass of protein enzymes; in many cases the metal ion or ions participate in determining the enzymatic properties of the protein by forming the active center in conjunction with a highly specific metal-binding complex. The most familiar example of this specificity is the Fe-porphyrin complex found in the proteins hemoglobin and myoglobin where the heme group confers the important property of reversible oxygen binding. Porphyrin-magnesium complexes form the center responsible for primary photosynthesis in chlorophylls; iron not bound in a heme moiety binds oxygen reversible in the misnamed protein hemerythrin.

Iron is also an important constituent of another class of proteins (Fig. 1), the iron-sulfur proteins, which function as electron-transfer agents, and which shall be the subject of this work. Iron is also, of course, carried by several proteins (e.g., transferrins and conalbumin), and stored by others (e.g., ferritin and hemosiderins), as it is a necessary element for most life processes. The iron storage protein, ferritin, whose principle function is related to binding iron reversibly, has been investigated thoroughly by a number of physical-chemical techniques (Brady et al., 1968) including magnetic susceptibility, electron paramagnetic resonance, Mossbauer spectroscopy, and low-angle x-ray scattering.

FIGURE 1. PROPOSED CLASSIFICATION OF IRON PROTEINS.

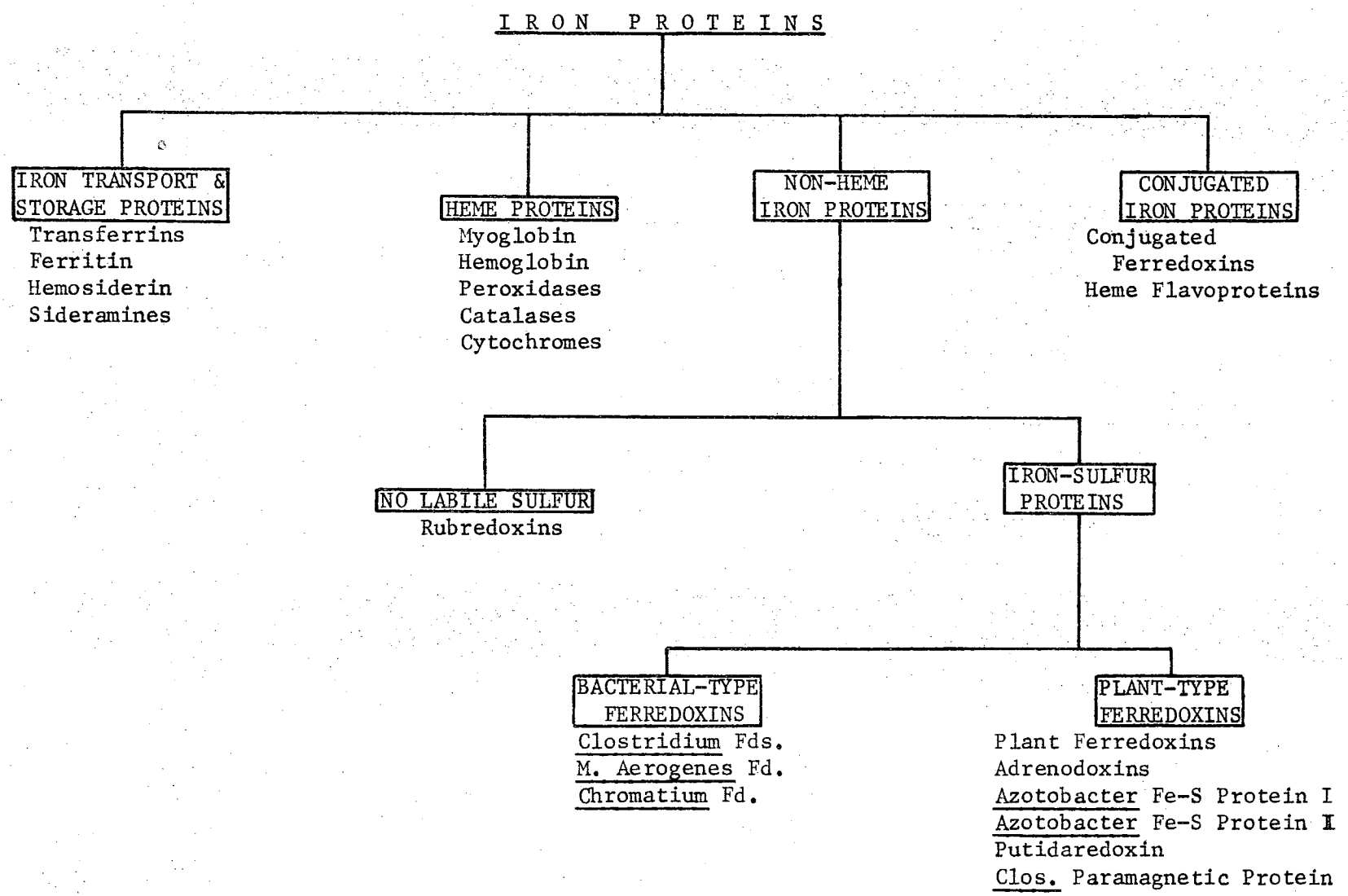
IRON PROTEINS
IRON TRANSPORT & STORAGE PROTEINS
Transferrins
Ferritin
Hemosiderin
Sideramines
HEME PROTEINS
Myoglobin
Hemoglobin
Peroxidases
Catalases
Cytochromes
NON-HEME IRON PROTEINS
CONJUGATED IRON PROTEINS
Conjugated Ferredoxins
Heme Flavoproteins
NO LABILE SULFUR
Rubredoxins
IRON-SULFUR PROTEINS
BACTERIAL-TYPE FERREDOXINS
Clostridium Fds.
M. Aerogenes Fd.
Chromatium Fd.
PLANT-TYPE FERREDOXINS
Plant Ferredoxins
Adrenodoxins
Azotobacter Fe-S Protein I
Azotobacter Fe-S Protein II
Putidaredoxin
Clos. Paramagnetic Protein

Heme proteins have been investigated fully by a variety of chemical and physical techniques. These investigations (Chance et al., 1966) have shown that the wide range of biochemical properties, including oxygen-transport as in myoglobin and hemoglobin and electron-transfer as in cytochromes, depend intimately on the configuration of the iron atom within a porphyrin ring (Falk, 1964) and on the details of the incorporation of this iron-porphyrin complex in the protein. Although the studies on heme compounds have given precise information on the character of the iron bound in these molecules (Moss et al., 1968), this information is not directly applicable to the present study of the plant-type ferredoxin for these two types of iron proteins never have similar iron environments, even when their functions are analogous, i.e., electron transfer reactions.

Iron proteins which have more than one type of prosthetic group (for example, xanthine oxidase) are called "conjugated iron proteins" (Beinert, 1969). Xanthine oxidase is a large molecule (MW = 275,000) containing two molybdenum and eight iron atoms as well as two flavin adenine dinucleotide (FAD) moieties per protein molecule. The heme-flavoproteins such as yeast lactate dehydrogenase, are also in this group. It has been suggested that the iron complex of the plant-type ferredoxins is sometimes a constituent in these proteins (Orme-Johnson and Beinert, 1969).

The non-heme proteins can be divided into two groups: the iron-sulfur proteins and the rubredoxins. Rubredoxin has a single iron atom per protein molecule. This single iron atom has been recently shown by x-ray crystallography to be tetrahedrally ligated by

the sulfur atoms from four cysteine residues (Herriott et al., 1970). These are one electron-transfer proteins, characterized chiefly by color (red-brown when oxidized) and by a g = 4.27 electron paramagnetic resonance signal (referenced in Palmer and Brintzinger, 1966; Newman and Postgate, 1968). Two distinct chemical differences distinguish the iron-sulfur proteins from the rubredoxins: 1) the iron-sulfur proteins contain "labile" sulfur, that is, sulfur which is not part of the amino acid backbone, and 2) the iron-sulfur proteins always contain more than one iron per molecule. The iron-sulfur proteins with more than two iron atoms per molecule and, generally, eight iron atoms per molecule (Orme-Johnson and Beinert, 1969) are called bacterial-type ferredoxins, as they were first discovered in nonphotosynthetic bacteria (Mortensen et al., 1962). Those with two iron atoms per protein molecule are called plant-type ferredoxins.

There are two other non-heme iron proteins: hemerythrin, and the high-potential iron protein (HiPIP) found in Chromatium D and Rhodopseudomas gelatinosa. Hemerythrin is an oxygen-transport protein found in some marine invertebrates: for example, sipunculid worms. There are two iron atoms and one cysteine residue in each of the eight subunits of the protein (Love, 1957; Boeri and Magaldi, 1957). The cysteine in this protein is involved in binding the subunits together (Keresztes-Nagy et al., 1965); therefore the iron complexes in this protein are not similar to that in rubredoxin (Lovenberg and Sobel, 1965), nor is the iron in hemerythrin analogous to that found in the iron-sulfur proteins (Fry and San Pietro, 1962).

The unique properties of HiPIP have given rise to studies of its chemical properties (Dus et al., 1967), but to date its function is unknown. HiPIP contains four iron atoms and four labile sulfur atoms per protein molecule. However, its reduction potential ($E_o' = +0.35V$) is not characteristic of any other iron protein, and it is not expected to contain an active center similar to the other iron-sulfur proteins.

As mentioned above, the name "plant-type ferredoxin" refers to iron-sulfur proteins with two iron atoms per molecule. The origin of this name is historical and not particularly descriptive for there are plant-type ferredoxins in animals and bacteria as well as in plants. Thus far, however, all iron-sulfur proteins in plants contain just two iron atoms per molecule, and all iron-sulfur proteins which have more than two iron atoms per molecule occur only in bacteria. In this research we have studied the best-characterized plant-type ferredoxins from plants, animals and bacteria:

Spinach Ferredoxin

Parsley Ferredoxin

Pig Adrenodoxin

Azotobacter Iron-Sulfur Protein I

Azotobacter Iron-Sulfur Protein II

C. pasteurianum Paramagnetic Protein

Putidaredoxin

The above designation of the iron-sulfur proteins in *Azotobacter* is in accordance with Shethna *et al*. (1968). *C. pasteurianum* paramagnetic protein (Hardy et al., 1965) is not to be confused

with the bacterial-type ferredoxin from C. pasteurianum known as Clostridial ferredoxin (Hong and Rabinowitz, 1967).

B. FUNCTION OF THE PLANT-TYPE FERREDOXINS

The main reactions of the plant-type ferredoxins included in this study are shown in Fig. 2. In plants, ferredoxin is involved in photosynthetic processes which are located very close to the chlorophyll in the electron-transport chain. It has been thought that ferredoxin was the primary electron acceptor in photosystem I in plants. Recently, however, Yocum and San Pietro (1969) have assigned this position in the chain to a different molecule which they named ferredoxin-reducing substance (FRS). Adrenodoxin and putidaredoxin are involved in the hydroxylation of deoxycorticosterone and camphor, respectively. The plant-type ferredoxins from C. pasteurianum and Azotobacter vinelandii have unknown functions; it is presumed that they are involved in nitrogen fixation.

Thus, the plant-type ferredoxins are participants in nitrogen fixation, photosynthesis, and steroid and camphor hydroxylations. Regardless of origin, however, these proteins show remarkable similarities in their chemistry. All the plant-type ferredoxins whose function is known, participate in electron transport chains with both one and two-electron transfer reactions present. In each chain, the switch between one and two electron transfer reactions takes place at the point where the ferredoxin reacts with a flavoprotein. Since Foust et al. (1969) have shown that spinach ferredoxin forms a 1:1 complex with the appropriate flavoprotein from spinach, it seems likely that the reaction in spinach involves two consecutive

FIGURE 2. ELECTRON-TRANSFER REACTIONS OF THE PLANT-TYPE FERREDOXINS.

Abbreviations:

ATP	- Adenosine triphosphate
Ad	- Adrenodoxin
Fd	- Ferredoxin
fp	- Flavoprotein
FRS	- Ferredoxin-reducing substance
NADPH	- Reduced nicotinamide adenine dinucleotide phosphate
P-450	- Cytochrome P-450
$P\text{-}450_{cam}$	- camphor specific cytochrome P-450
Put.	- Putidaredoxin
(r)	- Reduced form

I. PLANT FERREDOXINS

A. Cyclic Phosphorylation (Arnon, 1967)

$$4Fd_{ox} + 2ADP + 2P_i + 2H_2O \xrightarrow{h\nu} 4Fd_{red} + 2ATP + O_2 + 4H^+$$

B. Reduction of $NADP^+$ (Yocum and San Pietro, 1969)

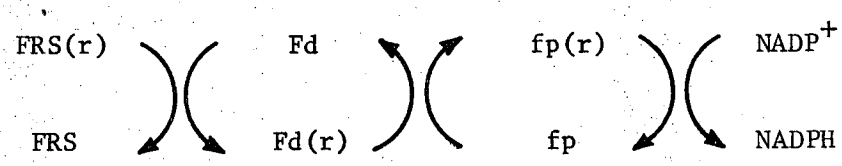

II. ADRENODOXIN

Deoxycorticosterone Hydroxylation (Kimura, 1968)

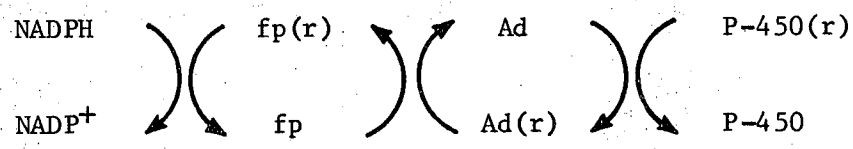

III. PUTIDAREDOXIN

Methylene Hydroxylation of Camphor

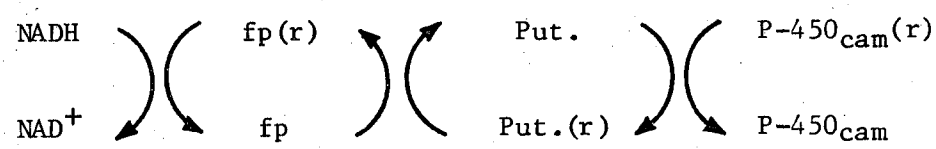

IV. AZOTOBACTER FE-S PROTEINS, CLOSTRIDIAL PARAMAGNETIC PROTEIN

Nitrogen Fixation?

reductions of the flavoprotein by reduced ferredoxin molecules. Thus, the role of the plant-type ferredoxins seems to be linked to an ability, in conjunction with a flavoprotein, to switch an electron transport chain from one to two electron transfer reactions or *vice versa*.

The importance of protein conformation in the reactions of the plant-type ferredoxins is not clear. The bacterial ferredoxins (Arnon, 1965; Tagawa and Arnon, 1962) and most of the plant-type ferredoxins will substitute for the plant ferredoxins in the photoreduction of nicotine adenine dinucleotide triphosphate (NADP). The iron-sulfur proteins from *Azotobacter* have no biological activity in the photoreduction of NADP (Shethna *et al.*, 1968). Here we note that the *Azotobacter* proteins have twice the molecular weight as any other plant-type ferredoxin (Table 1). However, none of the plant-type ferredoxins will substitute for adrenodoxin in steroid hydroxylation (Kimura *et al.*, 1969). Many of the above observations can be explained on the basis of thermodynamic arguments and known reduction potentials, although it is obvious that steric factors also play an important part in determining the biological activity of these proteins. Since we are interested here in the active site of these proteins, it is important to realize that the amino-acid residues not directly involved in the active site binding are surely of some importance in determining the chemical properties of these proteins. Thus, the measured reduction potentials of these proteins need not be a property which is determined solely by the physical properties of the active site.

C. PHYSICAL PROPERTIES OF THE PLANT-TYPE FERREDOXINS

The plant-type ferredoxins are small proteins with molecular weights between 12,000 and 24,000. Table 1 shows that four of the proteins examined have molecular weights around 12,000; this weight consists of 97 amino acid residues, two iron atoms and two sulfur atoms. Since disulfide bonds have not been detected in the plant-type ferredoxins, they are assumed to consist of a single amino acid chain with the iron and sulfur atoms bound to the protein via amino acid side chains.

The two iron and two sulfur atoms are labile; that is, they are released to the solution when the pH is lowered to around four. Since the protein contains no prosthetic group such as flavin or heme, and since the apoprotein is biologically inactive, the biological activity of the plant-type ferredoxin must result from a complex involving the apoprotein, the iron, the sulfur, or all three.

There are two oxidation states in plant-type ferredoxins: an oxidized state which then accepts a single electron to form the reduced state of these proteins. It will be important to keep in mind that even a strong reducing agent such as dithionite will only transfer a single electron to the plant-type ferredoxin (Mayhew et al., 1969). Once reduced, the plant-type ferredoxins are strong reducing agents themselves with reduction potentials between -240 and -420 millivolts at pH 7.5 (Table 1). Moreover, the plant-type ferredoxins exhibit no electron paramagnetic resonance (EPR) signal in the oxidized state, but in the reduced state, they show the "g = 1.94" EPR signal at low temperatures. (As a convenience, the abscissa in EPR data (Fig. 3) are

TABLE 1. PROPERTIES OF THE PLANT-TYPE FERREDOXINS INVESTIGATED. List of references used.

a. Bendall *et al.* (1963)

b. Cushman *et al.* (1967)

c. DerVartanian *et al.* (1967)

d. Evans *et al.* (1968)

e. Hall and Evans (1969)

f. Hardy *et al.* (1965)

g. Hollocher *et al.* (1966)

h. Kimura and Suzuki (1967)

i. Kimura *et al.* (1969)

j. Matsubara and Sasaki (1968)

k. Matsubara *et al.* (1968)

l. Orme-Johnson *et al.* (1968)

m. Palmer, G. (1967)

n. Palmer, G. - unpublished data

o. Palmer and Sands (1966)

p. Palmer *et al.* (1967a)

q. Shethna *et al.* (1964)

r. Shethna *et al.* (1968)

s. Tagawa and Arnon (1968)

t. Tsibris *et al.* (1968)

u. Watari and Kimura (1966)

	Fe	S=	Electrons Trans-ferred	MW	Eo'*** (mV)	EPR g-values	Ref
Azoto-bacter Fe-S Pro-tein I	2	2	1	21,000	-300 to -400*	gx=1.93 gy=1.95 gz=2.02	c,g, q,r
Azoto-bacter Fe-S Pro-tein II	2	2	1	24,000	-300 to -400*	gx=1.90 gy=1.95 gz=2.04	q
Parsley Ferre-doxin	2	2	1	12,000	-300 to -400*	gx=1.89 gy=1.96 gz=2.04	a,m
Adreno-doxin	2	2	1	12,000	-370	gx=1.93 gy=1.94 gz=2.02	e,h, i,l, n,u
Spinach Ferre-doxin	2	2	1	12,000	-420	gx=1.89** gy=1.96** gz=2.04**	d,j, k,p, o,s
C. Pas-teurianum Paramag-netic Pro-tein	2	2	1	24,000	-300 to -400*	gx=1.93 gy=1.95 gz=2.00	e,f
Putida-redoxin	2	2	1	12,000	-240	gx=1.94 gy=1.94 gz=2.02	b,c, e,t

*Personal communication, W.H. Orme-Johnson
**Personal communication, R.H. Sands
***Eo' = reduction potential at pH 7. (Mahler and Cordes, 1966).

sometimes given in terms of g, the spectroscopic splitting factor. "g" is defined as $\beta H/h\nu$ where ν is the microwave frequency and H is the applied field for a point along the abscissa. "g" is near the Lande g-value in the above experiments, but may vary widely for other compounds [Abragam and Pryce, 1951]).

This EPR signal has been critical for the identification and purification of these compounds (for example, see Shethna et al., 1964). The "g = 1.94" EPR signal has been observed from 4.2°K to between 80°K and 200°K, depending on the protein. The "high temperature" disappearance of this signal due to line broadening is attributed to spin relaxation effects (personal communication, G. Palmer; Shethna et al., 1968). The EPR signal (Fig. 3) is anisotropic with two g-values around 1.94 ($g_{\perp}$) and a third g-value around 2.04 ($g_{\parallel}$). Thus, the weighted average of these g-values is less than 2.0023, the g-value of the free electron. Although the "g = 1.94" EPR signal in itself attracts attention and gives rise to numerous theoretical implications with respect to the position of electronic energy levels (Brintzinger et al., 1966), we shall first turn to a consideration of a group of experiments in which changes in this EPR signal were observed.

These experiments consist of substituting isotopes with non-zero nuclear spin for native iron or sulfur atoms in the protein and then observing the resulting hyperfine interaction in the EPR spectrum of the reduced proteins at low temperature. The rationale and results of the experiments are as follows: 1) the oxidized protein does not show an EPR signal, whereas the reduced protein exhibits a signal characteristic of an S = 1/2 ground state doublet

FIGURE 3. EPR SIGNAL OF SPINACH FERREDOXIN. This spectrum was taken on 10^{-5}M spinach ferredoxin in 0.1Mtris (pH 8.1 at 25°C), reduced with sodium dithionite. The spectrum was recorded at a microwave power (9.203GHz) of 1mW, a modulation amplitude of 4 gauss, a scanning rate of 500 gauss/min. and at 20°K. The receiver gain of the Varian E-3 EPR Spectrometer was 3.2×10^5.

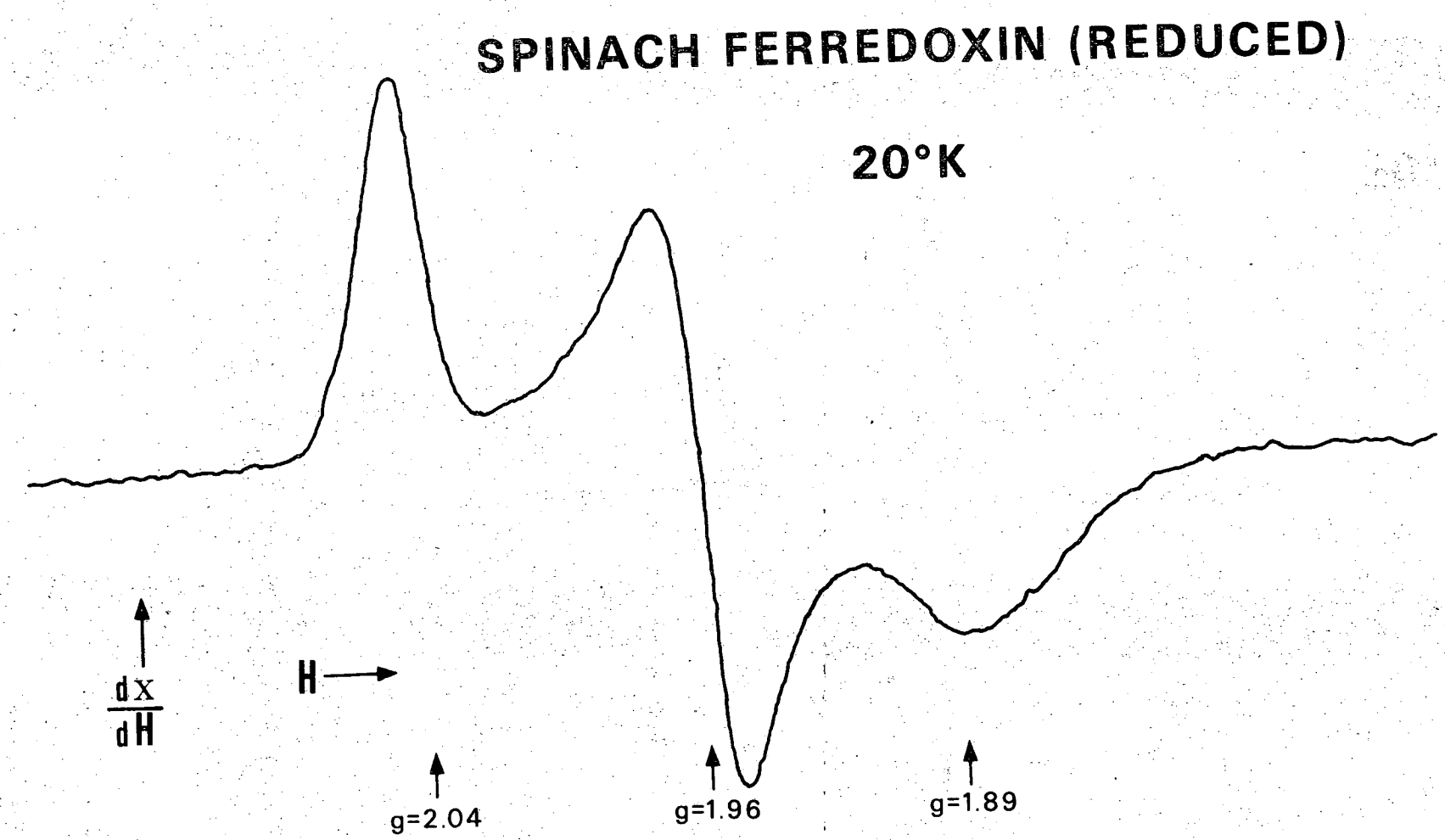
SPINACH FERREDOXIN (REDUCED)
20°K
dX/dH
H
g=2.04
g=1.96
g=1.89

(Beinert et al., 1965). In addition, the EPR signal quantitates to a single electron by double integration of the EPR signal (Palmer et al., 1967), and by spectrophotometric titration with dithionite (Mayhew et al., 1969). Since the proteins are known to take up a single electron during reduction, the electron spin which causes the EPR signal is located at the active site of the protein. 2) If atoms in the native protein are interchanged with isotopes having non-zero nuclear spin and if these atoms are involved with this reducing electron through a molecular orbital, then one can expect to see a broadening of the EPR signal due to the magnetic hyperfine interaction. Certainly, if broadening is observed upon isotopic substitution, this would mean that the substituted atom is part of the active site of the protein. Since Malkin and Rabinowitz (1966) have been able to reconstitute ferredoxin after the iron and inorganic sulfide has been removed, it would seem possible to induce hyperfine broadening by substituting ^{57}Fe ($I = 1/2$) or ^{33}S ($I = 3/2$) for their counterparts in the native protein. Alternatively, one could grow the cells in a medium enriched in ^{57}Fe or ^{33}S and obtain the desired protein in this way. The latter method is the more expensive in terms of time and money, and it is obviously not very feasible to produce enriched pig adrenodoxin in this way. However, the advantage of the growth experiments is that one is assured by this approach that enriched protein is structurally identical to the non-enriched protein.

The results of the above experiments show that enrichment with either ^{57}Fe or ^{33}S results in a broadening of the EPR signal in many of the plant-type ferredoxins (references in Table 1). These studies have

shown that both iron nuclei and both inorganic sulfide nuclei interact magnetically with the electron spin. The magnitudes of the hyperfine interactions with ^{57}Fe and ^{33}S nuclei indicate that the iron and sulfur atoms are bonded to form a complex at the active center of the plant-type ferredoxins. In addition, cysteine sulfur has been implicated in the active site of putidaredoxin by growth experiments on ^{33}S (Der Vartanian et al., 1967). Thus, the results of these EPR experiments imply that the active site of the plant-type ferredoxin consists of a complex with two iron atoms and two sulfur atoms ligated by the side chains of the protein amino acids. The absence of disulfide bonds in the proteins and the ^{33}S growth experiments for EPR study indicate that cysteine is a ligand in this complex.

The amino-acid sequences of several plant-type ferredoxins are known (Fig. 4). Since x-ray crystallography has not as yet been successfully applied to the study of any plant-type ferredoxin, the chief use of this amino-acid data has been to point out similarities in the sequences (Sasaki and Matsubara, 1967) and to draw conclusions on the evolution of these proteins from correlations in their sequences (Matsubara et al., 1968a). Since cysteine has been implicated as a ligand in the iron-sulfur complex of these protein, mention of its characteristics in these proteins is warranted.

The position of the five cysteine residues which are present in most plant-type ferredoxins is one of the most obvious and constant features in the sequences. In particular, cys44 and cys47 would seem to provide a most inviting binding site for the iron-sulfur complex. However, the incidence of amino acids with side chains having charged

FIGURE 4. AMINO ACID SEQUENCES OF PLANT-TYPE FERREDOXINS. References:

Alfalfa - Keresztes-Nagy *et al.*, 1969

L. Glauca - Benson and Yasunobu, 1969

Scenedesmus - Sugano and Matsubara, 1968

Spinach - Matsubara and Sasaki, 1968

	1	2	3	4	5	6	7	8	9	10	11	12	13	14	15	16	17	18	19	20
1. L. Glauca	----	Ala	Phe	Lys	Val	Lys	(Leu)	Leu	Thr	Pro	Asp	Gly	(Pro)	Lys	Glu	Phe	Glu	Cys	Pro	Asp
2. Spinach	Ala		Tyr			Thr		Val			Thr		Asn	Val			Gln			
3. Alfalfa	Ala	Ser	Tyr					Val			Glu		Thr	Gln						
4. Scenedesmus	Ala	Thr	Tyr			Thr		Lys			Ser		Asp	Gln	Thr	Ile				

	21	22	23	24	25	26	27	28	29	30	31	32	33	34	35	36	37	38	39	40	41	42	43	44
1.	Asp	Val	Tyr	Ile	Leu	Asp	Gln	Ala	Glu	Glu	Leu	Gly	Ile	(Asp)	Leu	Pro	Tyr	Ser	Cys	Arg	Ala	Gly	Ser	Cys
2.							Ala				(Glu)		(Ile)											
3.							His				Glu			Val										
4.		Thr					Ala				Ala		Leu										Ala	

	45	46	47	48	49	50	51	52	53	54	55	56	57	58	59	60	61	62	63	64	65	66	67	68	69
1.	Ser	Ser	Cys	Ala	Gly	Lys	Leu	Val	Glu	Gly	Asp	Leu	Asp	Gln	Ser	Asp	Gln	Ser	Phe	Leu	Asp	Asp	Glu	Gln	Ile
2.								Lys	Thr		Ser		Asn		Asp								Asp		
3.							Val	Ala	Ala		Glu	Val			Ser		Gly						Asp		
4.							Val	Glu	Ala		Thr	Val											Ser		Met

	70	71	72	73	74	75	76	77	78	79	80	81	82	83	84	85	86	87	88	89	90	91	92	93	94
1.	Glu	Glu	Gly	Trp	Val	Leu	Thr	Cys	Ala	Ala	Tyr	Pro	Arg	Ser	Asp	Val	Val	Ile	Glu	Thr	His	Lys	Glu	Glu	Glu
2.	Asp												Val				Thr								
3.										Val		Ala	Lys				Thr								
4.	Asp	Gly		Phe					Val				Thr			Cys	Thr		Ala						Asp

	95	96	97
1.	Leu	Thr	(Ala)
2.			
3.			
4.		Phe	---

or polarized atoms is quite high in the plant-type ferredoxins; thus, there are many side chains in the proteins which could provide ligands to the iron-sulfur complex. Although methionine is not always present in plant ferredoxins, "backbone" sulfur could be provided to the complex via this amino acid residue.

Although the optical spectra of these proteins have been extremely helpful in their identification and purification, their importance to the characterization of the active site has been less than gratifying. However, an absorption peak at 420 nanometers has been shown to lose one-half of its intensity upon reduction of the protein (Tsibris et al., 1968). Also EPR, CD (circular dichroism) and ORD (optical rototary dispersion) data have been correlated with OD_{420} (Palmer et al., 1967). The results of these experiments would indicate that OD_{420} is characteristic of a charge-transfer band in the iron-sulfur complex.

In summary, plant-type ferredoxins are 97 amino acid proteins with two iron atoms and two sulfur atoms bound in a complex with the ligands supplied by the amino acid side chains. Single electron reduction of this protein results in a material exhibiting a low-temperature EPR signal with absorptions centered around $g = 1.94$. Other physical techniques which give information on the active site of these proteins are magnetic susceptibility, Mossbauer spectroscopy and electron nuclear double resonance (ENDOR). The results of studies with these techniques are the subject of Chapter V.

D. WHY MOSSBAUER SPECTROSCOPY?

The function of the plant-type ferredoxins is to accept a single electron from one protein and pass it on to another. This electron, while in the ferredoxin molecule, is localized to a complex which contains two iron and two sulfur atoms which are not from the amino acid residues. As will be shown in Chapter V, however, the experimental data which have been presented heretofore are not sufficient to substantiate a definitive model for the active site of these proteins. There is also no small molecular weight iron-sulfur compound which has all the physical properties of the active site.

Since the problem is essentially to find the structure of the active site, the logical first choice for such a study is x-ray crystallography. This technique demands large, stable crystals of the native protein and one or more isomorphous-replacement derivatives. Since these demands have not been met thus far with any plant-type ferredoxin, x-ray crystallography has not been possible.

Thus we are forced to study non-crystalline preparations of the holo-proteins in order to discern the nature of the active site. Here, also, we are faced with a problem common to the study of all proteins: the active site of the protein is represented by around one-fiftieth of the total weight of the protein. We are interested in the oxidation state and coordinating ligands of two iron atoms which are surrounded by 97 amino acids. It is in this context that Mossbauer spectroscopy seems most appropriate to the study of the plant-type ferredoxins. Mossbauer spectroscopy is an absorption spectroscopy in which transitions between nuclear quantum states are observed. The

properties of this spectroscopy are such that the extremely small perturbations of the nuclear energy levels become measurable. These perturbations result from interactions of nuclei with surrounding electrons. One is thus able to derive information on the electronic environment of a particular nucleus by Mossbauer spectroscopic experiments.

The energy measurement made through Mossbauer spectroscopy is also completely noise-free with respect to any other nucleus than the one being studied. Thus, if a spectrometer is set up to observe transitions in an ^{57}Fe nucleus, 100% of the relative absorption seen at the detector is due to ^{57}Fe transitions. This specificity can be especially helpful in protein study as it allows one to see a particular locus in a large molecule. However, iron is one of the few elements present in biological compounds which has an isotope (^{57}Fe) that can exhibit a Mossbauer spectrum. Since the natural abundance of ^{57}Fe is 2.19%, enrichment with this isotope facilitates a study of the plant-type ferredoxins.

Another characteristic of Mossbauer spectroscopy is that it is most efficient at low temperatures (for frozen-aqueous solutions, below 250°K). As discussed previously, the "g = 1.94" EPR signal was observable only at low temperatures. Thus, the temperature dependence of Mossbauer spectroscopy allows correlation of the Mossbauer spectroscopic results directly with those of EPR under identical experimental conditions.

II. ^{57}Fe MOSSBAUER SPECTROSCOPY

A. THE MOSSBAUER EFFECT

As Mossbauer spectroscopy is a newer field than other fields of resonance spectroscopy, its literature is not yet organized to the point where a new investigator in the field can easily find the answer to as basic a question as, "What is the Mossbauer effect?" The bibliography presents a listing of the basic articles and works which deal with Mossbauer spectroscopy in general, and in its application in particular to biological problems. Three monographs (Wertheim, Frauenfelder, and Abragam) are good starting places to learn about Mossbauer spectroscopy, although a more thorough understanding of the field can carry one deeply into the literature of associated disciplines such as solid-state and nuclear physics. The following remarks on the theory of Mossbauer spectroscopy are meant to provide a feeling of the physical parameters as seen in the Mossbauer literature. In biological contexts, the Mossbauer spectroscopy literature is almost exclusively restricted to ^{57}Fe although other isotopes (^{129}Xe, ^{119}Sn, ^{127}I, ^{129}I) are of potential value to experimenters in biology.

Decay of the I = 3/2 nuclear state of ^{57}Fe to the I = 1/2 ground state takes place either by internal conversion or by the emission of a gamma ray. About ten internal conversion events occur for each gamma ray emission (Kistner and Sunyar, 1965). The emitted gamma ray has an energy of 14.41keV and a line width of 4.7×10^{-9}eV which arises from the lifetime of the I = 3/2 state through the Heisenberg uncertainty principle ($\Delta E = \hbar/\tau$ where τ is the mean lifetime

of the nuclear excited state). The monochromaticity of the gamma ray should in principle allow one to measure the perturbations of a ^{57}Fe nucleus produced by the electronic environment, since these perturbations are around 10^{-7}eV, thus much larger than the linewidth of the gamma ray. Normally, nuclear absorption spectroscopy is not particularly monochromatic because the energy of the emitted (and absorbed) gamma ray is modified by Doppler energy shifts due to nuclear recoil. These Doppler shifts are many orders of magnitude larger than either the linewidth of the gamma ray or the range of energy perturbations produced by atomic electrons on the iron nucleus. Therefore, nuclear resonance is difficult to observe by normal absorption techniques, since the probability is small that energy of a gamma ray emitted by one ^{57}Fe nucleus corresponds to the energy needed to excite the nucleus of another ^{57}Fe atom. The Mossbauer effect increases the probability of resonant events which occur when the temperatures are lowered in the gamma-ray source and the absorber.

This increase in resonance at low temperatures results from an increase in the probability that a nucleus can emit a gamma ray without recoiling. In these recoil-less events, the conservation of momentum principle applies, but the recoil momentum is carried by the entire lattice of which the emitting nucleus is a part. Upon emission the gamma ray has the full energy of the nuclear transition since the energy contained in the recoil of the massive lattice is negligible.

Consider a source of this gamma radiation which results from "recoil-less" emissions. The radiation source must consist of the

Mossbauer transition which will be excited in the absorbing material since other sources of radiation cannot meet the requirements for monochromaticity and energy. In ^{57}Fe Mossbauer spectroscopy, the sources are ^{57}Co nuclei imbedded in a transition metal matrix; the purpose of the matrix is to provide a uniform environment for the ^{57}Co nuclei and thus to prevent any ^{57}Co – ^{57}Co interaction which could result in a multiple line source. ^{57}Co decays via electron capture to the 136 keV isomeric state (I = 5/2) of ^{57}Fe. After 10^{-9} S this state cascades via a 14.41 keV isomeric state (I = 3/2) to the ground state of ^{57}Fe (I = 1/2). The lifetime of the 14.41 keV isomeric state is 10^{-7} S. The source gamma radiation can be energy-modulated by moving the source relative to an absorber, by employing the first-order relativistic Doppler shift:

$$E = E_\gamma \left(1 + \frac{v}{c}\right) \tag{1}$$

where E_γ is energy of the gamma ray when the nucleus is at rest, v is the velocity of source relative to the absorber and c is the velocity of light. For the 14.41 keV gamma ray of ^{57}Fe the linewidth (FWHM) corresponds to a velocity of 0.2 mm/S and the velocity range needed in practice to scan the energy spectrum of any absorber is 12 mm/S.

Let us now consider the means by which a nucleus can recoil when this nucleus is part of a protein in frozen aqueous solution.

1) The emitting nucleus cannot recoil as a free particle since the energy of recoil ($E_R = E_\gamma^2/2Mc^2 = 1.9 \cdot 10^{-3}$ eV for ^{57}Fe) is much smaller than the energy required to break chemical bonds in the protein molecule.

2) Rotational and translational motion of the protein molecule are precluded for such a macromolecule in frozen solution.

3) The only remaining means of motion for a nucleus is vibration within the crystal lattice (phonons). Although center-of-mass momentum may not be transferred to the lattice via phonon interactions, it is possible to destroy the Mossbauer effect by this means. Remembering the Einstein model for a crystal, nuclear vibrations in a crystal are described by wave functions which span the width of the crystal. Thus a nucleus is allowed certain quantized vibrational frequencies: there exists a minimum ground state frequency below which nuclear vibrations are not allowed. In the Debye solid, there is a characteristic energy, which represents the difference between this ground state and the first excited phonon state. This energy is given in terms of temperature, Θ_D, the Debye temperature.

As the temperature in a Debye solid is lowered, the ground phonon state becomes more and more populated until the energy needed to excite a vibrational transition in the solid becomes equal to $k\Theta_D$. If the recoil energy from a nuclear gamma ray is less than $k\Theta_D$, then it is possible for a nucleus to emit a gamma ray <u>without</u> a phonon excitation. In this case, momentum is conserved by recoil of the crystal as a whole. The velocity of the lattice corresponding to this momentum is so small that any Doppler effect on the emitted gamma ray is negligible. Thus the emission is said to be "recoil-free". The probability for recoil-free emission is given by f, the recoil-free fraction. The details of the above argument are given in the general

references to Mossbauer spectroscopy (Bibliography). The results define f as:

$$f = \exp\left\{-\frac{E_R}{k\Theta_D}\left[\frac{3}{2} + \frac{\pi^2 T^2}{\Theta_D^2}\right]\right\} \quad \text{where } T \ll \Theta_D \qquad (2)$$

Experimentally, this fraction approaches 0.7 for sources at 298°K and for frozen-protein solutions at temperatures around 100°K. Therefore it is not advantageous to cool the source.

A typical Mossbauer spectrometer consists of) a radioactive source of Mossbauer gamma rays placed in a source mover b) a dewar system which controls the absorber temperature and allows the transmission of gamma rays, and c) a gamma-ray counting system which is synchronized with the motion of the source mover and which is capable of filtering out non-resonant radiation. (The spectrometer used in this research will be considered in greater detail in Chapter III.) A Mossbauer effect spectrum results from an increase in absorption as the velocity of the source produces a gamma ray which corresponds to the difference in energy between two nuclear states in the absorber. For this reason, Mossbauer data are usually presented as per cent absorption vs. velocity.

Information about the electronic environment of an ^{57}Fe nucleus can be gained by obtaining Mossbauer spectra. These spectra will vary depending on the perturbations produced by the electronic environment on the ^{57}Fe nuclear isomeric states. It is important to note that <u>both</u> isomeric states will undergo energy perturbations, although the I = 1/2 ground state may not sense electrostatic interactions other than the electric monopole interaction as this state has zero electric moments. Relation of the observed Mossbauer spectra to

electronic configurations can be made by the use of perturbation theory applied to the nuclear energy levels as in no case does the Mossbauer experiment deal with the full energy of the nuclear isomeric transition but rather with extremely small changes in this energy ($1:10^{12}$) as produced by the various electronic environments. Thus, in constructing a perturbation Hamiltonian to describe the interaction between the nucleus and its electronic environment, no term need be included to represent the energy of the excited nuclear state relative to the ground state. In fact, Mossbauer spectra contain no information concerning the total energy of nuclear transition in the absorber since the energy unit in these spectra is relative to the energy of the nuclear transition in the source at rest. There are three types of perturbations to the energy levels of a bare nucleus: the isomer shift, the electric quadrupole interaction, and the interactions between the nuclear magnetic moment and any magnetic fields present at the nuclear position.

B. ISOMER SHIFT

The isomer shift term results from an electric monopole interaction between the charged nucleus and the charge of the surrounding electrons. Therefore, this term is a scalar in the perturbation Hamiltonian and produces a shift in velocity of a Mossbauer spectrum as a whole. The "shift" results from a difference in the interaction between the nuclear ground state ($I = 1/2$) and 14.41 keV first isomeric state ($I = 3/2$) of ^{57}Fe, hence the name isomer shift. Since this shift is dependent on the electronic environment, it is different in the source, a standard reference material, and the absorber (Fig. 5).

FIGURE 5. (A) EFFECT OF ELECTRON-CHARGE DENSITY ON BARE NUCLEI.

(B) RESULTING MOSSBAUER SPECTRUM.

A

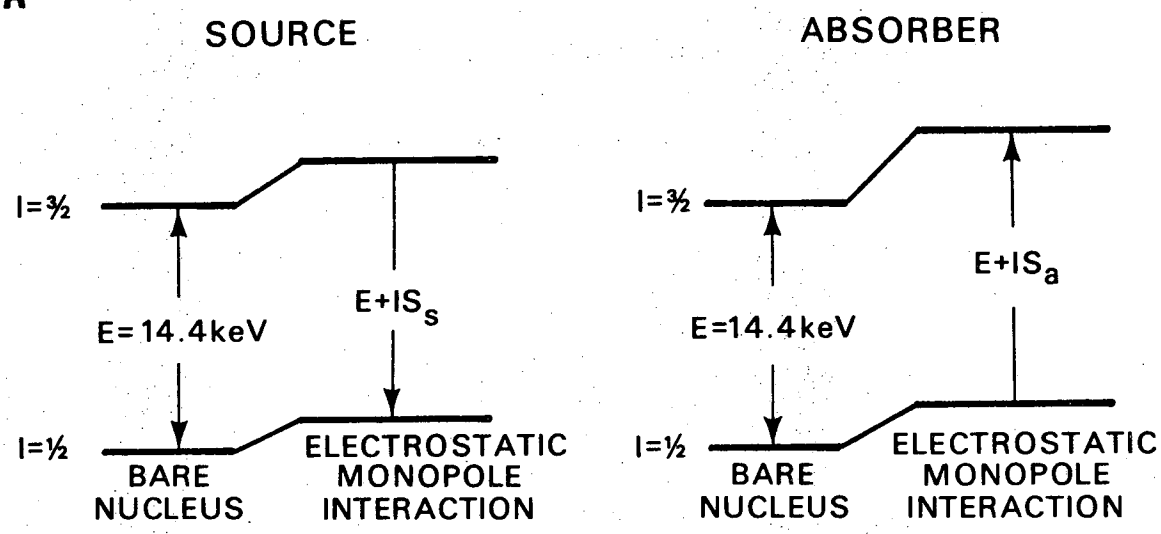

EFFECT OF ELECTRON CHARGE DENSITY ON BARE NUCLEI

B

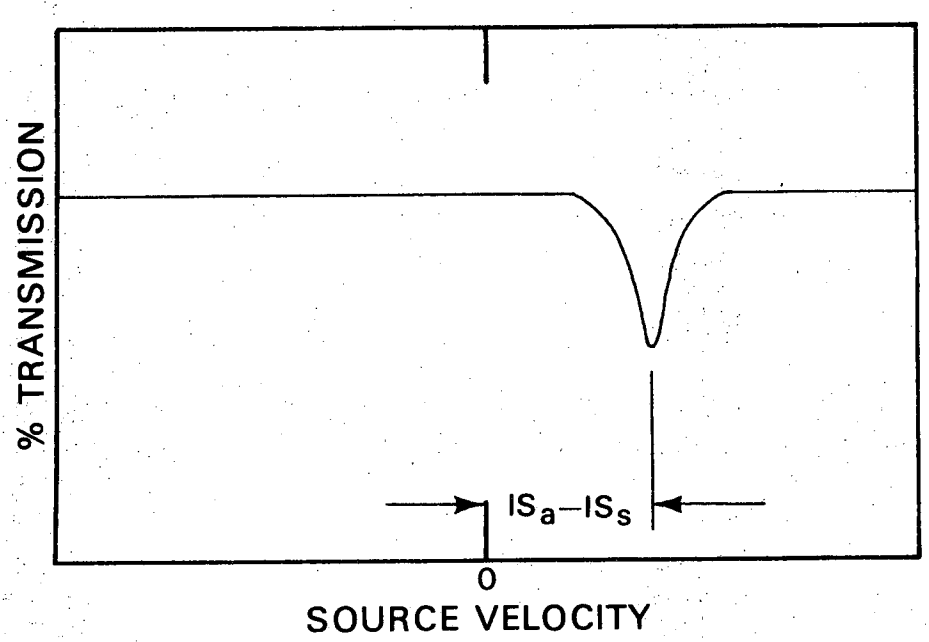

RESULTING MOSSBAUER SPECTRUM

Since the only electrons with a non-zero probability at the nucleus are s-electrons, the isomer shift is determined by s-electron density at the nucleus.

It is conventional to define positive velocities as motion of the source toward the absorber. With this convention, increased electron density at the absorber nucleus shifts a Mossbauer spectrum to more negative velocities. S-electron densities can be affected by variations in electron density in other atomic orbitals. In the case of iron chemistry, the largest variations in s-electron density result from variations in 3d orbitals. Since added d-electron density increases shielding of s-electrons from the nucleus, added d-electrons in the absorber shift a Mossbauer spectrum to higher energies (more positive velocities). Thus we have, in principle, a way to determine the oxidation state in the absorber by comparing an experimental spectrum to spectra of known standards. In practice, however, the situation is not as straightforward. The spin state of the iron and the bonding character of the 3d electrons are factors which affect the degree to which 3d electrons contribute to electron density at the nucleus. These effects have been discussed by Schulman and Sugano (1965):

1) The amount of 4s character in a valence electron contributes directly to the electron density at the nucleus. The ligand field will give an indication as to the probability of this occurring (Walker et al., 1961).

2) The shielding effects of 3d electrons depend on the type of bonding in which these electrons are involved. Principally, there are three bonding types to be considered:

a. The $3d^n$ configurations (ions) assign n electrons to the 3d shell. The contributions to $\sum |\Psi(0)|^2$ have been estimated for n = integer by Walker et al. (1961).

b. Covalency between 3d and filled ligand orbitals increases d-electron density, thereby increasing the isomer shift.

c. Covalency between 3d and empty ligand orbitals decreases d-electron density via back donation, thus resulting in a more negative isomer shift.

As a result of the complexity of the isomer shift interaction, the experimenter is seldom able to make a definitive assignment of oxidation state from isomer shift data alone. High-spin ferrous ($3d^6$, S = 2) compounds are the exception; this case will be discussed in greater detail during the description of the nuclear quadrupole interaction.

C. NUCLEAR QUADRUPOLE INTERACTION

The quadrupole term in the perturbation Hamiltonian originates from an interaction between the quadrupole moment of the nucleus and the electric field gradient (EFG) at the nuclear position resulting from the electrons in the iron atom and surrounding ligands. Since the quadrupole moment of the ground state (I = 1/2) of ^{57}Fe is necessarily zero (Evans, 1955), the interaction is absent for this state. However, in the excited state (I = 3/2) the quadrupole interaction splits the fourfold degeneracy of this state into $m_I = \pm 1/2$ and $m_I = \pm 3/2$ states.

The EFG is a second-rank tensor which can be diagonalized by a suitable choice of coordinate system. The mathematics of the quadrupole interaction is shown below in three equivalent representations; each has a specific advantage either in simplifying calculations or in aiding the experimenter to visualize the three-dimensional aspect of the EFG.

$$\mathcal{H}_Q = -\frac{eQ}{6}\left[V_{xx} I_x^2 + V_{YY} I_Y^2 + V_{zz} I_z^2\right] \tag{3}$$

where eQ = quadrupole moment of the I = 3/2 nuclear state in ^{57}Fe. V_{xx}, V_{yy}, V_{zz} are the diagonal components of the EFG.

$$\mathcal{H}_Q = \frac{e^2 q Q}{12}\left[3I_z^2 - I(I+1) + \eta\left(I_x^2 - I_Y^2\right)\right] \tag{4}$$

where $-eq = V_{zz}$; $\eta = (V_{xx} - V_{yy})/V_{zz}$.

Since it is customary to choose $|V_{zz}| \geq |V_{YY}| \geq |V_{xx}|$, the range of is limited: $0 \leq \eta \leq 1$. Notice also that there are only two variables (q, η) in Eq. 4. This reduction in parameters is possible because the components of the EFG must satisfy Laplace's equation at the nuclear position; that is,

$$V_{xx} + V_{yy} + V_{zz} = 0 \tag{5}$$

The following form of the quadrupole interaction is used in Chapter IV.

$$\mathcal{H}_Q = 2DI_z^2 + (E-D)I_x^2 + (-E-D)I_Y^2 \tag{6}$$

where $D = \frac{e^2qQ}{12}$ and $E = \eta D$.

The EFG at the nucleus is the result of non-spherical charge densities in the iron atom and in the surrounding ligands. Although the EFG at the nuclear position is the tensor which enters in the Hamiltonian for the quadrupole interaction, it is not this EFG but an

EFG which would arise from only the ligands and valence electrons that is of principal interest to the chemist. Since the effect of the inner electrons is to diminish the quadrupole interaction, the Hamiltonian is usually written with the "outer" electron EFG reduced by "Sternheimer anti-shielding constants" (Danon, 1968). The value of the quadrupole moment for $^{57}Fe_{3/2}$ is not known precisely (Grant, 1966). The uncertainty in this parameter and in the value of the anti-shielding constants makes the precise calculation of the quadrupole interaction from basic principles very difficult. An alternate way to treat the problem is to deal exclusively with the parameters in Eq. 6.

First define a new parameter, QS, which is convenient in matching computed spectra to Mossbauer data.

$$QS = \frac{e^2 q Q}{2} \left(1 + \frac{\eta^2}{3}\right)^{1/2} \tag{7}$$

Since $D = \frac{e^2 qQ}{12}$ then QS can be written as

$$QS = 6D\left(1 + \frac{\eta^2}{3}\right)^{1/2} \tag{8}$$

By taking only the positive square root in Eq. 8, the quadrupole Hamiltonian is defined in terms of QS and η, the EFG asymmetry parameter. Note that QS has the same sign as both D, the quadrupole coupling constant, and V_{zz}, the largest principal component of the EFG tensor. In addition, QS is the observed splitting of a single quadrupole pair (Wertheim, p.64) and can thus be easily specified in units of mm/S. η can be varied at will without changing the observed splitting while the parameter QS is held constant. For a simple quadrupole interaction in a powder sample the resultant Mossbauer

spectrum consists of two lines of equal intensity split by an amount QS (Fig. 6). However, the Goldanskii-Karyagin effect (Goldanskii and Marakov, 1968) can give rise to two-line quadrupole spectra for powders in which the lines are of unequal intensity. If a powder is envisioned as a random orientation of microcrystals, then this effect is explained by assigning different recoil-free fractions to different directions in the crystal coordinate frame. In other words, the microcrystal can have different Debye temperatures which depend on the direction of the phonon mode which can be excited during a gamma-ray absorption.

When the internal magnetic field at the nucleus is zero, the application of an external magnetic field is necessary in order to determine the sign of QS and the magnitude of η (Collins, 1964). Fig. 7 contains computed spectra which illustrate the effect of an applied magnetic field on powder samples with a simple quadrupole interaction. Note that when η is not equal to one, these spectra are not centro-symmetric along the velocity axis. Given a specific magnitude of QS and the magnetic field at the nucleus, the shape of these spectra is determined by the value of η as shown in Fig. 7. (Changing the sign of QS results in spectra which are the mirror images of these spectra.) Thus, by matching experimental data to calculated spectra, one can determine the major components of the quadrupole tensor for powder samples in applied magnetic field.

A quadrupole spectrum will appear when there is no magnetic field at the nucleus ($H_{nuc} = 0$) or when a magnetic field at the nucleus does not have an axis of quantization for a time comparable to the nuclear Larmor precession time. (If the magnetic field at an

FIGURE 6. (A) ELECTRIC QUADRUPOLE SPLITTING OF NUCLEAR LEVELS.

(B) RESULTING MOSSBAUER SPECTRUM.

A

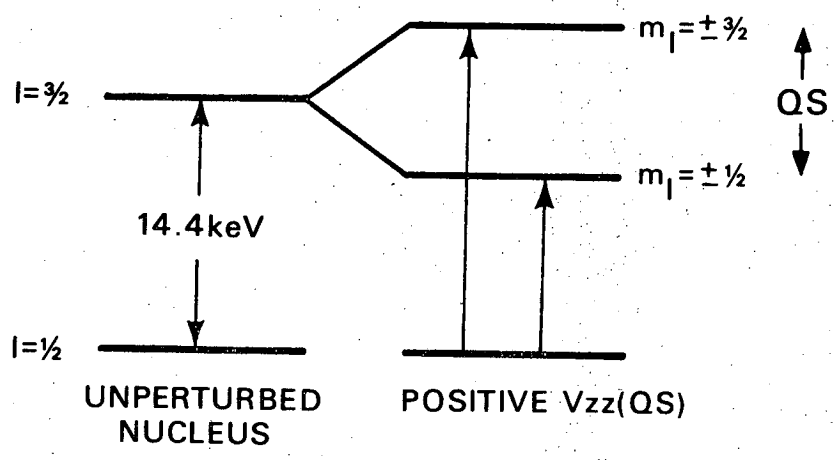

QUADRUPOLE SPLITTING OF NUCLEAR LEVELS

B

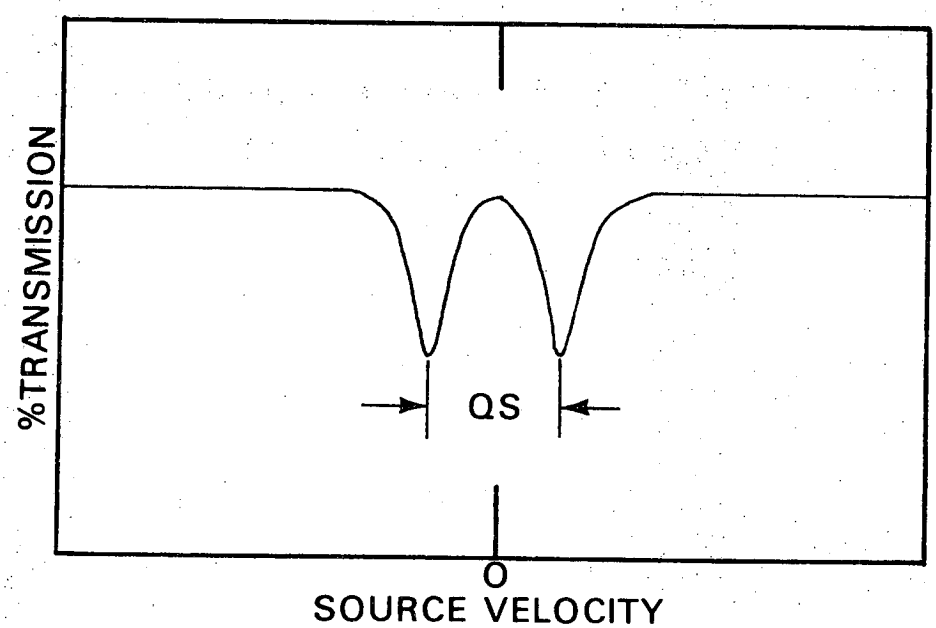

RESULTING MOSSBAUER SPECTRUM
FOR POWDER SAMPLE

FIGURE 7. COMPUTER PLOTS FOR PARAMAGNETS IN APPLIED MAGNETIC FIELDS. These plots are the output of program ANIMO and represent solutions to the Hamiltonian in Eq. 13 for powder samples in applied magnetic fields. These spectra are suitable for comparison with ^{57}Fe Mossbauer spectra of diamagnets or of materials with isotropic hyperfine interactions. The isomer shifts are zero for all spectra. Changing the sign of QS for any spectrum will reverse the spectrum along the velocity axis. Note that when η approaches one, these spectra become centro-symmetric. The effective magnetic field at the nucleus, H, is parallel to the gamma ray direction and is given in kilogauss. The left and right boundaries in each plot are at -6.00 mm/S and +6.00 mm/S, respectively.

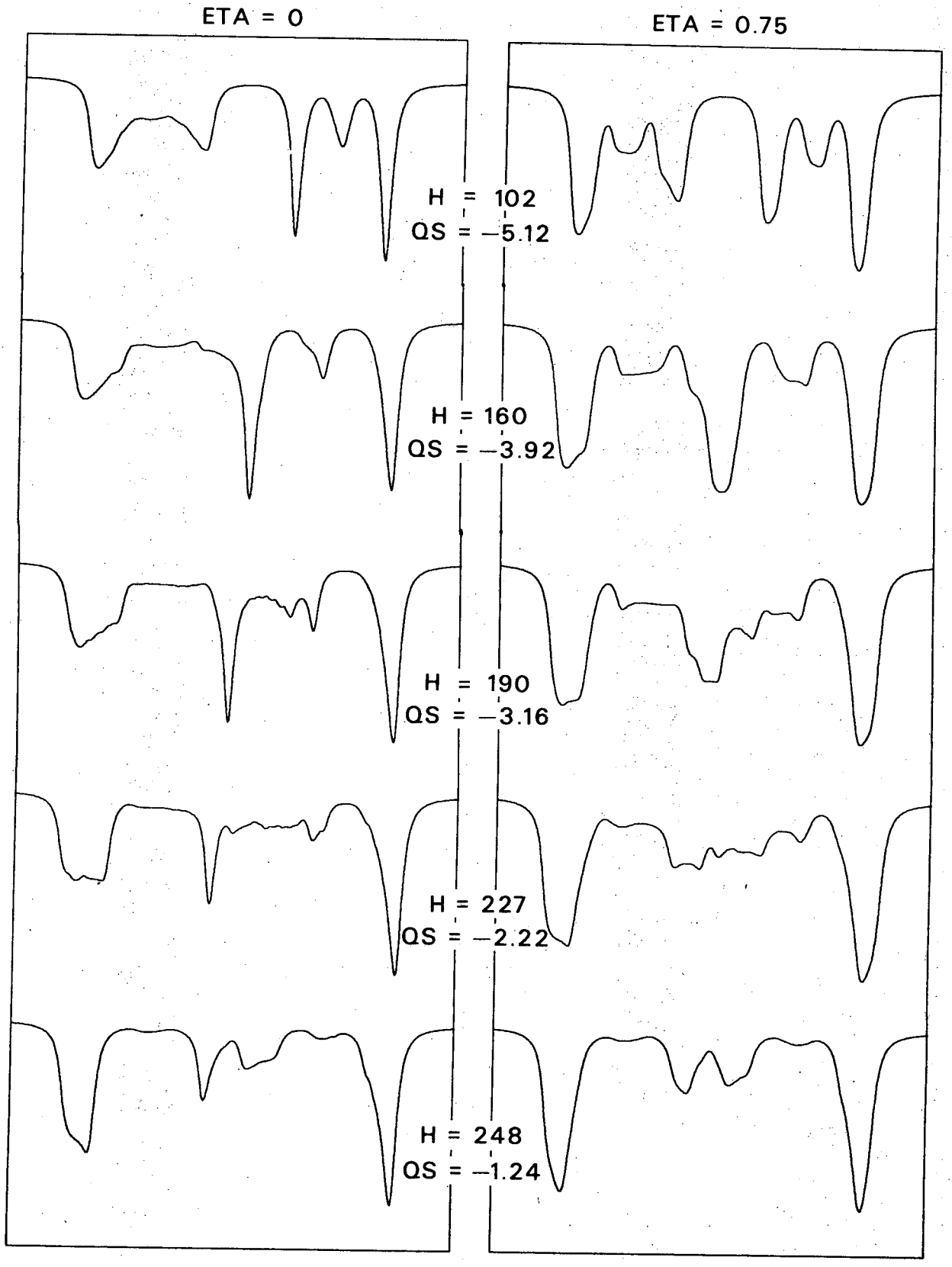
ETA = 0
ETA = 0.75
H = 102
QS = −5.12
H = 160
QS = −3.92
H = 190
QS = −3.16
H = 227
QS = −2.22
H = 248
QS = −1.24

$^{57}Fe_I$ = 1/2 nucleus equals 3 kG, then $1/\omega_L$ is $3 \cdot 8 \cdot 10^{-7}$S.) The zero applied field Mossbauer spectra of oxidized plant-type ferredoxins are quadrupole spectra (Fig. 16); therefore, one may assume that one of the above is true. There is, however, other information available from simple quadrupole Mossbauer spectra.

High-spin ferric and low-spin ferrous ions have spherical electron charge distributions about the nucleus (Unsold's theorem: see Pitzer, 1953). For low-spin ferric and high-spin ferrous ions the electron charge distribution is usually non-spherical; however, in high-spin ferrous, the electrostatic interaction between the 3d electrons is less than that for low-spin compounds, which accounts for their comparatively large quadrupole splitting and more effective shielding of the outer s-electrons (Section II-C). Thus, a quadrupole splitting of 2-4 mm/S and an isomer shift which is $\sim$ 1 mm/S more positive than most ferric compounds is characteristic of high-spin ferrous. (Most other iron compounds give quadrupole splittings of 0-1 mm/S.) An example of high-spin ferrous Mossbauer spectra will appear during the discussion of the high-temperature, reduced protein spectra.

In addition, q and η have been calculated for the crystal field basis set of d-orbitals (Ingalls, 1964).

TABLE 2

ORBITAL CONTRIBUTIONS TO EFG

Orbital	q	η
$d_{x^2-y^2}$	$4/7 \langle r^{-3} \rangle$	0
d_{z^2}	$-4/7 \langle r^{-3} \rangle$	0
d_{xz}	$-2/7 \langle r^{-3} \rangle$	+3
d_{yz}	$-2/7 \langle r^{-3} \rangle$	-3
d_{xy}	$4/7 \langle r^{-3} \rangle$	0

We shall return to the calculation of quadrupole parameters in Chapter V.

D. MAGNETIC EFFECTS

The basic magnetic interaction is the nuclear Zeeman interaction:

$$\mathcal{H}_m = -\tilde{\mu}_N \cdot \tilde{H}_{eff} = -g_N \mu_N \tilde{I} \cdot \tilde{H}_{eff} \tag{9}$$

where $g_N \mu_N I$ is the magnetic moment of the nucleus and H_{eff} is the effective magnetic field at the nucleus. The magnetic field splits the m_I degeneracy of both the ground and excited states of the nucleus. Figure 8 illustrates this splitting and also shows the resulting Mossbauer spectrum for the powder sample in which the interaction is due to an internal field, i.e., iron metal.

If the effective field at the nucleus results solely from the application of an external magnetic field to the sample, the interaction is properly called the "nuclear Zeeman effect", and H_{eff} in

Eq. 9 is equal to H_{app}, the applied field. However, unpaired electron spin in the iron atom or its ligands results in an internal magnetic field, H_i, which interacts with the nuclear moment through the hyperfine term, $\underline{a}\tilde{I}\cdot\tilde{S}$.

It is well to keep in mind that the gross magnetic properties of a sample such as magnetic susceptibility do not always give rise to the same magnetic effects as measured by Mossbauer spectroscopy. For example, diamagnetism implies that electron spin-pairing is complete within the sample, thus the material has no residual magnetic moment in zero applied field. When a magnetic field is applied, the electrons respond by circulating around the applied field and a small, negative moment is thereby induced in the sample. Thus, for diamagnetic iron samples, one does not observe an internal magnetic field except when the "pseudo-nuclear Zeeman interaction" (Bleaney, 1967) is large enough to give rise to an internal field, which is induced by the application of an external magnetic field. In Chapter V, we shall illustrate the effect of this "pseudo-field" as it is present in the spectra of the oxidized plant-type ferredoxins.

In paramagnets, there is unpaired electron spin in the material. When a small magnetic field ($>$25 gauss, Johnson <u>et al</u>., 1968) is applied to this material, this unpaired electron spin becomes quantized along the direction of the applied magnetic field. If this quantized spin interacts with an ^{57}Fe nucleus through a hyperfine interaction, one could expect to see the effect by Mossbauer spectroscopy if, in addition, the effect is large enough. However, in order for the effect to be measurable by Mossbauer spectroscopy, the magnetic

field from the quantized spin must be present at the nucleus for a long time compared to the Larmor precession time of the nuclear excited state. If the electron spin states are relaxed faster than this Larmor precession time, the magnetic interaction will not be measurable by Mossbauer spectroscopy.

In ferromagnets, the internal magnetic field is present over long periods of time and also oriented with respect to the sample lattice. In this case, the magnetic interaction is always measurable by Mossbauer spectroscopy. When an external field is applied, the effect is to align the internal field with the applied field. If the applied field is coaxial with the gamma ray direction, its effect is exhibited in the Mossbauer spectra by a disappearance of the $\Delta m_I = 0$ transitions (Fig. 8). Although the applied field will be present at the nucleus in addition to the internal fields, the effect of the applied field on the energy of the nuclear states is usually negligible since applied fields are usually much smaller than internal fields (150 to 600 kGauss). In anti-ferromagnets, the spectra at zero applied field are identical to those of ferromagnets since an antiferromagnet consists of superimposed ferromagnetic lattices. Thus, if there is no quadrupole interaction, the Mossbauer spectrum of these materials has six lines of intensity 3:2:1:1:2:3. When a quadrupole interaction is present, the m_I nuclear states are mixed such that all eight lines (Fig. 8) are present in the spectrum. Kundig has written a computer program for these spectra and his paper (Kundig, 1966) contains spectra which span the parameter space for the Mossbauer Hamiltonian of ferromagnetic and antiferromagnetic compounds.

FIGURE 8. (A) EFFECT OF MAGNETIC FIELD ON NUCLEAR LEVELS.

(B) RESULTING MOSSBAUER SPECTRA FOR FERROMAGNETIC MATERIALS.

A

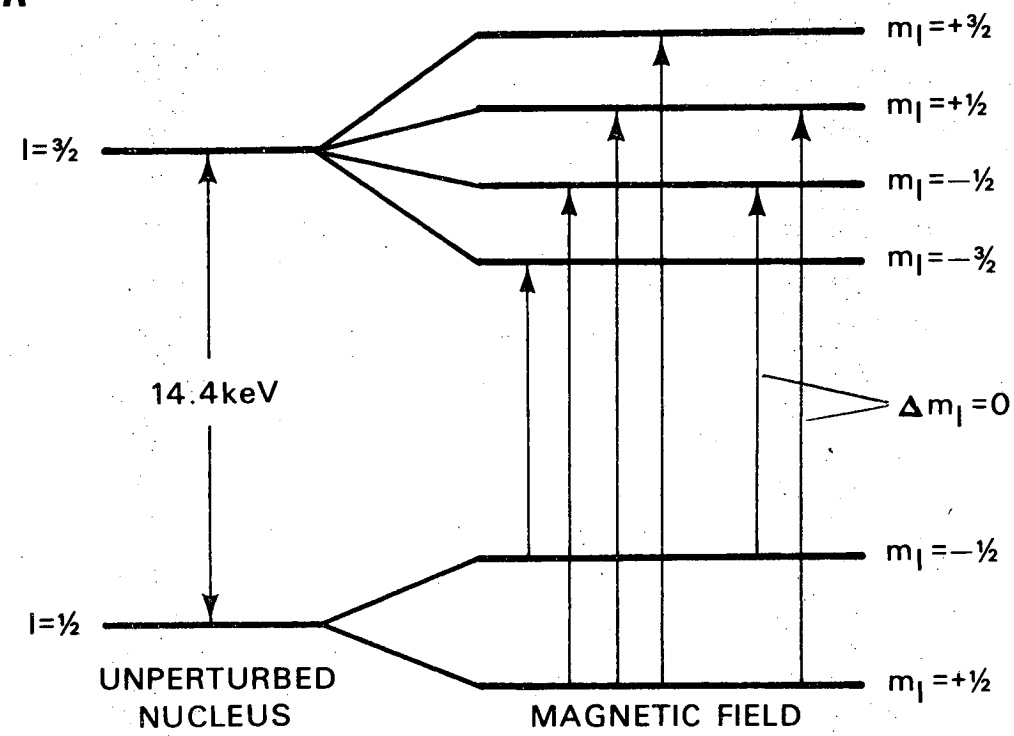

EFFECT OF MAGNETIC FIELD ON NUCLEAR LEVELS

B

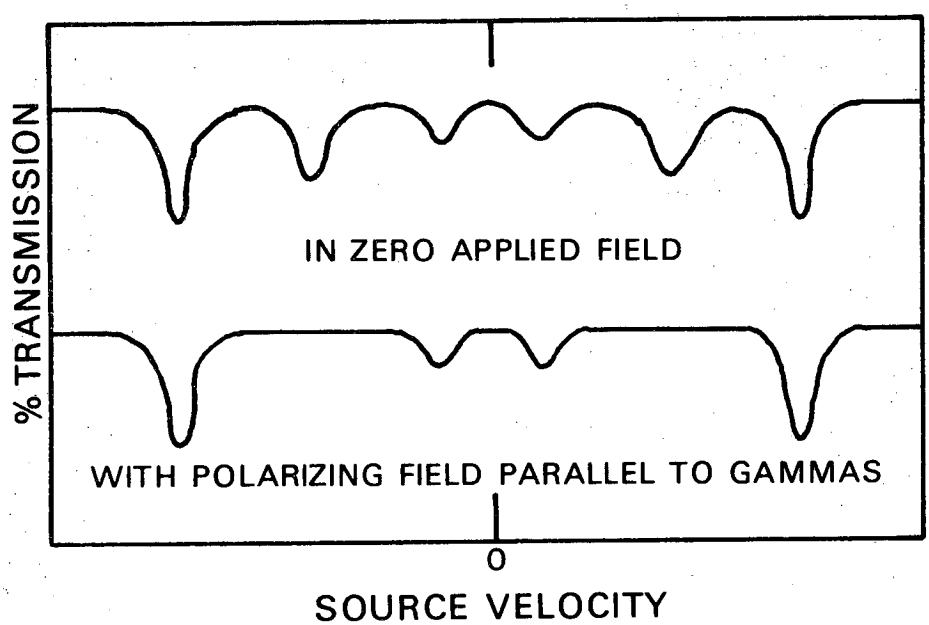

RESULTING MOSSBAUER SPECTRA (FERROMAGNETS)

A paramagnet at zero applied field deserves special attention for it is a case apart from the other magnetic materials. In the present discussion, it is assumed that the spin-relaxation times are infinite and that the hyperfine interaction is isotropic.

The Hamiltonian for the hyperfine interaction is:

$$\mathcal{H}_m = \underline{a}\,\tilde{I}\cdot\tilde{S} \tag{10}$$

where $\tilde{I}$ and $\tilde{S}$ are nuclear and electron spin vectors and $\underline{a}$ is the hyperfine coupling constant with the dimension of energy. Very often $\underline{a}$ is given in gauss through the following relationship:

$$\underline{a} = g_e \beta_e H \tag{11}$$

where g = 2.0023. β_e is the Bohr magneton, and H is the field in gauss. The reason for this convention stems from EPR measurements where the observed splitting in gauss from a hyperfine term is equal to $\underline{a}$ (Carrington and McLaughlin, p.15).

At zero applied magnetic field, $\tilde{I}$ and $\tilde{S}$ are coupled to form a resultant $\tilde{F}$. Rewriting the Hamiltonian in terms of this quantum number gives:

$$\mathcal{H}_m = \frac{a}{2}\left(F^2 - I^2 - S^2\right) \tag{12}$$

Assuming that $\underline{a}$ is negative and that S = 1/2, Fig. 9 shows the energy level scheme and resulting Mossbauer spectrum for this case. When a quadrupole interaction is present or when the hyperfine interaction is anisotropic, or both, a computer program is needed to generate the desired Mossbauer spectra. We have not written this program; thus, in Section V-D the zero applied magnetic field spectra for the reduced plant-type ferredoxins (paramagnets) are interpreted by comparison with the spectrum in Fig. 9.

FIGURE 9. (A) EFFECT OF MAGNETIC HYPERFINE INTERACTION ON NUCLEAR LEVELS.

(B) RESULTING MOSSBAUER SPECTRUM.

A

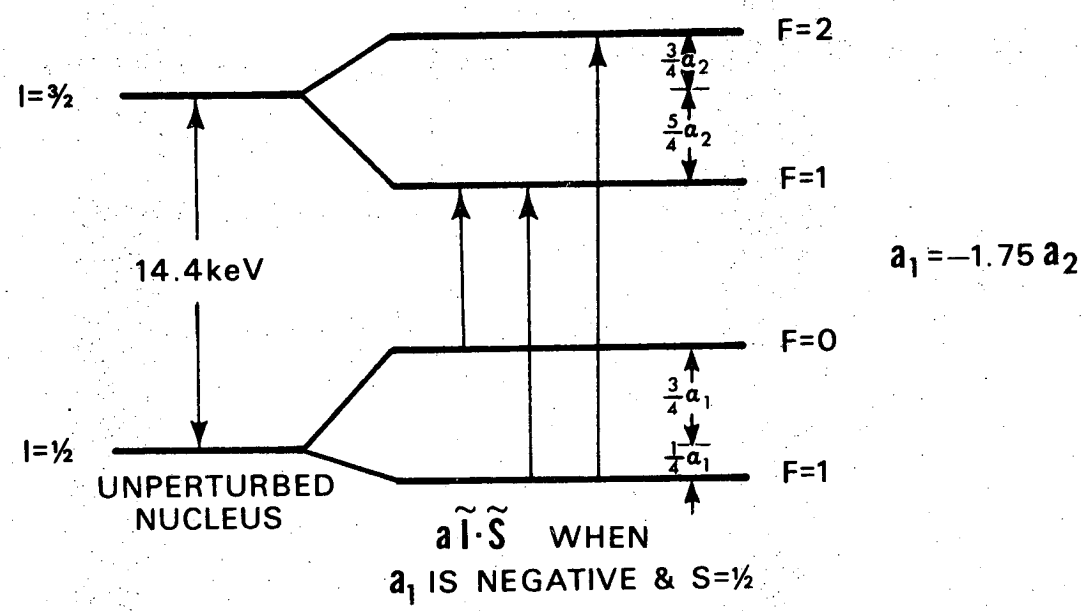

EFFECT OF MAGNETIC HYPERFINE INTERACTION ON NUCLEAR LEVELS

B

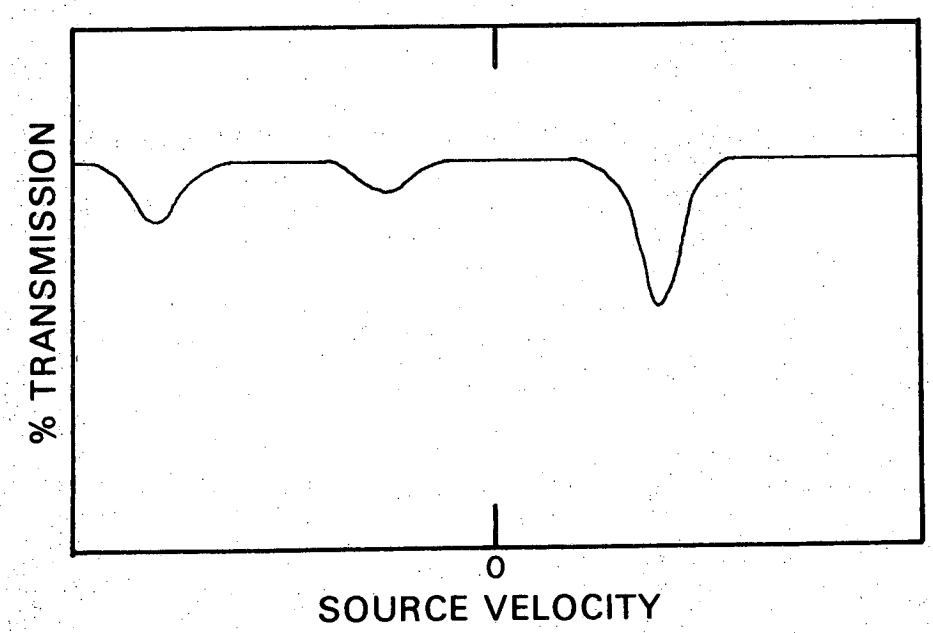

RESULTING MOSSBAUER SPECTRUM

When the applied magnetic field becomes greater than the hyperfine coupling constant in gauss, the coupling is destroyed and both nuclear and electron spins precess independently about the applied field. Since this is the case which is most pertinent to the study of plant-type ferredoxins, Section E will be devoted to a discussion of paramagnets in an applied field.

E. PARAMAGNETS IN APPLIED FIELD

Assuming that the $\tilde{A}$ and $\tilde{G}$ tensors are isotropic and that the applied field is along the Z-direction, the total Hamiltonian for paramagnets in applied field is:

$$\mathcal{H} = I.S. + \tilde{I}\cdot\tilde{\tilde{P}}\cdot\tilde{I} - g_N \beta_N H_z I_z + a \langle S_z \rangle I_z \tag{13}$$

where the first two terms are the isomer shift and quadrupole terms, the third term is nuclear Zeeman interaction and the last term is the hyperfine interaction. It is helpful to collect the last two terms in order that the effective field at the nucleus and the internal magnetic field can be defined. Thus:

$$\mathcal{H} = \cdots + \left[-g_N \beta_N H_z + a \langle S_z \rangle \right] I_z \tag{14}$$

For the electronic ground state $\langle S_z \rangle = -1/2$, therefore:

$$\mathcal{H} = \cdots + \left[-g_N \beta_N H_z - \frac{a}{2} \right] I_z = \cdots - g_N \beta_N H_{eff} I_z \tag{15}$$

If we now define the internal field, H_i, as:

$$H_i = a / 2 g_N \beta_N \tag{16}$$

the Hamiltonian becomes:

$$\mathcal{H} = I.S. + \tilde{I}\cdot\tilde{\tilde{P}}\cdot\tilde{I} - g_N\beta_N |H_a + H_i| I_z \tag{17}$$

Since a is usually given in gauss, the following expression is useful:

$$H_i\,(\text{gauss}) = \frac{g\beta H_a}{2 g_N \beta_N} = 1.0174 \cdot 10^4\ \underline{a}\ (\text{gauss}) \tag{18}$$

Note that in Eq. 17, if a is negative, the internal field opposes the applied field for the ground electronic state. Using H_{eff} as the magnetic field parameter, one can generate a family of curves for the different relative values of the quadrupole coupling constant and the effective field at the nucleus. Figure 7 shows this family of curves for powder samples in a magnetic field. Since the source of H_{eff} does not affect the spectra, Fig. 7 is also the same curves which would apply to diamagnetic powders in a magnetic field. When fitting these curves to experimental data it is well to keep in mind that the shapes of the spectra are changed little when the magnitude of the parameters QS and H_{eff} are varied while holding their ratio constant. We have found empirically that the energy interval from the lowest energy line to the highest energy line in a Mossbauer spectrum of this type can be fit by the following expression:

$$TS = 0.0288\ H_{eff} + 0.954\ QS \tag{19}$$

where TS is the total splitting in mm/S, H_{eff} is defined as before and given in kilogauss and QS is the observed quadrupole splitting given in mm/S.

All the computed spectra in this work were made under the assumption that the spin-relaxation times were infinitely long.

Wickman (1965) has treated the problem for the case when the relaxation times are in the order of the Larmor precession time of the nuclear paramgnet.

The number of variable parameters in the above spectra is essentially three: H_{eff}, QS and η. Isomer shift is usually not handled by the computer since its determination by sliding the computed spectra over the experimental data is more efficient. If the $\overset{\approx}{G}$ and $\overset{\approx}{A}$ tensors are allowed to be anisotropic, the situation becomes a great deal more complex. The total Hamiltonian in this case is:

$$\mathcal{H} = I.S. + \tilde{I}\cdot\overset{\approx}{P}\cdot\tilde{I} - g_N \beta_N H_z I_z + \widetilde{\langle S_{eff}\rangle}\cdot\overset{\approx}{A}\cdot\tilde{I} \qquad (20)$$

There are three second-rank tensors in this Hamiltonian: $\overset{\approx}{P}$, $\overset{\approx}{A}$ and $\overset{\approx}{G}$. The $\overset{\approx}{G}$ tensor is needed to compute $\langle S_{eff}\rangle$. Thus, there are nine Eulerian angles needed to specify the orientations of these tensors relative to the lattice coordinate system. These Euler angles are reduced to a single parameter in the following way: 1) the $\overset{\approx}{A}$ and $\overset{\approx}{G}$ tensors are assumed to be diagonal and coaxial (this assumption can lead to errors only if <u>both</u> $\overset{\approx}{A}$ and $\overset{\approx}{G}$ are anisotropic) 2) the coordinate system of these tensors is chosen to be identical with that of the lattice, and 3) it is found that the quadrupole tensor can be rotated through all its orientations by keeping QS constant and varying η from $-\infty$ to $+\infty$.

Thus, there are nine unknown parameters for a single iron environment material: I.S., QS, η, the three principal components of the $\overset{\approx}{G}$ tensor and the three principal components of the $\overset{\approx}{A}$ tensor. The data from other techniques, such as EPR and ENDOR, can further reduce the uncertainty in these parameters by giving the magnitudes of the

principle components of the $\tilde{\tilde{A}}$ and $\tilde{\tilde{G}}$ tensors. However, a computer program is essential if one expects to derive these parameters from experimental data. Appendix I contains this computer program, and a more detailed explanation of its calculation and parameters is the subject of Chapter IV. Since the spectra from this program are so varied as to defy organization, no "family of representative spectra" is here included. However, examples of the output of the program appear in Section V during the discussion of the low-temperature, reduced protein, Mossbauer data.

F. MAGNETIC HYPERFINE INTERACTIONS IN ^{57}Fe IONS

The magnetic hyperfine interaction is defined as the interaction between the nuclear magnetic moment and the resultant magnetic moment of the surrounding electrons:

$$\mathcal{H} = \tilde{I} \cdot \tilde{\tilde{A}} \cdot \tilde{S} \tag{21}$$

where $\tilde{\tilde{A}}$ is the hyperfine tensor. We shall assume that this tensor has been diagonalized by a suitable choice of coordinate system relative to coordinate system of the crystal field which surrounds the ion. The ground nuclear state of ^{57}Fe has a magnetic moment of 0.1806 nuclear magnetons (Locher and Geschwind, 1965), with I = 1/2. The electronic spin is assumed to result from unpaired d-electron density. Consider first the interaction of a single 3d electron with the nuclear magnetic moment.

In the Fermi contact interaction, unpaired d-electron density results in a non-zero, s-electron spin density at the nucleus which gives rise to the hyperfine interaction. The process by which the

d-electrons cause a non-zero, spin at the nucleus is called "core polarization" (Watson and Freeman, 1967) and arises in the following manner. In the ferric ion, for example, the 3d electron density, as determined from Hartree-Fock wavefunctions, is such that the expectation value of the position of the 3d electrons, $\langle r_{3d} \rangle$, is greater than that of the 2s electrons, but less than that of the 3s electrons, but less than that of the 3s electrons. For any pair of s-electrons, the overlap of the d and s-orbitals causes an exchange interaction with the electron spin which is not equivalent for the "spin up and "spin down" s-electrons. The result of this exchange interaction is that s-electrons with spin anti-parallel to that of the d-electrons are more strongly repelled by the d-electrons than are s-electrons with spin parallel. Thus in the ferric ion, core polarization results in a negative spin density at the nucleus from 1s and 2s electrons, while the spin density at the nucleus from 3s electron is positive, i.e., parallel to d-electron spin. Watson and Freeman (1961) have calculated the contact term and the internal fields for ferric and ferrous ions using a Hartree-Fock formalism which allows exchange polarization. Their values are shown below in Table 3.

TABLE 3

CALCULATED CONTACT TERMS
(Watson & Freeman, 1961)

	Fe^{+++}	Fe^{++}
X (a.u.)	-3.00	-3.29
1-s contribution to X	-0.25	-0.21
2-s contribution to X	-8.51	-7.80
3-s contribution to X	+5.77	+4.72
H_i (kOe)	-630	-550

Note that in both cases shown above, the effective moment at the nucleus opposes the magnetic moment of the d-electron density.

The orbital moment, L, of the d-electrons can also interact with the nuclear magnetic moment. In iron compounds, however, the orbital angular momentum of the d-electrons is "quenched" by the crystal field of the surrounding ligands (Hecht, 1967). Here we shall consider the d-electrons as occupying the crystal field set of d-orbitals, d_{xy}, d_{xz}, d_{yz}, d_z2 and $d_x2_{-y}2$, for which the expectation value of angular momentum is zero. Within this approximation the hyperfine interaction involving orbital spin is zero. Also, the Fermi contact interaction results solely from the interaction with the intrinsic spin of the d-electrons. When spin orbit coupling mixes the d-electron wave functions, this orbital term does not vanish, although its effect on the hyperfine tensor is usually small.

The final term in the hyperfine interaction is the magnetic dipole term between the d-electron spin and the nuclear spin.

Griffith (1961, p.325) has constructed an operator for this interaction by the method of operator equivalents. The following expression includes this operator as well as the contact and orbital terms for a single d-electron.

$$\mathcal{H} = 2 g_N \beta_N \beta \langle r^{-3} \rangle \left\{ \tilde{\ell} \cdot \tilde{I} + \tfrac{1}{7} \left[4 \tilde{s} \cdot \tilde{I} - (\tilde{\ell} \cdot \tilde{s})(\tilde{\ell} \cdot \tilde{I}) - (\tilde{\ell} \cdot \tilde{I})(\tilde{\ell} \cdot \tilde{s}) \right] - \kappa \tilde{s} \cdot \tilde{I} \right\} \tag{22}$$

where κ is a scaling constant for the contact interaction and $\langle r^{-3} \rangle$ refers to the 3d radial wave functions of the particular atom of interest.

Within a term ^{2S+1}L, the above operator is written as the following for a system with n d-electrons:

$$\mathcal{H} = P \left(\tilde{L} \cdot \tilde{I} - \kappa \tilde{S} \cdot \tilde{I} + \tfrac{1}{7} \sum_{k=1}^{n} \tilde{a}_k \cdot \tilde{I} \right) \tag{23}$$

where $\tilde{a}_k = 4 \tilde{s}_k - (\tilde{\ell}_k \cdot \tilde{s}_k) \tilde{\ell}_k - \tilde{\ell}_k (\tilde{\ell}_k \cdot \tilde{s}_k)$ AND $P = 2 g_N \beta_N \beta \langle r^{-3} \rangle$

In the following table, the matrix elements for the hyperfine interaction in Eq. 22 are tabulated for single d-electron configurations.

TABLE 4

MATRIX ELEMENTS FOR THE MAGNETIC HYPERFINE INTERACTION
(In Multiples of P)

Orbital	A_x	A_y	A_z
$d_{x^2-y^2}$	$2/7-\kappa$	$2/7-\kappa$	$-4/7-\kappa$
d_{z^2}	$-2/7-\kappa$	$-2/7-\kappa$	$4/7-\kappa$
d_{xz}	$2/7-\kappa$	$-4/7-\kappa$	$2/7-\kappa$
d_{yz}	$-4/7-\kappa$	$2/7-\kappa$	$2/7-\kappa$
d_{xz}	$2/7-\kappa$	$2/7-\kappa$	$-4/7-\kappa$

To calculate the hyperfine interaction for a particular ion, then, one constructs the wavefunction for the electron spin from the sum of d-orbitals and chooses the proper values from Table 4 to form the components of the hyperfine tensor. In order for this table to be useful, however, it is necessary to choose a value for the parameters, P and κ. Lang and Oosterhuis (1969) quote a value of κ, 0.35, from their calculations on the spin=1/2 iron compounds. The parameter, P, can be calibrated by assuming the following rule of thumb: the internal magnetic field resulting from the contact interaction in iron compounds of approximately 110 kOe per unpaired electron in the iron atom (Wickman, 1965).

With the above assumptions for the values of P and κ one can calculate a hyperfine constant for iron compounds for which the term, ^{2S+1}L, is known. Conversely, one can use the Mossbauer data on a particular compound to choose between the terms available to that compound. In this case any knowledge of the iron ligands is valuable. For example, if the iron ligands are expected to give rise to a high-spin situation in iron atom, then inspection of Table 4 reveals that the ferric state will give rise to an isotropic $\tilde{A}$ tensor which is the sum of contact terms only. Any knowledge of the symmetry and strength of the ligand field will give information on the probability of spin-orbit coupling, which can be the determining factor in the calculation of hyperfine fields. This is the case in low-spin, ferric compounds in octahedral symmetry (Wickman, 1965).

When Mossbauer spectra is available on two or more oxidation states of a compound, the calculation of the hyperfine fields must

correlate with the changes observed in isomer shift and quadrupole splitting. Information on the degree of covalency and s and p orbital mixing into d-orbitals is available in these correlations since $\langle r^{-3} \rangle$ is a parameter common to all three perturbations.

G. EXCHANGE COUPLING

As mentioned in Section II-F, exchange interactions arise from the combined effects of coulombic interaction and the Pauli exclusion principle. For the interaction of two electronic systems with spin, S_1 and S_2, we write the operator for this interaction as:

$$\mathcal{H} = -2J\tilde{S}_1 \cdot \tilde{S}_2 \tag{24}$$

where $\tilde{S}_1$ and $\tilde{S}_2$ are the spin vectors and J is the exchange-coupling constant. J was originally defined as the Heisenberg exchange integral, which is always positive. This type of interaction is called "direct exchange" and results in ferromagnetism. It was found, however, that this formulation for the exchange-coupling constant is seldom applicable to problems concerning exchange coupling and that a more complicated integral was needed to explain the coupling of most spin systems (Anderson, 1963). Here we shall treat the constant, J, as an experimental parameter and discuss the different types of mechanisms which give rise to exchange coupling.

"Superexchange" is spin coupling of systems through bridging atoms and most often results in J being negative; thus, antiferromagnetic coupling. When the spin-coupling mechanism is seen as a resonance between non-equivalent ionic spin systems the interaction is termed "double exchange" (Zener, 1951). This formalism does not

imply, however, that spin coupling through bridging atoms always results in negative values of J, and that without the bridging atom, the coupling always gives rise to ferromagnetism. For example, most chemical bonds result in spin pairing: an indication that the "direct exchange" formalism of Heisenberg does not explain most exchange interactions!

In the following, we shall restrict ourselves to exchange interactions which give rise to anti-ferromagnetic coupling (negative values of J). In this case, the spin systems (S_1 and S_2) are coupled to form a resultant, S. We write the Hamiltonian (Anderson, 1963) as:

$$\mathcal{H}_E = -J(S^2 - S_1^2 - S_2^2) \tag{25}$$

where $(S_1+S_2) \geq S \geq |S_1-S_2|$. Consider specifically the cases in which 1) $S_1 = 5/2$ is coupled to $S_2 = 5/2$, and 2) $S_1 = 5/2$ is coupled to $S_2 = 2$. If J is negative, one obtains the following energy level schemes for these interactions.

FIGURE 10

ENERGY LEVEL SCHEMES FOR EXCHANGE-COUPLED SYSTEMS
[$J_i < 0$]

System 1		System 2	
$S_1 = 5/2$, $S_2 = 5/2$		$S_1 = 5/2$, $S_2 = 2$	
$S = 5$	$-12.5J_1$	$S = 9/2$	$-10J_2$
$S = 4$	$-2.5J_1$	$S = 7/2$	$-1J_2$
$S = 3$	$5.5J_1$	$S = 5/2$	$6J_2$
$S = 2$	$11.5J_1$	$S = 3/2$	$11J_2$
$S = 1$	$15.5J_1$	$S = 1/2$	$14J_2$
$S = 0$	$17.5J_1$		

At low enough temperatures, System 1 in Fig. 10 is diamagnetic (spin = 0) and System 2 has spin = 1/2. As the temperature is increased, population of excited states in the above systems will increase the magnetic susceptibilities of these systems above what would be expected for non-coupled systems. Thus, System 2 is expected for non-coupled systems. Thus, System 2 is expected to have a higher susceptibility at high temperatures than would be predicted by Curie-law behavior of a paramagnetic, spin = 1/2 material. In the above discussion, zero field splittings (Owen, 1961) have been ignored. We note that this approximation is valid only if J is much larger than the spin-orbit interaction. This assumption is valid for the plant-type ferredoxins with the exceptions cited in Section V-E. The

properties of the above spin systems will be expanded in Section V-E as they are important in the explanation of the model for the active site of the plant-type ferredoxins.

III. EXPERIMENTAL PROCEDURE

A. THE MOSSBAUER SPECTROMETER

There are three basic components to a Mossbauer spectrometer: 1) the source velocity-drive system 2) the sample and its associated dewar system for temperature variation, and 3) the gamma ray detection apparatus (Fig. 11). Since these spectrometers are usually constructed by the experimenter, their design reflects greatly the type of experiment for which they are planned. For example, if ^{57}Fe is the isotope to be studied, the technology surround the detection of 14.41 keV gamma rays has established that the use of proportional gas counters is recommended because of their efficiency, adaptability, cost, and durability. The electronics between the gas counter and the data-display device is also the product of a well-developed technology, so that the experimenter need merely choose between the many commercially available sources for these components. However, the dewar system and the source velocity-drive system are unique to Mossbauer spectroscopy; thus the experimenter must rely more on his own experience in designing and building these components.

In this design problem, the most significant choice to be made is the type of source velocity-drive system. Mossbauer data consists of gamma ray counts versus source velocity. Since the velocity scan is divided into increments, one must decide whether to collect the counts at the velocity increments simultaneously or sequentially. In other words, he must choose between 1) a drive system which scans the velocity scale over a short period of time

FIGURE 11. BLOCK DIAGRAM OF MOSSBAUER SPECTROMETER.

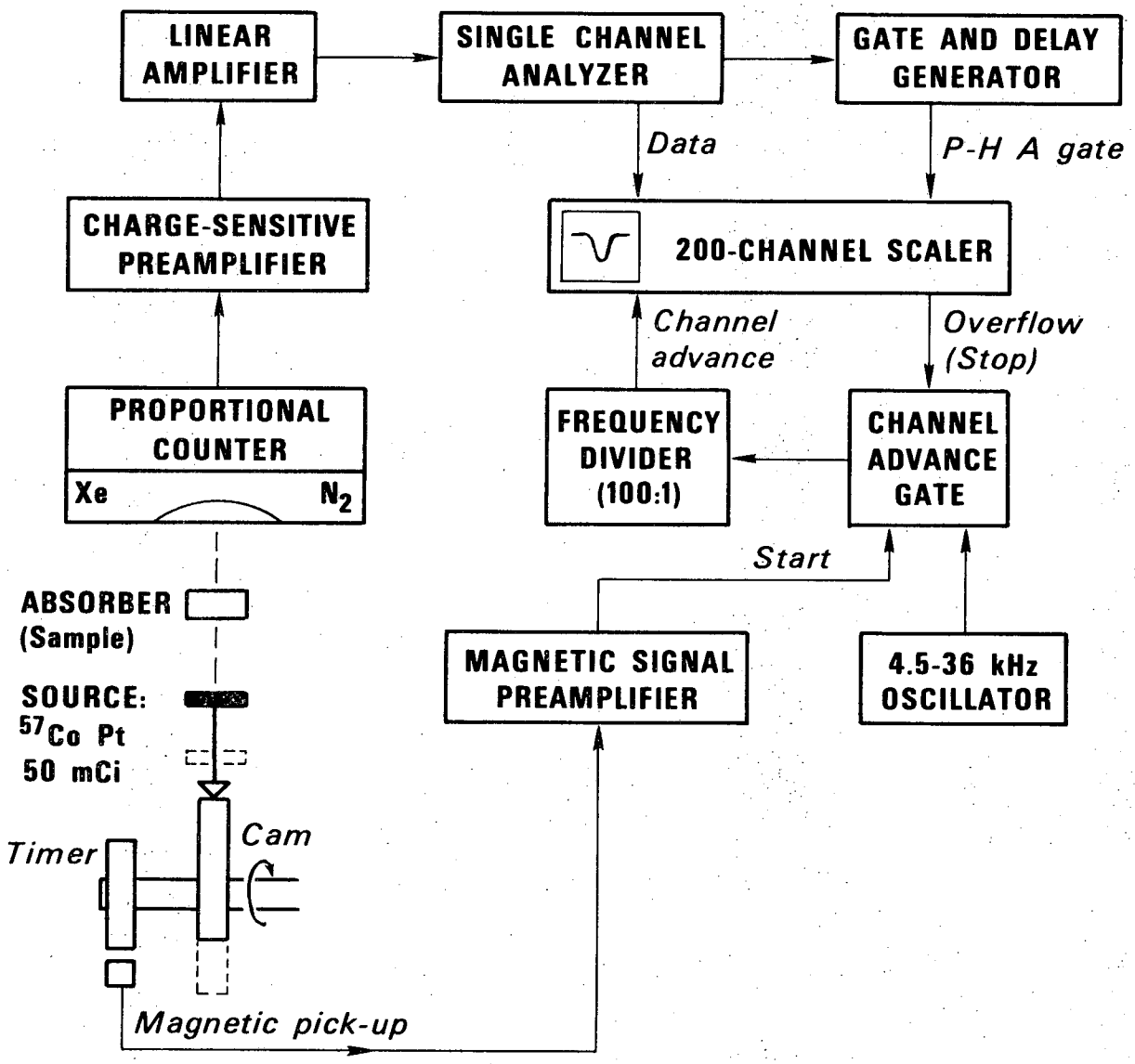
LINEAR AMPLIFIER
SINGLE CHANNEL ANALYZER
GATE AND DELAY GENERATOR
Data
P-H A gate
CHARGE-SENSITIVE PREAMPLIFIER
200-CHANNEL SCALER
Channel advance
Overflow (Stop)
PROPORTIONAL COUNTER
Xe
N2
FREQUENCY DIVIDER (100:1)
CHANNEL ADVANCE GATE
Start
ABSORBER (Sample)
SOURCE: 57Co Pt 50 mCi
MAGNETIC SIGNAL PREAMPLIFIER
4.5-36 kHz OSCILLATOR
Timer
Cam
Magnetic pick-up

(constant acceleration) and then rescans until the desired counts per channel are acquired, or 2) a drive system which maintains a constant velocity over a long period of time thus collecting the data in a single velocity scan. If a constant velocity-drive system is chosen, then one must decide between a mechanical drive (cam) or an electromagnetic drive (loudspeaker) system. The choice of drive system seems to be quite subjective as it is the subject of a continuing debate between experimenters. The constant-acceleration cam driven system used in this research is quite adequate for ^{57}Fe Mossbauer studies; however, the reader is referred to the work, Mossbauer Effect Methodology (Gruverman, 1965-70), for a review of the different types of spectrometer design.

The constant-acceleration, cam drive system has been described by Bearden et al. (1965). The cam consists of a cylinder of radius, s, whose axis of rotation is displaced by an amount, a (Fig. 12). The cam rider is a small cylinder of radius, b. It was found that for 50 degrees in both directions from bottom dead center on the cam, the motion of the cam rider is very close to linear in velocity when the cam is rotated with a constant angular velocity (Moss, 1965). The velocity of the source (cam rider) at some time t, where t = 0 correspond to the cam rider's being at bottom dead center, is given by the following expression where ω is the angular velocity of the cam:

$$V(t) = a\omega \sin\omega t \left\{ 1 - a\cos\omega t / \left[(b+s)^2 - a^2 \sin^2 \omega t \right]^{1/2} \right\} \qquad (26)$$

For the cam used in this research: a = 0.1272 in., s = 0.4922 in., b = 0.003 in. One of the advantages of the cam is that there is little uncertainty in the velocity at a particular

FIGURE 12. (A) ONE-LOBE CAM DIAGRAM. In this diagram, rotary motion of the offset cylinder results in vertical motion of the cam rider which, in turn, moves the source. (Three times actual size.)

(B) THREE-LOBED CAM WITH TIMING WHEEL. The slots in the timing wheel trigger a magnetic pick-up which generates the starting pulse for the channel advance in the analyzer (Fig. 11). The cam consists of three identical cylindrical surfaces as shown in (A) with bottom dead centers (BDC) spaced at 120° intervals. The analyzer operates during the 50° arc on either side of BDC for each lobe. (Drawing in actual size.)

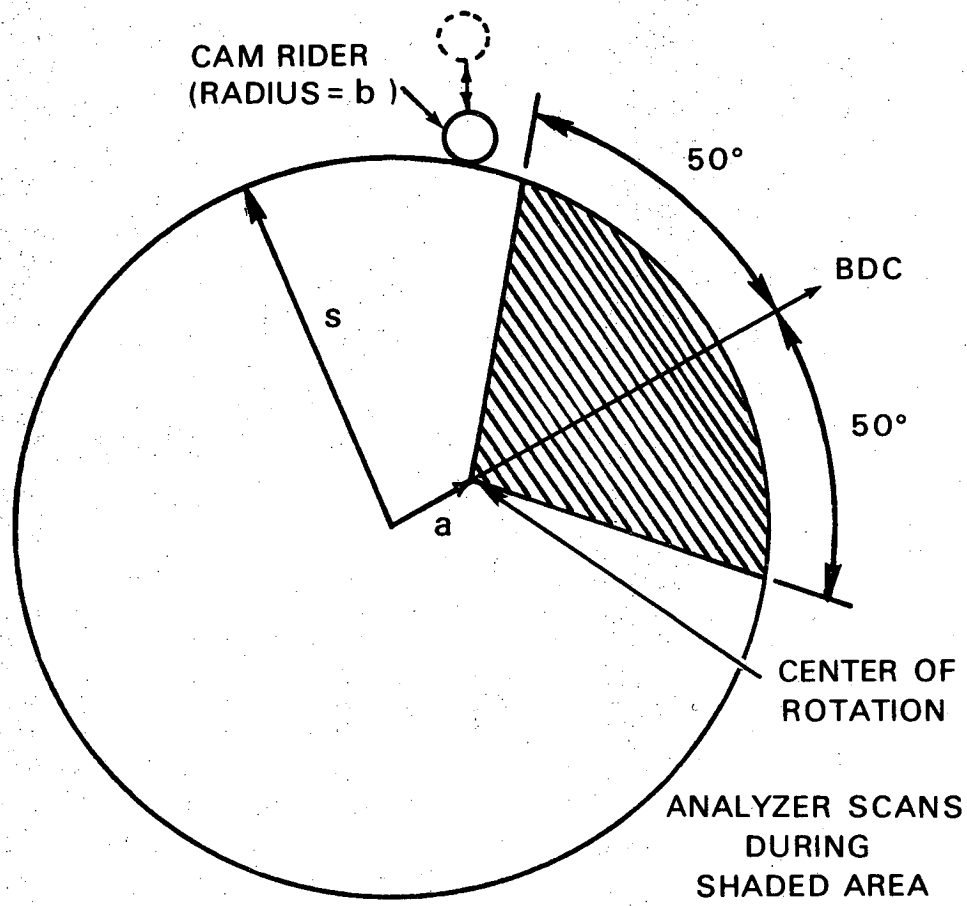

1-LOBE CAM

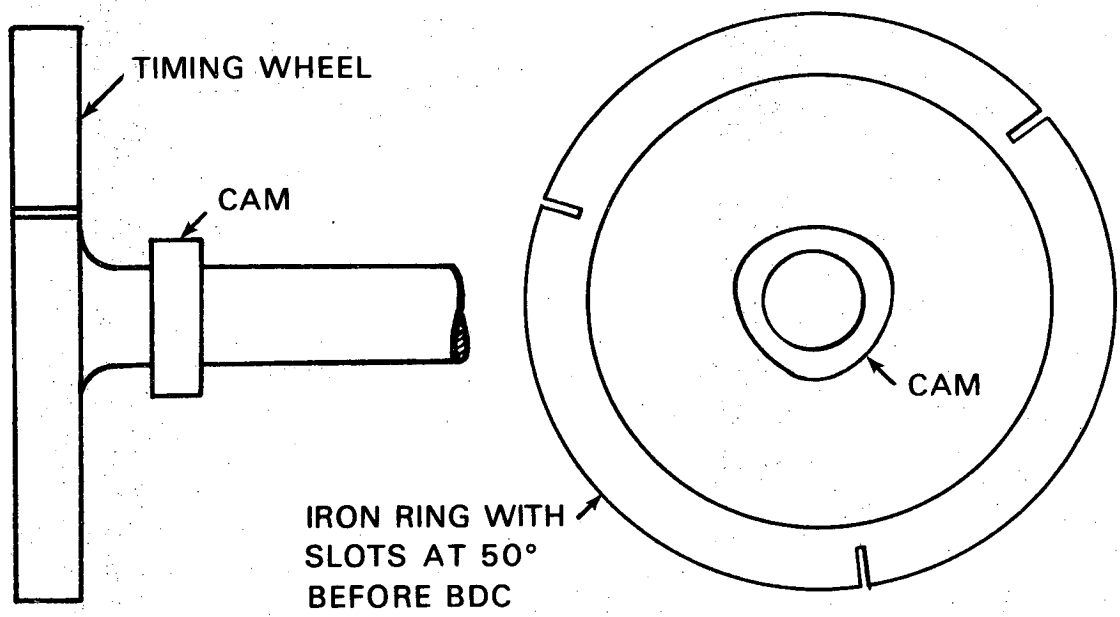

3-LOBED CAM AND TIMING WHEEL

channel if the above parameters are known to better than .001". However, a disadvantage of the cam as shown is that only 100° of the 360° in a cam rotation can be used for collecting data. This fault has been corrected by grinding three lobes on the cam as shown in Fig. 12. Thus the duty cycle for the cam is increased to 83 per cent. Cam wear is not a problem in this case as it was recently measured to be less than 0.0002 in. over three years usage. From this and other checks made on the spectrometer it is found that for any one channel in the data here presented, the absolute velocity is correct to less than half the width of a channel. Thus, isomer shift and quadrupole splittings here measured are correct to 0.2 per cent of the total velocity-scan range of the spectrum from which they are measured, as these spectra are all taken over a 200 channel scan.

The dewar system on this spectrometer is, however, its most impressive component. Figure 13 illustrates the dewar in cross section with the caption to this figure explaining the most important aspects of its construction. Since the magnetic field within the sample chamber is provided via a superconducting solenoid (Westinghouse, Model #3-3225), it is necessary to maintain the liquid helium level above the top of the solenoid whenever the spectra are taken with applied magnetic field. The liquid nitrogen jacket is necessary to thermally insulate the liquid helium dewar. The thermal properties of this dewar are reflected in its liquid helium consumption rate, which is at a maximum when the solenoid operates at its highest field and when the sample temperature is lowest. With the solenoid operating at 46 kilogauss (20A magnet current) and with the sample

FIGURE 13. DEWAR ASSEMBLY FOR MOSSBAUER SPECTROMETER. The dewar assembly is constructed of stainless steel with the following exceptions: 1) at the bottom of the liquid N_2 dewar is a copper heat shield with an aluminum window 2) the wall of the sample chamber is copper to height just above the top of the solenoid 3) the solenoid leads are three feet of coiled, #18 copper wire (times three) and 4) the windows between the vacuum areas and the liquid helium chamber are 0.010" Mylar. Samples are removed through the bottom of the inner dewar assembly with all joints made with indium compression seals.

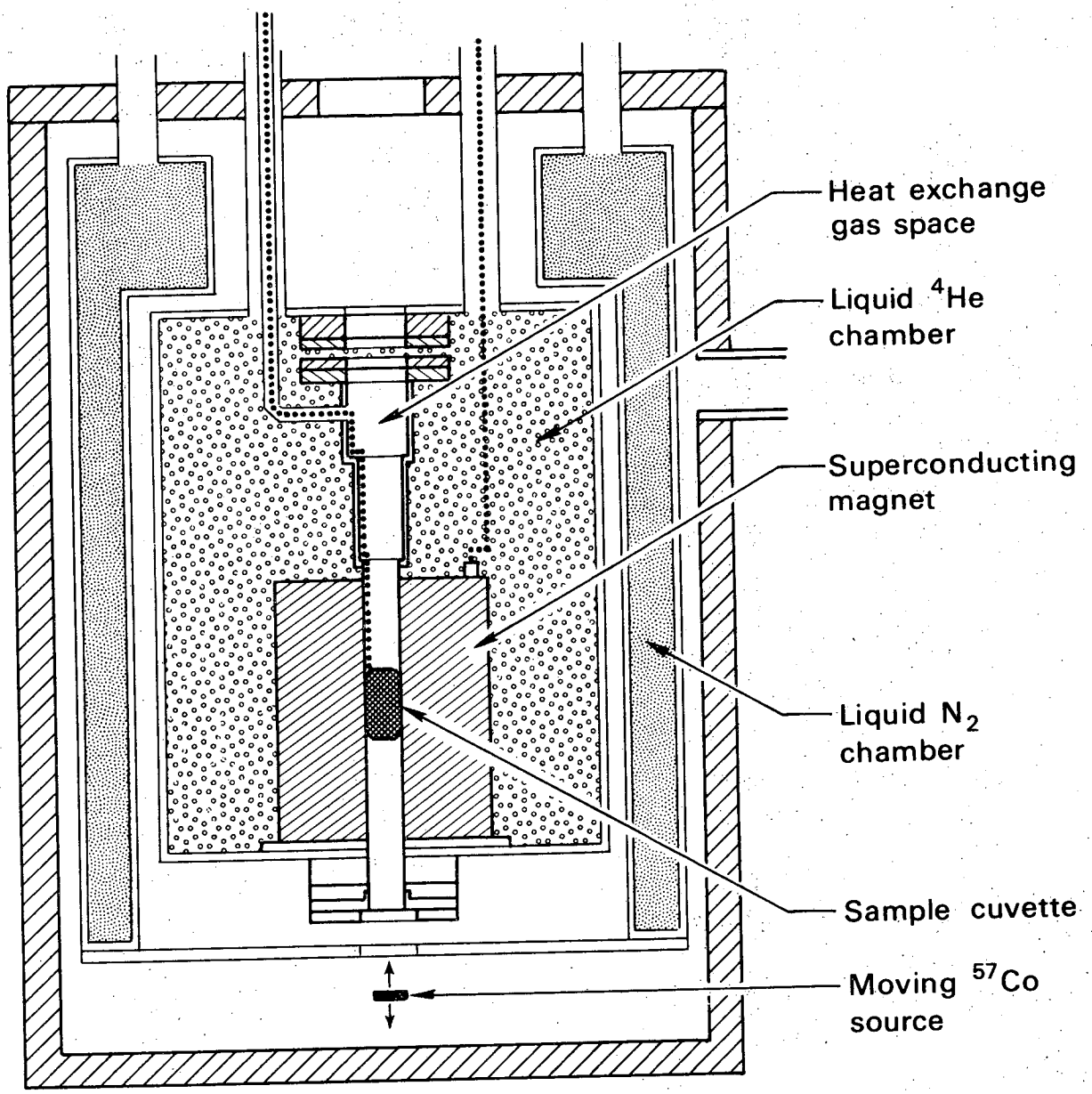
Heat exchange gas space
Liquid ^{4}He chamber
Superconducting magnet
Liquid N_2 chamber
Sample cuvette
Moving ^{57}Co source

temperature at 4.2°K, the liquid helium consumption rate is about one liter per hour. Raising the sample temperature or decreasing the field lowered the helium consumption rate to around 1/4 liter per hour at a minimum. Whenever liquid helium was used in this apparatus, the dewar vacuum was maintained at 10^{-7} torr by means of a two-inch, oil diffusion pump with the dewar itself acting as the cold trap.

The sample temperature was maintained in two ways: 1) the pressure of helium gas in the sample chamber (Fig. 13) was vaired to control thermal contact between the sample cuvette and the walls of the sample chamber which were held at 4.2°K and 2) the current through a constantan wire heater coil around the sample cuvette was varied to provide a fast response heat input directly to the sample (Fig. 14). The temperature was monitored and controlled electronically via a carbon resistor and a copper-constantan thermocouple, both mounted in the sample cuvette. Thermal equilibrium within the cuvette was insured by a helium gas pressure within the sample cuvette of one atmosphere (298°K).

Carbon resistors (unmodified Allen-Bradley Type TR 1/10W, 1500 ohm at 25°C) were calibrated at 25°C and 4.2°K; the resistance at 4.2°K rising to about 112 kohms with a variation from resistor to resistor of ±2 kohms. Once calibrated, a resistor held its 4.2°K resistance value within ±1 kohm. The temperature of the cuvette was determined by use of an empirical relation between T and R (Keesom and Pearlman, 1956); namely,

$$\left(\frac{\log R}{T}\right)^{1/2} = a + b \log R \tag{27}$$

FIGURE 14. SAMPLE CUVETTE.

SAMPLE CUVETTE

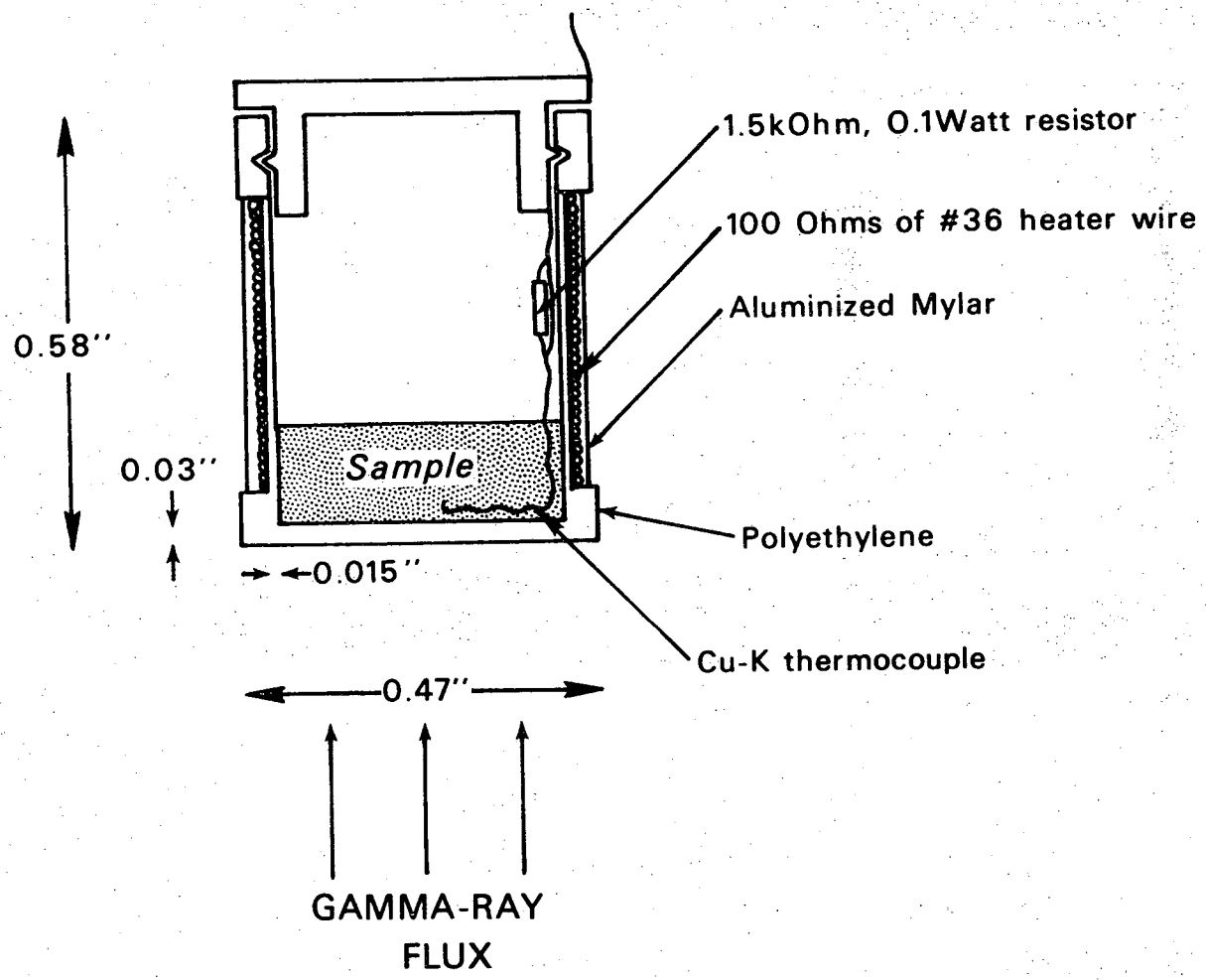

The function was tabulated by digital computation for 1°K intervals between 300°K and 10°K and 0.1°K intervals between 10°K and 4.2°K. Each cuvette was fitted with a resistor and the temperature resistors were checked before and after each set of runs. The effect of applied magnetic field on these resistors (Neuringer and Shapira, 1969) is so small that we can neglect the value of the applied field when making the temperature measurements.

The carbon resistor was used to monitor temperatures between 4.2°K and 100°K (at the low end of this range, temperatures are easily maintained and monitored to an accuracy of 0.1°K). From 30°K to 300°K the copper-constantan thermocouple allowed temperature control to an accuracy of 2°K. The details of the design of the sample cuvette and the placement of the thermocouple and resistor are shown in Fig. 14.

There are two possible modes for operation of a superconducting solenoid; a mode in which the superconducting current travels within a loop all below the critical temperature of the superconductor, and a mode in which the current is supplied continuously from an external power supply at room temperature. The first mode can be activated by the proper incorporation of a "heat switch" in the superconducting circuit and has the advantage of no wires running from room temperature to liquid helium temperature during the operation of the solenoid. A disadvantage is that monitoring of the current and the magnetic field produced by the solenoid is more difficult. In these experiments in which it is desired to know the magnetic field intensity to one-half per cent; it has become more favorable to design ohmic leads of

low heat conduction so that the continuously monitored current system can be used. This has been done by providing spiral leads, first three AWG #14 Cu conductors, and then in the He chamber fill tubes, three strand spirals of AWG #18 Cu conductors. The essential feature of this design is that the He boiloff produced by other heat leaks to the dewar cool the current leads in the fill tubes, thus lowering the resistance and reducing the ohmic heating and leaving a large temperature differential between the upper part of the current leads and the terminals at the top of the dewar vessel. This system has worked in such a fashion that there is very little increase in the boiloff rate with the magnet at full current.

The most outstanding characteristic of this system is that it is possible to take Mossbauer spectra with the superconducting solenoid operating at 46 kG (20A), while maintaining the sample temperature as high as 300°K. As will be shown in Chapter V, it was the spectra taken under these extreme conditions which allowed a successful interpretation of the low-temperature spectra for the reduced proteins.

B. PREPARATION OF BIOLOGICAL SAMPLES FOR MOSSBAUER SPECTROSCOPY

In general, Mossbauer samples are best when the ratio of ^{57}Fe atoms to all other atoms in the sample is at a maximum. However, special problems of aqueous protein solutions complicate this rule in protein studies. To illustrate this point, let us consider the types of radiation present in an ^{57}Fe Mossbauer spectrometer and their interactions with the material in the beam path.

The beam consists of three types of radiation: 1) electrons from Compton scattering processes, internal conversion of the gamma rays, and photoelectric effects 2) the resonant 14 keV gamma rays, and 3) the other gamma rays from the source and x-rays resulting from internal conversion and inelastic scattering processes of the gamma rays. Any count at the detector which is not from a 14 keV gamma ray is unwanted, background noise. Spectrometer design can reduce or eliminate the effect on the counter of all of these types of radiation. Thus, electrons are absorbed in the windows of the dewar and x-ray radiation is reduced by aluminum shields in the beam path. The photons counted at the detector are discriminated electronically to choose the 14 keV radiation. These precautions having been taken, it is still necessary to keep the number of 14 keV gamma rays reaching the detector at a maximum. That is, any material in the beam path other than ^{57}Fe nuclei decreases the rate at which Mossbauer effect information is collected by attenuating the 14 keV gamma rays via inelastic scattering processes. Since the inelastic cross section for atoms is proportional to Z^2, heavy atoms are to be especially avoided. In aqueous protein solutions, the chief offenders in this regard are sodium and chloride ions and the water molecules themselves. For this reason, lyophilyzed samples, with organic buffers such as tris(hydroxymethyl)amino methane, are most desirable.

C. IMPURITY SIGNALS

If an absorption occurs in a Mossbauer spectrum, the experimenter is assured that this absorption results from resonance

with an ^{57}Fe nucleus. Thus, with regard to impurities, the experimenter need only concern himself with ^{57}Fe nuclei which are not in the specific environment under study. In the study of the plant-type ferredoxins these impurities are of three types: 1) free-iron complexes in the solution 2) iron bound by denatured protein, and 3) iron bound by active protein which is not in the oxidation state under study. The amount of any of these impurities is a function of the handling of the protein. Remembering that it was necessary to reconstitute these proteins with ^{57}Fe, one is certain that impurities of type 1) and 2) were at one time present in the protein solution. It is found, however, that gel filtration can reduce these types of impurity to a nondetectable level. Further denaturation is held to a minimum by storing the samples at liquid nitrogen temperatures. The reduction of impurities of type 3) is also gained through experience in the handling of the proteins. By comparing the integrated intensity of the computed and experimental Mossbauer spectra, the absorption due to impurity in this study was found to be a maximum of 2 per cent of the total absorption in the oxidized proteins at low temperatures. In Fig. 16 the spectra for spinach and parsley ferredoxin contain this maximum impurity signal as a quadrupole pair (IS = -0.2 mm/S, QS = $\pm$0.5 mm/S). A quadrupole pair of this type would be expected for ferric iron in tris buffered solutions; therefore, the impurity signal for the oxidized is of type 1) or 2). For the reduced proteins, this maximum rose to 5 per cent, half of which was due to incomplete reduction of the proteins. Since different iron environments have different Debye temperatures, it was possible in some cases to

identify impurity signals by observing the temperature dependence of their recoil-free fractions. In other cases, impurity signals were identified by measuring differences in Mossbauer spectra which were taken under identical conditions on different preparations of the same protein.

D. MATERIALS AND METHODS

The ^{57}Fe exchanged Azotobacter vinelandii proteins, adrenodoxin, and C. pasteurianum paramagnetic protein samples were provided by Dr. W.H. Orme-Johnson and Prof. H. Beinert (Madison, Wisconsin) according to procedures set forth in previous papers (Orme-Johnson and Beinert, 1969; Shethna et al., 1966, 1968). ^{57}Fe exchanged putidaredoxin was provided by Dr. J.C.M. Tsibris and Prof. I.C. Gunsalus (Cushman et al., 1967; Tsibris et al., 1968). ^{57}Fe exchanged parsley ferredoxin was provided by Dr. G. Palmer (Ann Arbor, Michigan) according to unpublished preparative methods which are modifications of methods in the literature (Keresztes-Nagy and Margoliash, 1966; Hong and Rabinowitz, 1967). All the above protein samples were 2 to 6 mMolar aqueous solutions (pH 7.5-8.3) buffered anaerobically with 0.1M tris(hydroxyamino) methane. Comparison of spectra taken on different preparations of the same protein show that varying the concentration, even through lyophilization, has no effect on the shape of the resulting Mossbauer spectra.

^{57}Fe-exchanged spinach ferredoxin samples were provided by both the Ann Arbor and Madison groups. The spinach ferredoxin samples from Madison resulted from purification procedures which involved acetone (Tagawa and Arnon, 1962) or acetone-free preparations

(Keresztes-Nagy and Margoliash, 1966). The spinach ferredoxin samples from Ann Arbor were all acetone-free, but resulted from exchange procedures involving either mercurial or trichloroacetic acid, protein denaturations (Hong and Rabinowitz, 1967). Also, spinach ferredoxin samples of varying salt (tris-NaCl) concentrations were provided by Dr. G. Palmer and Dr. I. Salmeen.

For all the spinach ferredoxin samples, the resulting Mossbauer spectra were found not to be a function of sample preparation, with the exception of small absorptions at -1 mm/S and +1 mm/S. These absorptions were attributed, therefore, to impurity signals (Section III-C). Reduced adrenodoxin and reduced spinach ferredoxin samples were run as either frozen aqueous solutions or as lyophilized material. The resulting Mossbauer spectra show no change for the lyophilized samples other than a general increase in per cent absorption (Section III-B).

For each protein, reduction was effected by addition of solid dithionite to the aqueous solution of the oxidized protein. In the case of adrenodoxin, methyl viologen was also added to the extent of one mole per cent in protein. Since during the reducing procedures, it was necessary to thaw the protein solutions, these procedures must have been performed with extreme care in order to circumvent possible denaturation of the proteins. Accordingly, the following procedure was used for protein reduction.

The frozen material in a sample cuvette was placed into a fitted, copper cold finger and allowed to thaw. Before the sample became liquid, however, the top of the cuvette was removed and a

continuous helium flushing procedure was started. Upon liquification, the protein material was reduced with solid dithionite and allowed to equilibrate for five minutes to allow complete reduction. At the end of this time, the sample was refrozen by inserting the lower section of the copper cold finger into liquid nitrogen. If the reduced material was to be lyophilized, the copper cold finger and cuvette were then placed into the main dewar cavity of the Mossbauer spectrometer and a hard vacuum was immediately pulled on the frozen material by the combined action of the spectrometer roughing and diffusion pumps. As the cold finger and the sample warmed in the dewar cavity, the water in the sample was drawn off at its lowest possible temperature. It was necessary to take extreme care during this procedure to cope with any splattering that may take place in the sample cuvette. After the lyophilization was complete, the sample was withdrawn from the spectrometer vacuum system, and the helium flushing procedure was immediately resumed. The top of the cuvette was then reinstalled, the sample immediately refrozen and placed into the spectrometer for running.

The advantage of the above procedure is that it is essentially anaerobic while simultaneously providing the heat-exchange gas, helium, to the sample cuvette (Section III-A). One should also notice that for the lyophilized sample, the top to the sample cuvette is installed <u>before</u> the cuvette is frozen, as this procedure obviates sublimation of water vapor on the inside of the sample cuvette.

As a general note, we add that after the initial ^{57}Fe reconstitution and purification of the proteins, extreme care was

taken to maintain the temperature of the proteins to below 80°K. Even with these precautions, reoxidation of one of the reduced adrenodoxin samples and reduced adrenodoxin selenide (Orme-Johnson et al., 1968) was seen to take place at low temperatures during Mossbauer spectroscopy experiments. However, at the beginning and at the end of any set of Mossbauer spectroscopy experiments, the 4.2°K, polarizing magnetic field spectrum was taken as a check for any denaturation or reoxidation of the reduced proteins. We have never observed a change in any oxidized ferredoxin during Mossbauer spectroscopy experiments, even when the sample was repeatedly refrozen.

IV. THE CALCULATION OF ^{57}Fe MOSSBAUER SPECTRA IN APPLIED MAGNETIC FIELD

Gabriel and Ruby (1969, revised by Gabriel and Olson, 1969) have written a computer program, PDRHXT, for randomly oriented powder Mossbauer samples placed in an internal magnetic field. This program, as received in June, 1967, was not capable of calculating spectra for samples which contained anisotropies in either the $\tilde{\tilde{A}}$ or $\tilde{\tilde{G}}$ tensors (p. 52). This program was written to apply to any Mossbauer transition between nuclear levels with spin up to and including 9/2. This generality resulted in a complexity which, in turn, resulted in a number of errors in the program when it was applied by us to ^{57}Fe Mossbauer spectroscopy. Since, in addition, the program was quite inefficient when applied to ^{57}Fe materials, it was decided to retain the basic method of calculation and those subroutines which could be efficiently applied to ^{57}Fe, and then to rewrite the program specifically for iron Mossbauer spectroscopy in magnetic field.

The program which resulted from rewriting PDRHXT was named MOSSCAL. Basically, the computer plots in Fig. 7 are the output of MOSSCAL. When the output of MOSSCAL failed to provide adequate fits to the reduced spinach ferredoxin data, MOSSCAL was rewritten to include the anisotropies in the $\tilde{\tilde{A}}$ and $\tilde{\tilde{G}}$ tensors which had been shown to exist for the plant-type ferredoxins by EPR studies (Table 1). The resulting program, ANIMO, appears in Appendix I, and its method of calculation is described below.

Some of the subroutines in ANIMO are taken from the systems library of the Computer Center at the University of California at San Diego. Also, the subroutine, ALLMAT, which is capable of diagonalyzing any square array of complex numbers, was written by Rinzel and Funderlic (1968). This subroutine has been slightly amended to deal with the matrices encountered, specifically, in program ANIMO.

The total Hamiltonian for Mossbauer samples in an applied field is written as follows:

$$\mathcal{H} = I.S. + 2DI_z^2 + (E-D)I_x^2 + (-E-D)I_y^2 + g_N\beta_N H_z I_z + \widetilde{\langle S_{eff}\rangle}\cdot\tilde{\tilde{A}}\cdot\tilde{I} \tag{28}$$

The first term is dropped from the Hamiltonian since it can be easily handled by moving the computed Mossbauer spectrum along the velocity axis after the rest of the calculation has been completed. The next three terms represent the quadrupole interaction as given in Eq. 6. The definition of D and E are given in the following expressions:

$$D \equiv QS/6(1+\eta^2/3)^{1/2} \tag{29}$$

$$E \equiv \eta D \tag{30}$$

where QS is the observed splitting from a quadrupole pair when the magnetic field at the nucleus is zero. Before discussing the last two terms in Eq. 28, we shall present the following preview of the calculation.

1) We choose the basis set for this calculation as Pauli spin matrices (Brink and Satchler, 1962).

2) We choose a basis coordinate system.

3) The Hamiltonian operator matrices for both nuclear energy levels are constructed in the above basis set for a particular orientation of the lattice coordinate system relative to lab frame.

4) The above matrices are diagonalized to give a set of eigenvalues and a matrix of eigenvectors for each nuclear energy level.

5) The energy and intensity of the transitions are then calculated and stored as a line spectrum.

6) Steps 3-5 are repeated for each orientation of the lattice relative to laboratory frame through one octant of the 4π steradians. (121 orientations are sufficient to produce high-quality spectra.)

7) The line spectrum which is now the sum of the 121 lattice orientations is converted to a Mossbauer intensity spectrum with Breit-Wigner lineshapes (Wertheim, 1964, p.108).

The basis coordinate system for the calculation is in lab frame, with the z-axis coincident with the gamma-ray direction which is also coincident with the applied magnetic field direction. There are several advantageous consequences of this choice of basis coordinate system:

1) A specific orientation of the lattice coordinate system relative to lab frame is now denoted by Euler angles, α, β, and γ (Brink and Satchler, 1962), where the angles are all zero when the lattice coordinate system is coincident with that in the lab frame. Rotation through Euler angle, α, is then needless since it amounts to rotation of the lattice around an axis coincident with the applied magnetic field.

2) Since the basis coordinate system has its z-axis along the gamma ray direction, the elements of the magnetic dipole operator are related to the basis eigenvectors through a unit tensor. Thus the intensity calculation is much simplified.

3) This choice of basis set also allows closed-form integration of the magnetic dipole operator around the direction of propagation (Kundig, 1966).

The Hamiltonian operator for a particular lattice orientation is now written as:

$$\mathcal{H} = D_{J_z}(\beta)^{\dagger} \; D_{J_Y}(\gamma)^{\dagger} \; \tilde{I}\cdot\tilde{\tilde{P}}\cdot\tilde{I} \; D_{J_Y}(\gamma) \; D_{J_z}(\beta) + L_x k H_{eff} I_x + L_Y k H_{eff} I_Y + L_z k H_{eff} I_z \tag{31}$$

The first term is the rotated quadrupole matrix, with the rotating matrices, D_j, given as defined in Brink and Satchler (1962). The last three terms represent the combined magnetic hyperfine and Zeeman interactions. Here the effective magnetic field at the nucleus resulting from both interactions is given in terms of a scalar magnitude, H_{eff}, and the direction cosines relative to lab frame, L_x, L_y and L_z. I_x, I_y and I_z are Pauli spin matrices; k is a constant to convert the interaction to units of mm/S. The method for calculating the effective magnetic field follows:

1) From the value of the Euler angles β, γ, calculate the direction cosines, ℓ, for the applied field in lattice frame.

2) Calculate $\langle S \rangle$ in the lattice frame. The direction cosines, ℓ', for S can be calculated from the following expression for the

states of S with magnetic moment parallel to the applied field as opposed to antiparallel to the applied field where this expression changes sign.

$$\ell_i' = \ell_i g_i / (\ell_i^2 g_i^2 + \ell_j^2 g_j^2 + \ell_k^2 g_k^2)^{1/2} \tag{32}$$

where i, j, k are subscripts denoting the Cartesian axes in lattice frame x, y, z.

3) An effective hyperfine field, h, at the nucleus is then calculated from the following equation:

$$h_i = \ell_i' A_i g_N \beta_N / g_e \beta_e \tag{33}$$

where A_i is a principle component of the magnetic hyperfine tensor. Note that the $\tilde{\tilde{A}}$ tensor has been assumed to be coaxial with the $\tilde{\tilde{G}}$ tensor and that the $\tilde{\tilde{A}}$ tensor is correctly defined in this formulation only if S = 1/2. In cases where S is not equal to one-half, one must generate the $\tilde{\tilde{A}}$ tensor for this program from the real $\tilde{\tilde{A}}$ tensor by means of the following expression:

$$A_i(\text{Program}) = 2SA_i(\text{Real}) \tag{34}$$

4) The applied field is now added to or subtracted from the applied field depending on the value of a computational flag, ALIGN.

5) The direction cosines, L, and effective magnetic field, H_{eff}, are now generated in lab frame and are then used directly in the calculation of the Hamiltonian operator.

The calculation of the effective magnetic field at the nucleus is done in subroutine ANI. Note that this magnetic field is applied to Hamiltonian operator, Eq. 31, in terms of a nuclear Zeeman interaction. The total Hamiltonian is formed by summing the rotated

quadrupole matrix and magnetic matrix. Thus, when the eigenvalues are computed by diagonalyzing the Hamiltonian, the matrix of eigenvectors is the lab frame basis set.

The transition intensity subroutine, PDRHIN, was designed from the formulation given by Kundig (1966). Using the notation of Kundig, the probability, P, of a transition between states i and j is given by the following expression where the C's are the elements of the matrices of eigenvectors.

$$
\begin{aligned}
P_{(i,j)} = {} & \left| C^{\frac{1}{2}*}_{(\frac{1}{2},j)} C^{\frac{3}{2}}_{(\frac{3}{2},i)} \right|^2 + \frac{1}{3} \left| C^{\frac{1}{2}*}_{(\frac{1}{2},j)} C^{-\frac{1}{2}}_{(3/2,i)} \right|^2 \\
& + \frac{1}{3} \left| C^{-\frac{1}{2}*}_{(\frac{1}{2},j)} C^{\frac{1}{2}}_{(\frac{3}{2},i)} \right|^2 + \left| C^{-\frac{1}{2}*}_{(\frac{1}{2},j)} C^{\frac{3}{2}}_{(3/2,i)} \right|^2 + \frac{1}{3} \Big[C^{\frac{1}{2}}_{(\frac{1}{2},j)} C^{\frac{3}{2}*}_{(\frac{3}{2},i)} C^{-\frac{1}{2}*}_{(\frac{1}{2},j)} C^{\frac{1}{2}}_{(\frac{3}{2},i)} \\
& + C^{\frac{1}{2}}_{(\frac{1}{2},j)} C^{-\frac{1}{2}*}_{(\frac{3}{2},i)} C^{-\frac{1}{2}*}_{(\frac{1}{2},j)} C^{\frac{3}{2}}_{(\frac{3}{2},i)} + C^{-\frac{1}{2}}_{(\frac{1}{2},j)} C^{\frac{1}{2}*}_{(\frac{3}{2},i)} C^{\frac{1}{2}*}_{(\frac{1}{2},j)} C^{\frac{3}{2}}_{(\frac{3}{2},i)} \\
& + C^{-\frac{1}{2}}_{(\frac{1}{2},j)} C^{\frac{3}{2}*}_{(\frac{3}{2},i)} C^{\frac{1}{2}*}_{(\frac{1}{2},j)} C^{-\frac{1}{2}}_{(\frac{3}{2},i)} \Big]
\end{aligned}
\tag{35}
$$

Once the line spectra are available, it is a simple matter to construct Breit-Wigner lineshapes and then to plot the output as an absorption spectrum. Isomer shift; electron spin states; Boltzmann spin population; limits for the velocity in the spectrum, etc., are handled through input parameters which are described in Appendix I.

Complex mode is used extensively in the program; other than this, there are few library subroutines which are not common to most research computers, except, of course, the plotting routines. The execution time for the program on a CDC 6600 Computer is 3 seconds for 121 integration steps and is not a function of the complexity of the

input parameters. Most of this time is spent in subroutine ALLMAT and in the subroutine GRPLTR, the plotting routine.

The physics of ^{57}Fe Mossbauer spectroscopy with applied magnetic field is well represented by program ANIMO, with the following exceptions:

1) The formulation in ANIMO is one of stationary states. When the spin-relaxation time or the excited nuclear state's Larmor precession time approach the lifetime of the excited state (Section II-D), this formulation is not valid.

2) The $\tilde{\tilde{A}}$ and $\tilde{\tilde{G}}$ tensors are assumed to be coaxial. When both tensors have large anisotropies, this assumption can produce results which are in error. However, even in this case, the program is correct to first order.

3) Goldanskii-Karyagin effects (Goldanskii and Makarov, 1968) and thick absorber effects (Preston et al., 1962) are not treated by the program.

As will be shown in Chapter V, a successful interpretation of the plant-type ferredoxin Mossbauer data does not depend on the inclusion of the above "perturbations" to the physics already represented in program ANIMO. However, the program is written in a form which allows the inclusion of any of these modifications with a minimal rewriting of the existing subroutines.

V. DISCUSSION AND RESULTS

A. PREVIOUSLY-PROPOSED MODELS FOR THE ACTIVE SITE OF THE PLANT-TYPE FERREDOXINS

The g = 1.94 EPR signal exhibited in the reduced state of the ferredoxins was the basis for first models for the active site of these proteins. The identification of this EPR signal with an iron complex has been described in a review by Beinert and Palmer (1965). The complexity of the iron ligand field which is necessary to produce a g = 1.94 signal was demonstrated by Beinert et al. (1965), who proposed a model compound for this signal. This model compound was pentacyanonitrosylferrate (I), and therefore was not expected to be completely analogous to active site of the ferredoxin compounds. The properties of this compound were later related and expanded by Van Voorst and Hemmerich (1967).

Meanwhile, Blumberg and Peisach (1965) showed that the interaction between a low-spin ferrous atom and an adjacent free radical can give rise to a g = 1.94 EPR signal. Brintzinger, Palmer, and Sands (1966a) proposed the first two-iron model for the active center of a plant-type ferredoxin. Their model, which consisted of two spin-coupled, low-spin ferric atoms in the oxidized protein and one low-spin ferric and one low-spin ferrous atom in the reduced protein, explained much of the chemical data on the proteins. Later, they (Brintzinger, Palmer, and Sands, 1966b) presented EPR data for a compound, bis-hexamethylbenzeme, Fe(I), which demonstrated all the properties of the g = 1.94 signal observed in the ferredoxins.

FIGURE 15. PREVIOUSLY-PROPOSED MODELS FOR THE ACTIVE CENTER OF THE PLANT-TYPE FERREDOXINS.

A. Blumberg and Peisach, 1965

Reduced Protein

Fe^{II} (S=0) ——— Free Radical

B. Brintzinger *et al.*, 1966

Oxidized Protein

↑(S_1=1/2) ⟷ ↓(S_2=1/2)

Fe^{III} Fe^{III}

Reduced Protein

↑(S_1=1/2) ⟷ ●(S_2=0)

Fe^{III} Fe^{II}

C. Gibson *et al.*, 1966

Oxidized Protein

↑(S_1=5/2) ——— ↓(S=5/2)

Fe^{+++} Fe^{+++}

Reduced Protein

↑(S_1=5/2) ——— ↓(S=2)

Fe^{+++} Fe^{++}

D. Johnson *et al.*, 1969

↑Fe^{+++} low-spin ——— (S=0) ↓Fe^{+++} low-spin $\xleftrightarrow{e^-}$ ●Fe^{++} low-spin ——— (S=1/2) ↑Fe^{+++} low-spin

●Fe^{++} low-spin ——— (S=0) ●Fe^{++} low-spin $\xleftrightarrow{e^-}$ ↑Fe^{+} low-spin ——— (S=1/2) ●Fe^{++} low-spin

Oxidized Protein Reduced Protein

The above model was criticized by Gibson et al. (1966) and Thornley et al. (1966) who reported that the tetrahedral symmetry of the BPS model could not create the crystal-field splitting required for spin pairing in the iron atoms. They, instead, proposed a model with two high-spin ferric atoms in the oxidized protein which were exchange-coupled to render this state diamagnetic. In the reduced state, their model consists of a ferric (S = 5/2) state exchange-coupled to a ferrous (S = 2) state to give a resultant spin to the complex as a whole of S = 1/2. Thus, their reduced state was ferrimagnetic, and they attributed the high temperature disappearance of the EPR signal to two-phonon Orbach processes (Orbach, 1961). The g = 1.94 signal was explained by assuming a tetrahedral ligand field about the ferrous atom with a spin-orbit coupling constant of 75 cm^{-1}. This model explained all the properties of the g = 1.94 EPR signal; also, it has the advantage of being quite plausible in view of the known sulfur ligands around the iron atoms. The above models are illustrated in Fig. 15.

Several Mossbauer spectroscopic papers have dealt with members of the plant-type ferredoxins. In these papers, the Mossbauer spectra for a particular protein were interpreted to yield information such as the oxidation state and spin state of the iron atoms in the protein, and in some cases this information was extended to validate a proposed model for the active site. However, problems with denatured protein material or incorrect interpretation of the Mossbauer data have prevented any of these models from being accepted as valid. It is noted

that these studies show Mossbauer spectra which agree with our own if we exclude those studies performed on denatured material.

Bearden and Moss (1967) and Moss et al. (1968) presented the Mossbauer spectra of spinach ferredoxin in its oxidized and reduced states. These spectra showed the two iron atoms in the oxidized protein in identical electronic environments. Upon protein reduction, one of the iron atoms exhibited a spectrum characteristic of a high-spin ferrous ion. The Mossbauer spectra of the reduced proteins in the above study are not consistent with subsequent data for these proteins (Dunham et al., 1970). It is now believed (personal communications, W.H. Orme-Johnson and Graham Palmer) that 1) the samples in these experiments were impure, and 2) the buffers used in these experiments were not strong enough to maintain the pH during the dithionite reductions. Therefore, the Mossbauer spectra of reduced spinach ferredoxin in the above experiment resulted from a mixture of oxidized protein iron and iron from denatured protein material. These problems were overcome later by improvements in purification techniques, particularly with respect to gel filtration and increased buffer strengths.

Johnson et al. (1968a) interpreted the spectra on spinach ferredoxin (similar to those of Moss et al., 1968) as consistent with the following interpretation: 1) the oxidized protein contains two low-spin ferrous ions, and 2) the reduced protein contains one low-spin ferrous ion and one high-spin ferrous ion. Cooke et al. (1968) interpreted their data (similar to the data contained in the present work) on putidaredoxin in the following manner: 1) the electronic environments of both iron atoms are identical in the oxidized protein,

with the diamagnetism of this material resulting from spin pairing between the iron atoms, and 2) in the reduced state, a single electron is shared equally by both iron atoms and gives rise to the internal magnetic field observed in the Mossbauer spectra. Novikov et al. (1958) have published the results of a Mossbauer spectroscopic study on an iron-sulfur protein from Azotobacter. Both the data and the conclusions are similar to those made by Moss et al. on spinach ferredoxin. Recently, Johnson et al. (1968b) and Johnson et al. (1969) have published Mossbauer studies on the ferredoxins from Euglena and spinach. They now report their data as being most favorable to two models for the active site of these proteins (Fig. 15).

The above diversity in the interpretation of the Mossbauer spectra of the plant-type ferredoxins has stemmed from the complexity of the low-temperature spectra for the reduced proteins. In the following sections, we shall develop the computer program approach which led to our interpretation of the spectra and to the subsequent development of a model for the active site of these proteins.

B. DATA FOR THE OXIDIZED PROTEINS

Figure 16 shows the Mossbauer spectra of the oxidized state of all the plant-type ferredoxins. The isomer shift and quadrupole splittings for these spectra are listed below:

FIGURE 16. LOW-TEMPERATURE, ZERO APPLIED MAGNETIC FIELD MOSSBAUER SPECTRA FOR OXIDIZED PLANT-TYPE FERREDOXINS. Abbreviations:

AZI - Azotobacter Fe-S protein I, 4.6°K

AZII - Azotobacter Fe-S protein II, 4.2°K

Put. - Putidaredoxin, 4.2°K

Ad. - Pig adrenodoxin, 4.2°K

Clos. - Clostridial paramagnetic protein, 4.2°K

PPNR - Spinach ferredoxin, 4.5°K

Parsley - Parsley ferredoxin, 4.2°K

Velocity scale: relative to platinum source material.

Run numbers: D0035, D0025, D0063, 0J002, 0J011, B0193, B0235.

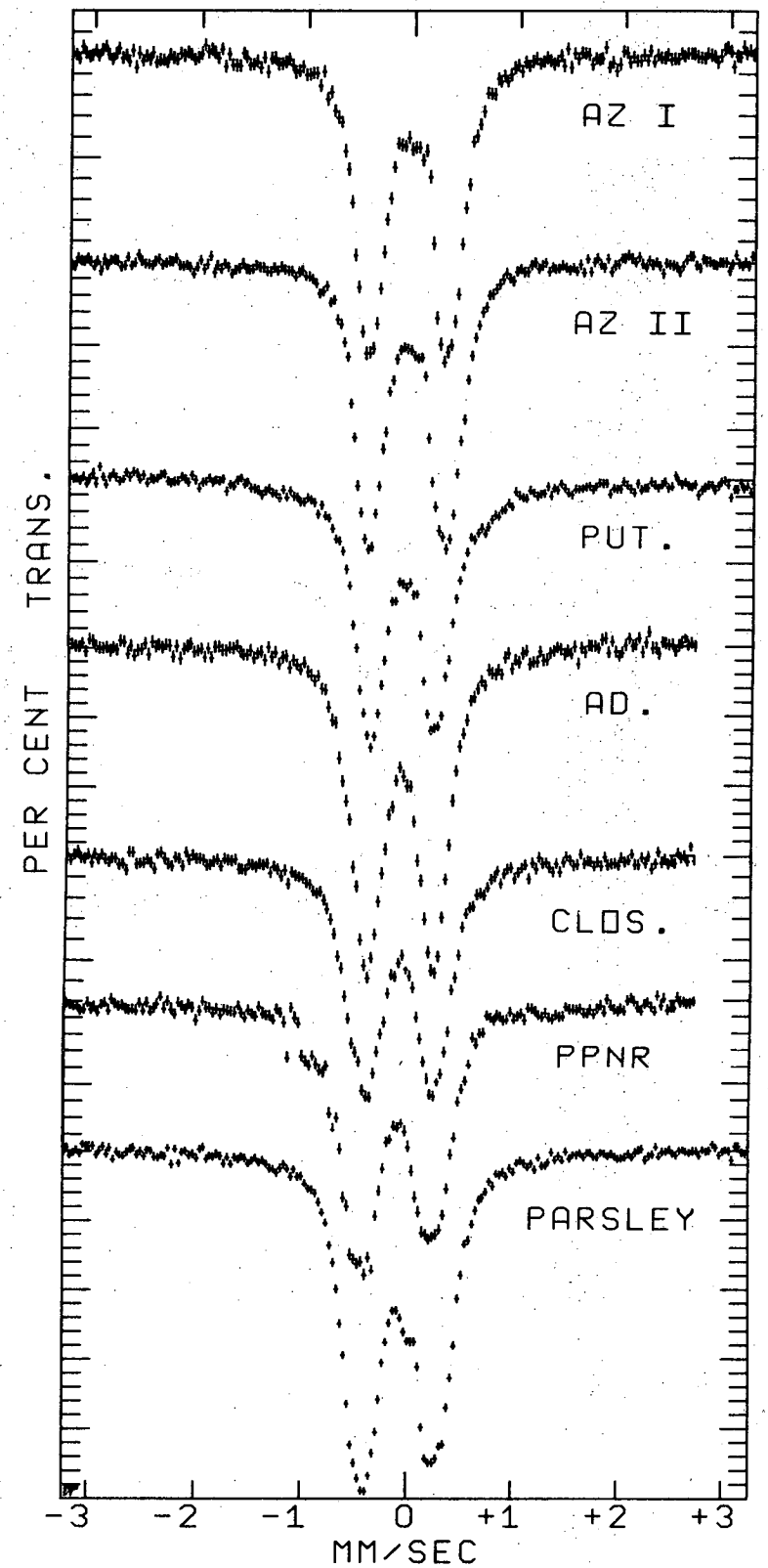
AZ I
AZ II
PUT.
AD.
CLOS.
PPNR
PARSLEY
PER CENT TRANS.
-3
-2
-1
0
+1
+2
+3
MM/SEC

FIGURE 17. LOW-TEMPERATURE, HIGH APPLIED MAGNETIC FIELD MOSSBAUER SPECTRA FOR OXIDIZED PLANT-TYPE FERREDOXINS. Abbreviations:

Ad. - Pig adrenodoxin, 4.2°K, 46 kG applied magnetic field

PPNR - Spinach ferredoxin, 4.5°K, 50 kG applied magnetic field

Clos. - Clostridial paramagnetic protein, 4.2°K, 46 kG applied magnetic field

AZI - Azotobacter Fe-S Protein I, 4.6°K, 46 kG applied magnetic field

AZII - Azotobacter Fe-S Protein II, 4.2°K, 46 kG applied magnetic field

Applied magnetic field parallel to gamma ray direction.

Velocity scale: relative to platinum source matrix.

Run numbers: 0J003, B0194, 0J012, D0034, D0027.

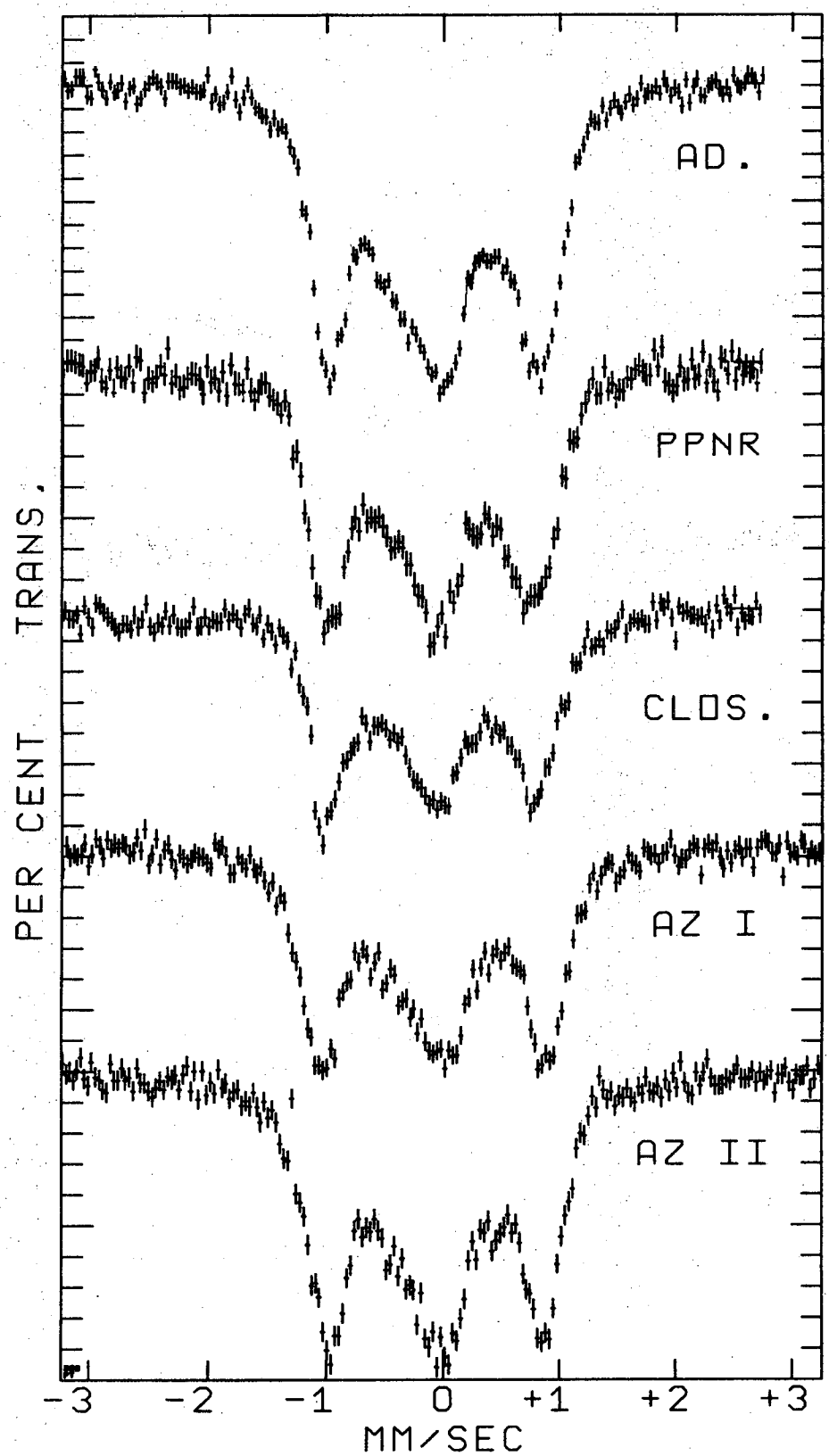
AD.
PPNR
CLOS.
AZ I
AZ II
PER CENT TRANS.
-3
-2
-1
0
+1
+2
+3
MM/SEC

TABLE 5

MOSSBAUER PARAMETERS FOR THE OXIDIZED PROTEINS

	IS/Pt* (mm/S)	QS (mm/S)	η
Spinach Fd.	-0.08 ± 0.01	0.65 ± 0.01	0.5 ± 0.2
Parsley Fd.	-0.07 ± 0.01	0.66 ± 0.01	0.5 ± 0.2
Adrenodoxin	-0.08 ± 0.01	0.61 ± 0.01	0.5 ± 0.2
Putidaredoxin	-0.08 ± 0.01	0.61 ± 0.01	0.5 ± 0.2
Clos. Paramag. Protein	-0.07 ± 0.01	0.62 ± 0.01	0.5 ± 0.2
Azoto. Fe-S Protein I	-0.04 ± 0.01	0.73 ± 0.01	0.5 ± 0.2
Azoto. Fe-S Protein II	-0.06 ± 0.01	0.71 ± 0.01	0.5 ± 0.2

*Isomer shifts quoted here are given relative to a gamma ray source consisting of ^{57}Co diffused into a platinum matrix.

The parameters, IS and QS, shown in Table 5 are measured at 4.2°K with zero applied field. The value of η and the sign of QS are derived by matching computed spectra to the Mossbauer data for the oxidized proteins taken at 4.2°K in 46 kilogauss applied magnetic field (Fig. 17). The above parameters do not exhibit any measurable temperature dependence over the temperature range from 4.2°K to 77°K. Thus, the best fit to the oxidized protein data is a single quadrupole pair with an isomer shift of -0.08 mm/S and an observed splitting of 0.65 mm/S.

The most probable electron configurations for iron atoms in a ligand field formed by amino acid side chains and sulfur are d^5 and d^6. The crystal field splitting required to pair spins in iron compounds is greater than 15,000 cm^{-1} (Ballhausen, 1962). Ligand

field theory calculations (Jørgensen, 1966) indicate that even in octahedral coordination, strong field ligands are required to cause spin pairing of iron atoms. The only side chains capable of supplying this strong field ligand are the aromatic residues: histidine, tryptophan and tyrosine. There are plant-type ferredoxins which contain only one of each of these amino acids (Newman et al., 1969; Kimura et al., 1969). Also, since sulfur is shown to be a ligand in the iron complex, low-spin iron configurations are doubtful for these proteins.

The small quadrupole splitting in the oxidized protein spectra imply that the electron density around the iron atoms is nearly spherical. A spherical charge density indicates that the iron is an S-state ion, although low-spin ferric atoms can have small quadrupole splittings (Wickman, 1965). In addition, the oxidized protein spectra show a single quadrupole pair, which indicates that the environments for the two iron atoms are nearly identical. The isomer shift for this quadrupole pair is most consistent with that of ferric iron, although ferrous iron cannot be ruled out as a possibility by the isomer shift value alone.

Thus, the most reasonable interpretation of the oxidized protein data is that the iron sites in this protein are either high-spin ferric or low-spin ferrous, with the high-spin ferric situation favored by the ligand field arguments set forth above. Combinations of electron configurations which give an odd total number of electrons for the two iron sites are not possible because the Mossbauer spectra do not exhibit the effects of the internal magnetic field

which would result from a paramagnetic system. In addition, the EPR results and the magnetic susceptibility data (Moss et al., 1969) are consistent with the conclusion that these proteins are diamagnetic in the oxidized state.

If the iron sites are high-spin ferric (S = 5/2), then an exchange-coupling mechanism is necessary to account for diamagnetism of the proteins in this oxidation state. Evidence for this exchange-coupling between the iron sites will be given during the discussion of the reduced protein spectra. Since high-spin ferric is an S-state ion, the EFG which gives rise to the quadrupole splitting in the oxidized spectra must result from anisotropies in the ligand field surrounding the iron sites. In this case, the value of η for these spectra indicate that both axial and rhombic distortions are present in the ligand field. It is important that this be true since the g = 1.94 EPR signal of the reduced state can only be explained if these distortions are present. Some of the verification that these iron sites are both spin-coupled, high-spin ferric irons rests with the interpretation of the reduced protein spectra. Accordingly, we shall return to the discussion of the oxidized proteins after the presentation of the reduced protein data.

C. THE HIGH-TEMPERATURE DATA FOR THE REDUCED PROTEINS

The Mossbauer spectra of spinach ferredoxin at 256°K is shown in Fig. 18; the solid line on these spectra is the result of computer-simulated Mossbauer spectra. A magnetic field of 46 kilogauss was applied to this sample (Fig. 18b) in order to establish the sign of QS and the value of η. Inspection of the four-line, zero-field

FIGURE 18. HIGH-TEMPERATURE MOSSBAUER SPECTRA FOR REDUCED SPINACH FERREDOXIN WITH COMPUTER FITS.

(A) Lyophilyzed spinach ferredoxin, 256°K, zero applied magnetic field.

(B) Lyophilyzed spinach ferredoxin, 256°K, 46 kG applied magnetic field parallel to gamma ray direction.

Computer input parameters in Table 6.

Velocity scale: relative to platinum source matrix.

Run numbers: D0119, D0120.

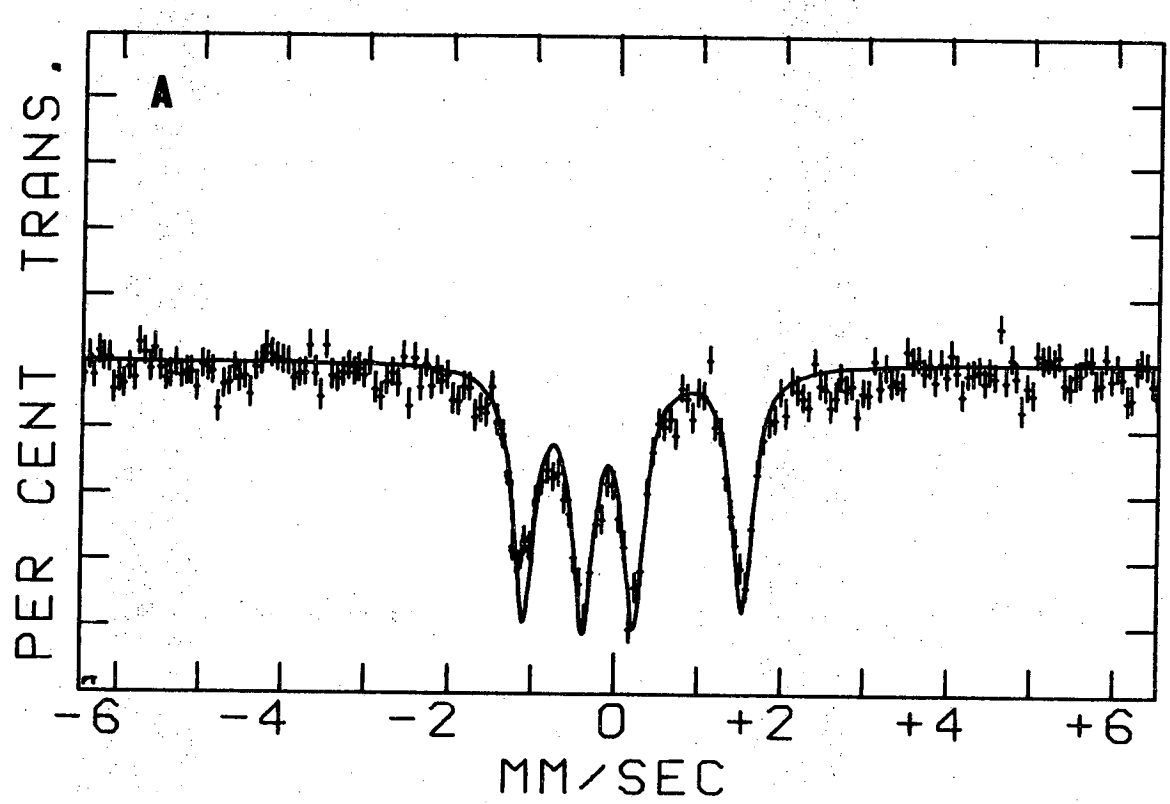
A
PER CENT TRANS.
-6
-4
-2
0
+2
+4
+6
MM/SEC

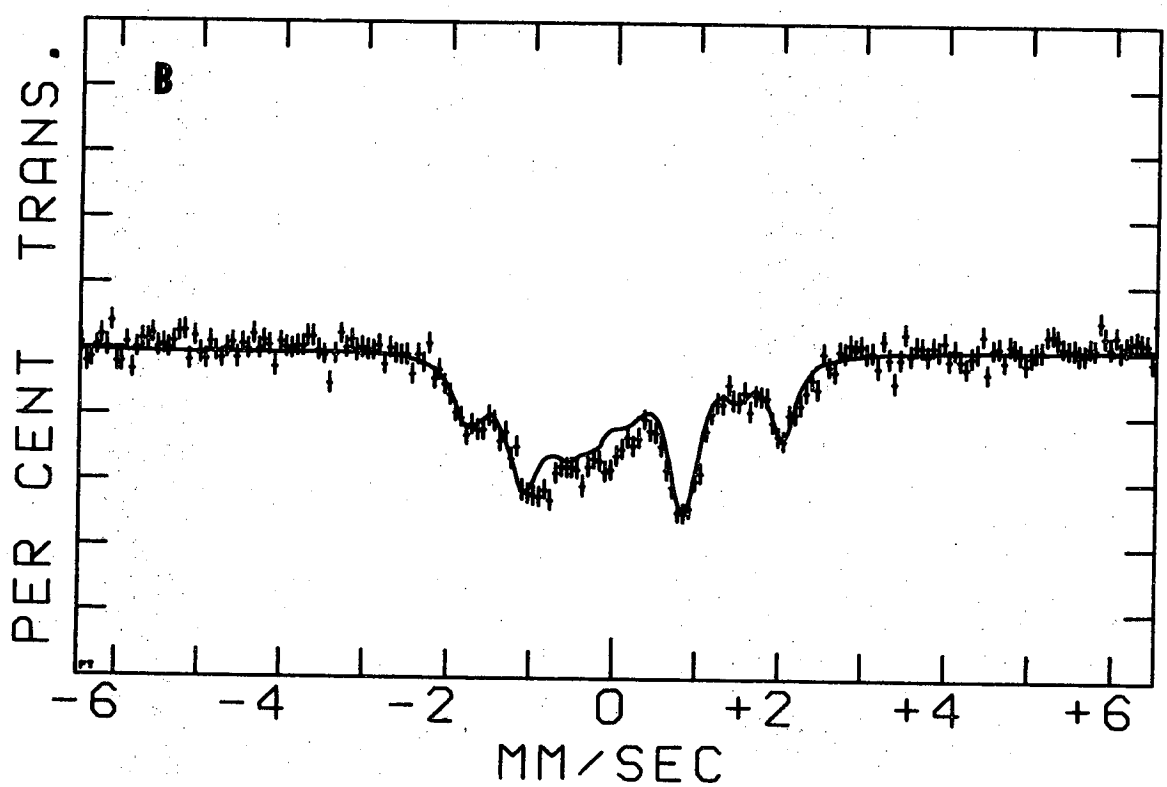
B
PER CENT TRANS.
-6
-4
-2
0
+2
+4
+6
MM/SEC

spectrum (Fig. 18a) reveals that this spectrum can be fit by two quadrupole pairs. The parameters for the computer simulated spectra shown in Fig. 18 are given below in Table 6.

TABLE 6

MOSSBAUER PARAMETERS FOR THE HIGH-TEMPERATURE REDUCED PPNR SPECTRA

	IS/Pt (mm/S)	QS (mm/S)	η
Iron Site #1	-0.08 ± 0.01	$+0.64 \pm 0.01$	0.5 ± 0.2
Iron Site #2	$+0.21 \pm 0.01$	-2.63 ± 0.01	0.25 ± 0.25

The assignment of quadrupole pairs shown in Table 6 is the result of a trial-and-error approach to fit the high-field data in Fig. 16b with computer simulated spectra. This approach establishes, unambiguously, the values for the isomer shift and magnitude of the quadrupole splitting shown for iron sites in Table 6. In addition, the sign of QS for iron site #2 is determined with no assumptions in interpretation during curve fitting procedures. Noticing that the values of IS and QS for iron site #1 are the same as for the sites in the oxidized proteins, we then assume that the value of η for iron site #1 is the same in oxidized and reduced proteins. With this assumption, the value of η for iron site #2 can be specified by the goodness of computer fits to the range, 0 to 0.5. The uncertainty in the value of η is diminished, however, by fitting the low-temperature spectra of the reduced proteins.

These data establish that there are two non-equivalent iron sites in the reduced proteins: site #1 is quite similar to that of

both iron atoms in the oxidized proteins, site #2 is characteristic of a high-spin ferrous ion. (The isomer shift and quadrupole splitting of site #2 leave little doubt that this site is high-spin ferrous (see Section II-C). Since the one-electron reduction of this protein is expected to change only a high-spin ferric ion to a high-spin ferrous ion, these data greatly reinforced the conclusion that the oxidized proteins contain two high-spin ferric ions. In addition, the reducing electron is seen to reside almost exclusively at site #2, since the Mossbauer parameters of site #1 are not affected by the reduction of the protein.

The magnetic susceptibility measurements of Moss et al. (1969) show a molecular paramagnetism in the reduced protein characteristic of a S = 1/2 compound. The absence of internal magnetic effects in the high-temperature, reduced protein spectra are explained by the Mossbauer spectra shown in Fig. 19. These spectra, taken at variable temperatures and a small polarizing applied magnetic field, show a temperature-dependent transition for spinach ferredoxin. As the temperature is lowered, the effects of an internal magnetic field on the Mossbauer spectra become more distinct until they result at around 30°K, in a spectrum which is characteristic of the low-temperature data of the plant-type ferredoxins (Fig. 20). We attribute this transition in the spectra to spin-lattice relaxation effects. This conclusion is preferred over a spin-spin mechanism as the transition was identical for both the lyophilized and 10 mM aqueous solution samples. Thus, the variable temperature data for reduced spinach ferredoxin indicate that the electron-spin relaxation time is around

FIGURE 19. VARIABLE-TEMPERATURE, LOW APPLIED MAGNETIC FIELD MOSSBAUER SPECTRA FOR REDUCED SPINACH FERREDOXIN. Lyophilyzed spinach ferredoxin with 580 gauss applied magnetic field parallel to gamma ray direction. Velocity scale: relative to platinum source matrix.

Run numbers: D0118, P0123, D0124, D0126, D0122, D0121, D0125.

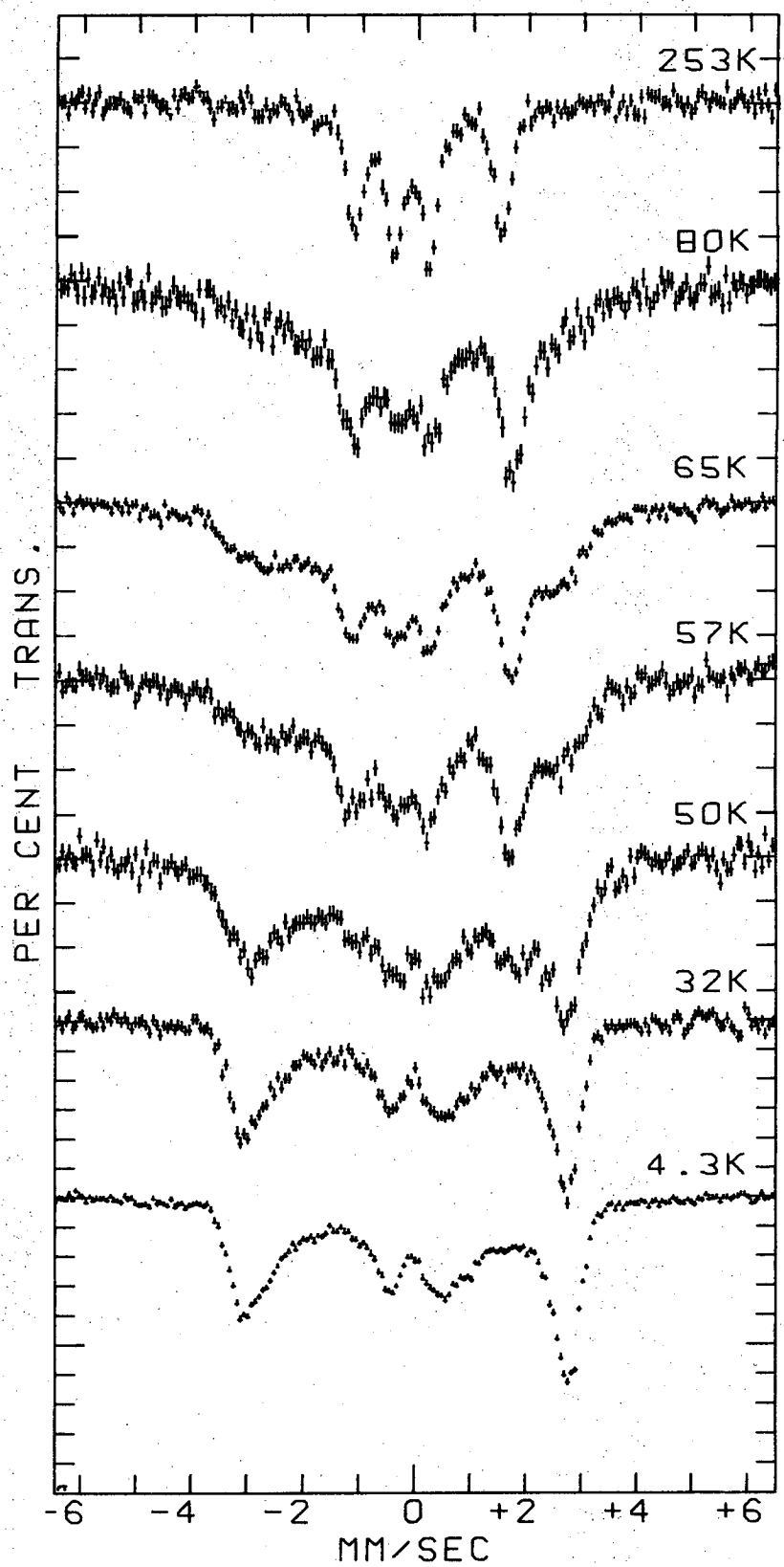
253K
80K
65K
57K
50K
32K
4.3K
PER CENT TRANS.
-6
-4
-2
0
+2
+4
+6
MM/SEC

10^{-7} seconds at 50°K. The temperature at which this transition in the Mossbauer spectra is half-complete is estimated to be the following: spinach ferredoxin, 50°K; parsley ferredoxin, 60°K; adrenodoxin, putidaredoxin, Clostridium and Azotobacter iron-sulfur proteins, 100°K.

D. THE LOW-TEMPERATURE DATA FOR THE REDUCED PROTEINS

The Mossbauer spectra of the reduced proteins at 4.2°K are shown in Fig. 20 for 3.4 kilogauss applied field and in Fig. 21 for 46 kilogauss applied field. Since the spectra are so similar, we shall speak exclusively in terms of the spinach ferredoxin data. Fig. 22 is low-temperature spinach-ferredoxin spectra with computed fits superimposed. By assuming that the isomer shift and quadrupole parameters for the low-temperature spectra are the same as for the high-temperature spectra and then adjusting magnetic parameters by trial and error, we were able to obtain a set of "best fit" magnetic parameters for the low-temperature spectra. The hyperfine constants for site #1 which resulted from this approach were very close to those measured independently by R.H. Sands, J. Fritz and J. Fee by ENDOR experiments (unpublished data). Since hyperfine constants measured by ENDOR are more precise than those measured by Mossbauer spectroscopy, the ENDOR results were adopted for site #1. Using these "improved parameters" for site #1, the trial-and-error approach was then resumed in order to find a best fit for the site #2 parameters. Subsequently, the ENDOR values for the hyperfine interaction at site #2 were also obtained by Sands and his co-workers. Since these values were also in agreement with our own, the final parameters for spinach ferredoxin shown in Table 7 incorporate the combined effort of ENDOR and Mossbauer

FIGURE 20. LOW-TEMPERATURE, LOW APPLIED MAGNETIC FIELD MOSSBAUER SPECTRA FOR REDUCED PLANT-TYPE FERREDOXINS. Abbreviations:

AZI - Azotobacter Fe-S protein I, 4.2°K, 1.15 kG applied magnetic field

AZII - Azotobacter Fe-S protein II, 4.2°K, 300 gauss applied magnetic field

Put. - Putidaredoxin, 4.6°K, 580 gauss applied magnetic field

Clos. - Clostridial paramagnetic protein, 4.7°K, 3.4 kG applied magnetic field

Ad. - Lyophilyzed pig adrenodoxin, 5.3°K, 580 gauss applied magnetic field

PPNR - Lyophilyzed spinach ferredoxin, 4.3°K, 580 gauss applied magnetic field

Parsley - Parsley ferredoxin, 5.1°K, 580 gauss applied magnetic field

Applied magnetic field parallel to gamma ray direction.

Velocity scale: relative to platinum source matrix.

Run numbers: D0045, D0032, B0244, OJ054, D0117, D0074.

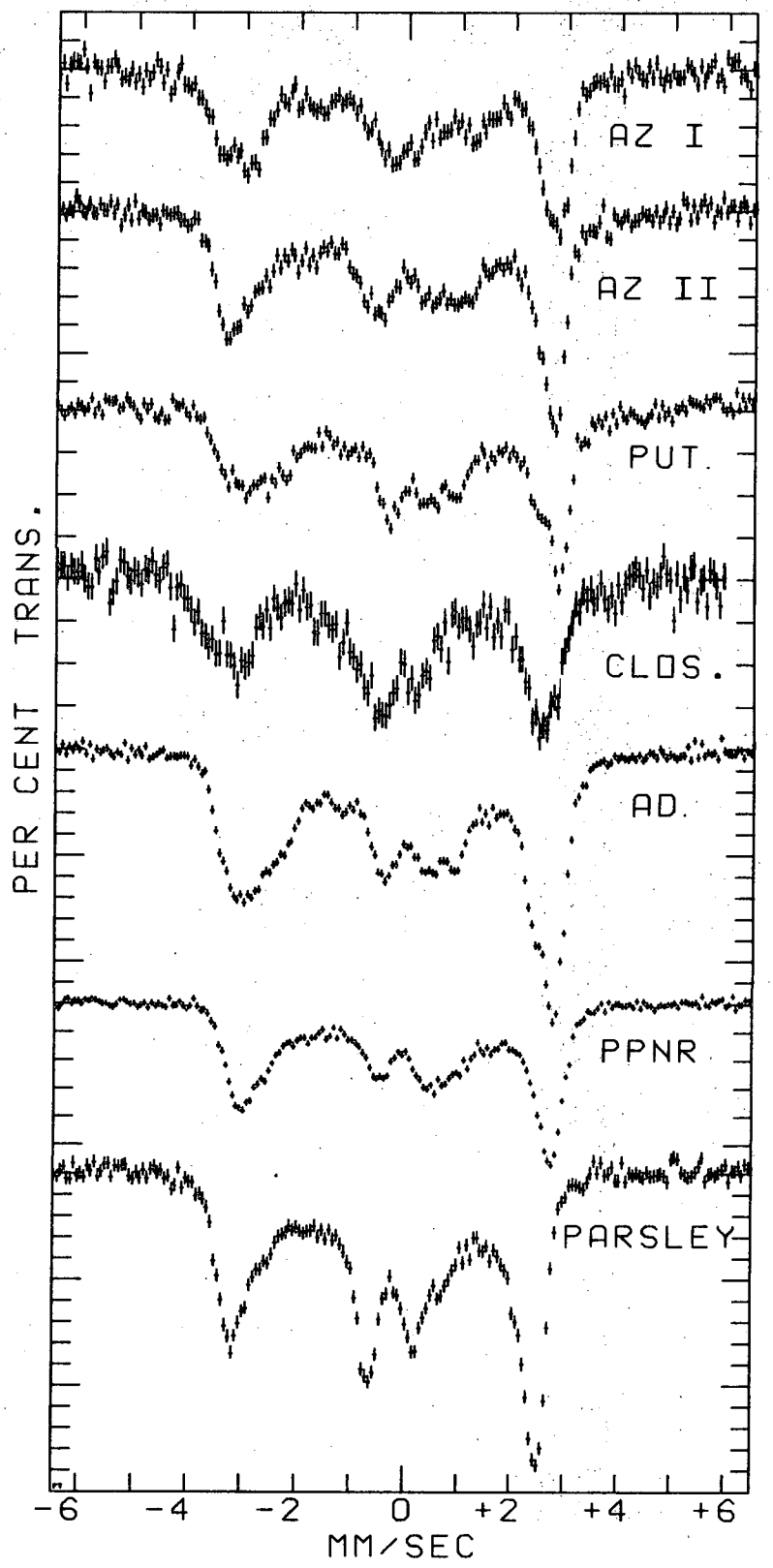
AZ I
AZ II
PUT.
CLOS.
AD.
PPNR
PARSLEY
PER CENT TRANS.
-6
-4
-2
0
+2
+4
+6
MM/SEC

FIGURE 21. LOW-TEMPERATURE, HIGH APPLIED MAGNETIC FIELD MOSSBAUER SPECTRA FOR REDUCED PLANT-TYPE FERREDOXINS. Abbreviations:

AZI - *Azotobacter* Fe-S protein I, 4.2°K, 46 kG applied magnetic field

AZII - *Azotobacter* Fe-S protein II, 4.2°K, 46 kG applied magnetic field

Put. - Putidaredoxin, 4.6°K, 46 kG applied magnetic field

Clos. - Clostridial paramagnetic protein, 4.2°K, 46 kG applied magnetic field

Ad. - Adrenodoxin, 4.2°K, 46 kG applied magnetic field

Parsley - Parsley ferredoxin, 4.3°K, 46 kG applied magnetic field

PPNR - Lyophilyzed spinach ferredoxin, 4.3°K, 46 kG applied magnetic field

Applied magnetic field parallel to gamma ray direction.

Velocity scale: relative to platinum source matrix.

Run numbers: D0041, D0031, B0245, OJ015, OJ007, D0083, D0115.

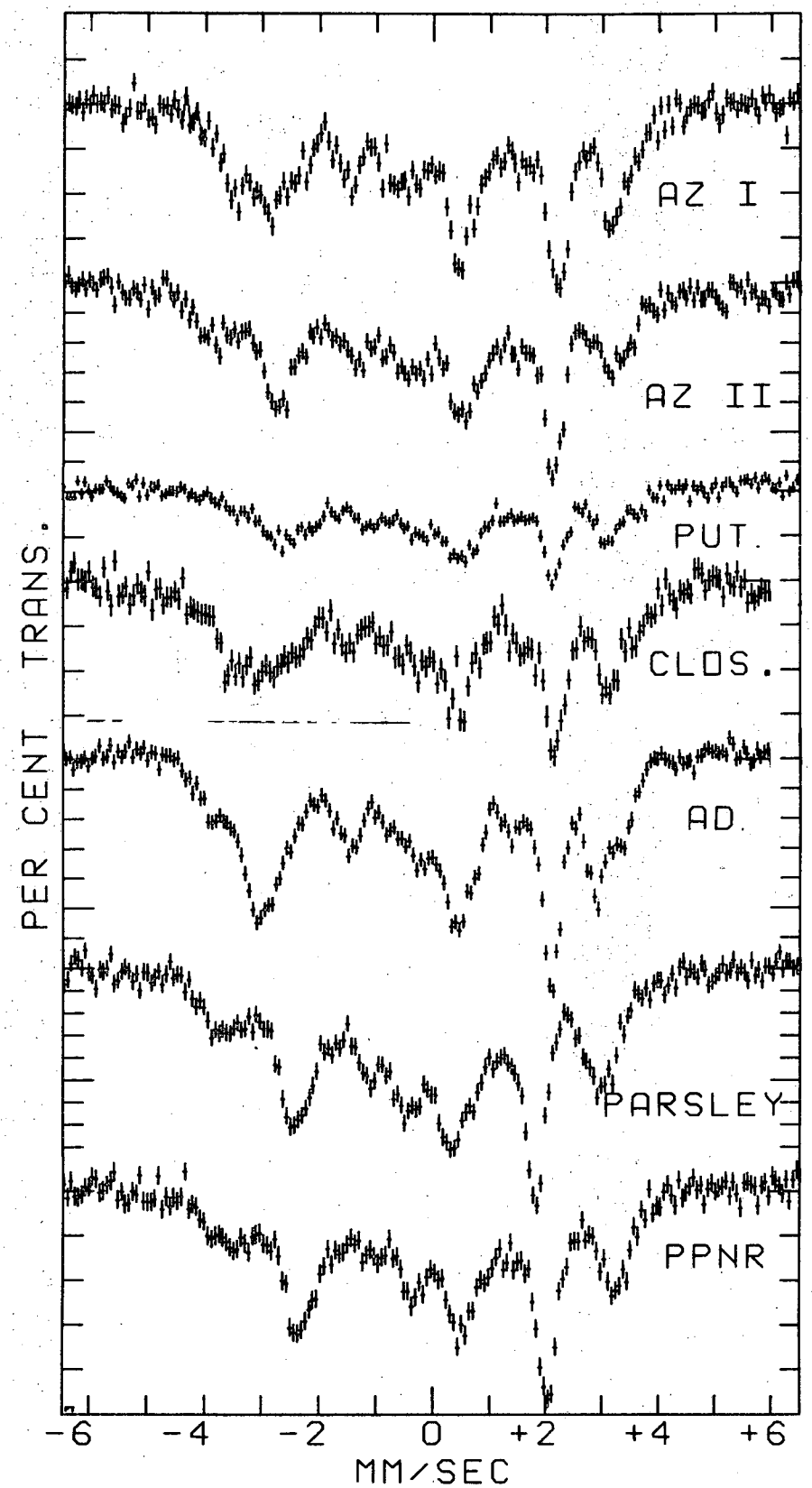
AZ I
AZ II
PUT.
CLOS.
AD.
PARSLEY
PPNR
PER CENT TRANS.
-6
-4
-2
0
+2
+4
+6
MM/SEC

FIGURE 22. LOW-TEMPERATURE MOSSBAUER SPECTRA FOR REDUCED SPINACH FERREDOXIN WITH COMPUTER FITS.

(A) Lyophilyzed spinach ferredoxin, 4.3°K, 580 gauss applied magnetic field

(B) Spinach ferredoxin, 4.3°K, 46 kG applied magnetic field parallel to gamma ray direction

Computer input parameters given in Table 7.

Boltzmann weighting factor for electronic excited state - 0.26.

Velocity scale: relative to platinum source matrix.

Run numbers: D0017, D0115.

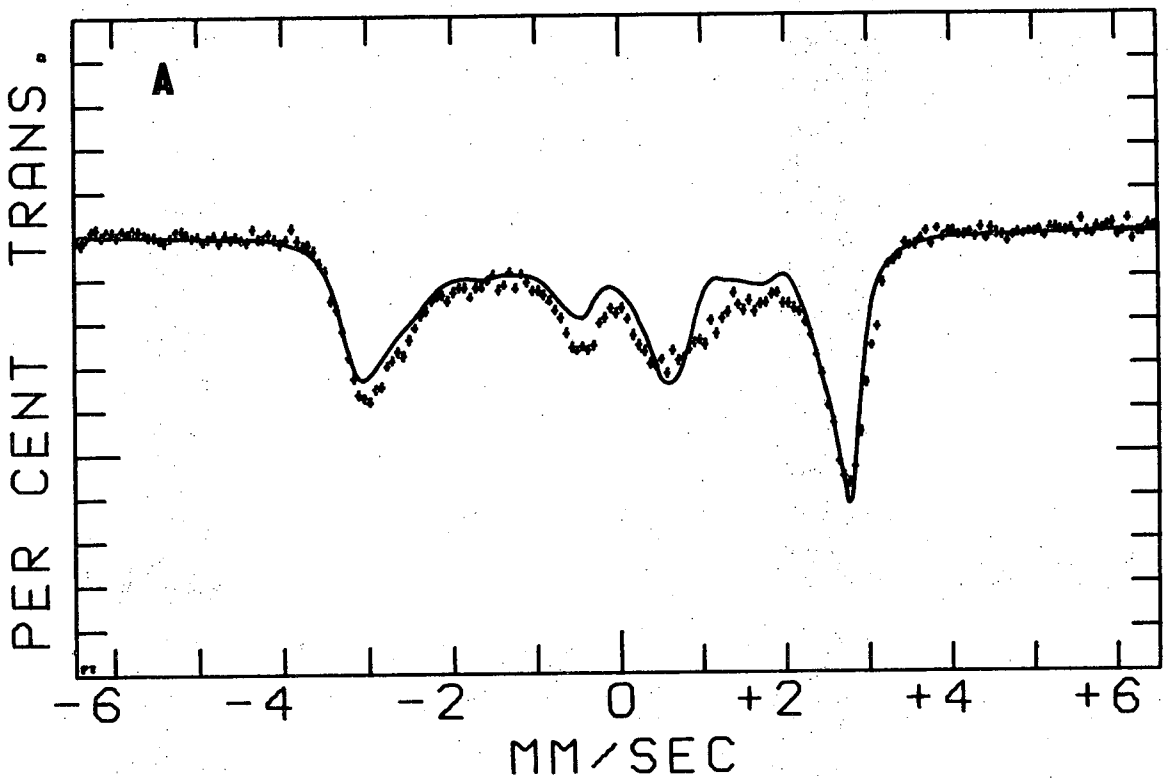
A
PER CENT TRANS.
-6
-4
-2
0
+2
+4
+6
MM/SEC

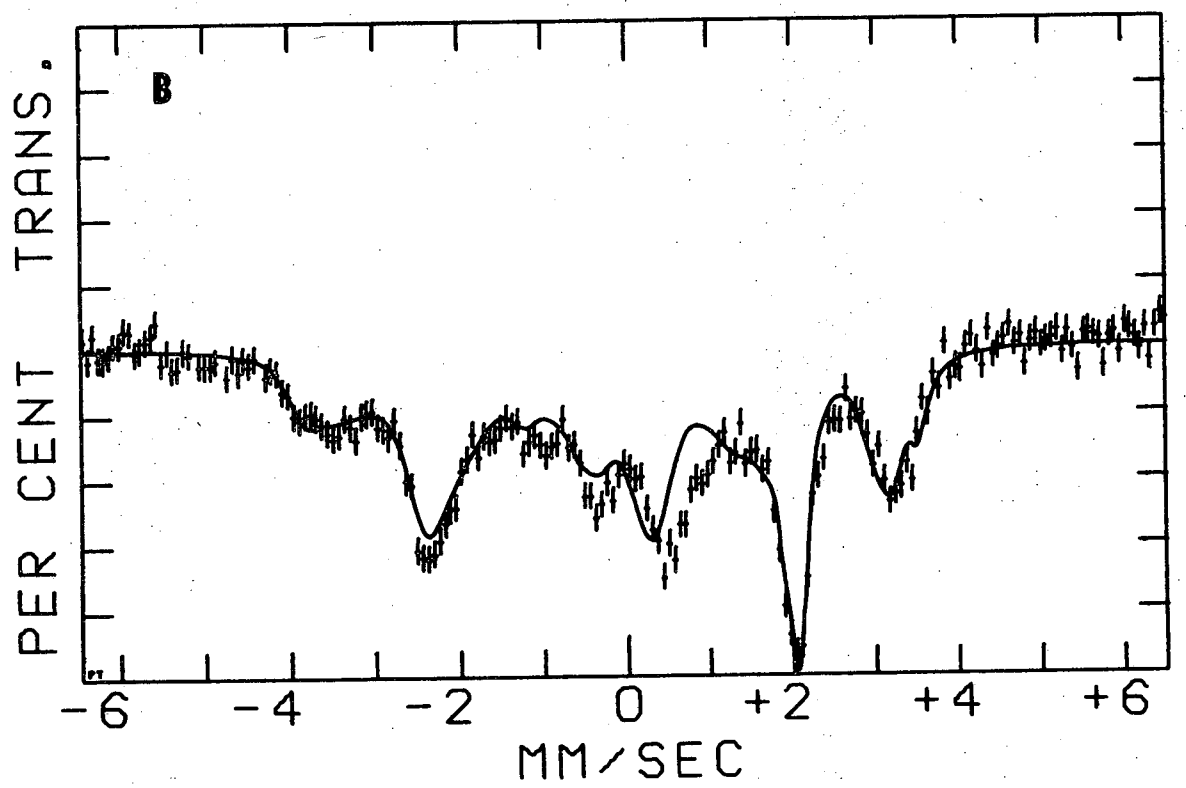
B
PER CENT TRANS.
-6
-4
-2
0
+2
+4
+6
MM/SEC

results, although the ENDOR results give no information on the sign of the principle $\overset{\approx}{A}$ tensor components. The spectra in Fig. 22 show the computed Mossbauer spectra which result from the parameters in Table 7.

TABLE 7

PARAMETERS FOR THE LOW-TEMPERATURE, REDUCED PPNR MOSSBAUER SPECTRA

	IS/Pt (mm/S)	QS (mm/S)	η	A_x	A_y	A_z	G_x	G_y	G_z
				(In electron gauss)					
Iron #1	-0.05 ±0.01	+0.64 ±0.01	.5 ±0.2	-17.8 ±0.1	-18.6 ±0.1	-15.1 ±0.1	1.89	1.96	2.04
Iron #2	+0.24 ±0.01	-2.63 ±0.01	.15 ±0.1	+5.0 ±0.7	+7.1 ±0.7	+12.5 ±0.4	1.89	1.96	2.04

In order to explain the spectra in Fig. 22, it is necessary to introduce another parameter into the discussion. Consider the effect of applying an external magnetic field to an S = 1/2 system. The effect of the field is to create two electron spin populations: one with spin parallel to the applied field and one with spin anti-parallel to the applied field. Further, these spin states will have different populations given by a Boltzmann factor. Note also that because the magnetic moment of the spin, with respect to the applied field, is reversed for the two spin states, the magnitude of the effective magnetic field at the nucleus differs for the two spin states by twice the amount of the applied magnetic field. An applied magnetic field of around 30 kilogauss is necessary in order that the Mossbauer spectra of the two spin states become distinct. When the applied field is around 30 kilogauss, low temperatures of approximately 5°K are needed to cause the differences in population of the

two states to become measurable by Mossbauer spectroscopy. When the applied field is 46 kilogauss and the temperature is 4.2°K, as is the case in Fig. 22, both of these criteria are met. Therefore, Fig. 22 contains Boltzmann parameters, 0.26 and 1.0 for the populations of the two spin states for the resultant spin one-half system of the reduced protein complex. We find that for samples which have different water mole fractions, but are measured to be at identical temperatures by the resistor, the spin temperature depends on the water mole fraction: lyophilized samples have lower spin temperatures than aqueous samples.

As added evidence for our confidence in the parameters shown in Table 7, the zero applied field spectra taken at low temperatures are shown in Fig. 23. Since the A-values for site #1 are almost isotropic, it is expected that the absorption peaks from this site would dominate the Mossbauer spectra in both zero and applied magnetic field. Comparison of Fig. 23 and Fig. 9 reveals that the absorption in these spectra at -6 mm/S results from an isotropic hyperfine interaction of about -17 gauss at one of the iron sites in the reduced proteins. The anisotropic hyperfine interaction at site #2 results in a broad, unresolved absorption which accounts for the difference in shape between the spectra.

The Mossbauer spectra for these proteins are consistent with the "spin-coupled" model proposed by Gibson et al. (Section IV-A) for the active site of these proteins. In the next section we shall discuss this model in detail.

FIGURE 23. LOW-TEMPERATURE, ZERO APPLIED MAGNETIC FIELD MOSSBAUER SPECTRA FOR REDUCED PLANT-TYPE FERREDOXINS. Abbreviations:

AZI - Azotobacter Fe-S protein I, 4.2°K

Put. - Putidaredoxin, 4.2°K

Clos. - Clostridial paramagnetic protein, 4.2°K

Ad. - Adrenodoxin, 4.2°K

Parsley - Parsley ferredoxin, 4.6°K

Velocity scale: relative to platinum source matrix.

Run numbers: D0048, D0059, OJ014, OJ006, D0084.

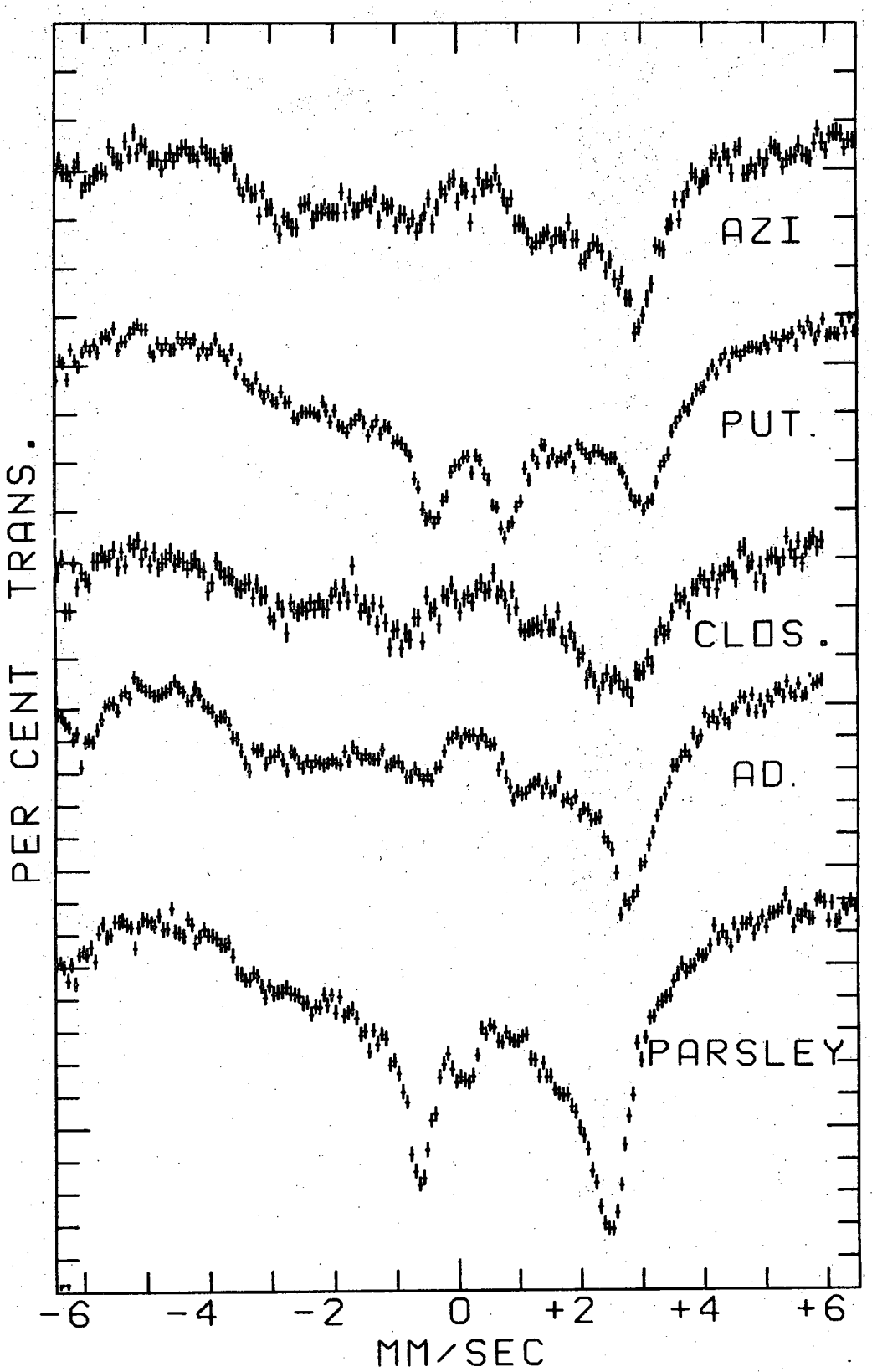
AZI
PUT.
CLOS.
AD.
PARSLEY
PER CENT TRANS.
-6
-4
-2
0
+2
+4
+6
MM/SEC

E. VALIDITY OF THE "SPIN-COUPLED" MODEL

The iron atoms in the oxidized protein are high-spin ferric ($^6S_{5/2}$) ions, exchange-coupled to give a resultant spin-zero complex. Upon reduction, one of the iron atoms changes to the high-spin ferrous state (S = 2). The exchange-coupling for this protein oxidation state gives a resultant spin of one-half. Lewis et al. (1967), Khedekar et al. (1967) and Gerloch et al. (1968) have observed a similar exchange-coupling mechanism in a number of Schiff's base iron salts. In every case in which the exchange-coupling constant was negative (anti-ferromagnetic), the structure of the salt is as shown below:

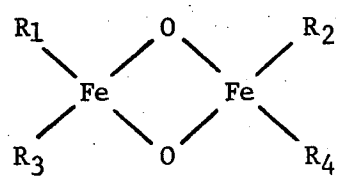

FIGURE 24. STRUCTURE OF OXY-BRIDGED Fe^{+++} SCHIFF-BASE COMPLEXES (LEWIS et al., 1967).

where the R's refer to the Schiff-base ligands. If this situation is analogous to that in the plant-type ferredoxins, then we may assume that the role of the labile sulfur in these proteins is to bridge the iron atoms in an analogous fashion and thus promote the exchange-coupling interaction.

The g = 1.94 EPR signal of the reduced proteins must be explained by any model for their active site. Using subscript 1 to specify the ferric-iron site and subscript 2 the ferrous-iron site, the "spin-coupled" model explains this EPR signal in the following way.

The electron magnetic moments (S_1 = 5/2 and S_2 = 2) are coupled to form a resultant spin, S, as shown below.

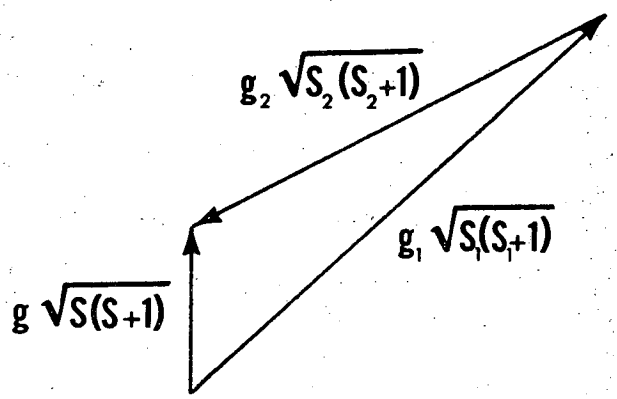

FIGURE 25. DIAGRAM FOR "SPIN-COUPLED" MODEL.

Relating Fig. 25 to the law of the cosines, the g-value for an S = 1/2 system is given by the following expression:

$$g = (7g_1 - 4g_2)/3 \tag{36}$$

Since g_1 arises from an S-state ion, spin-orbit interactions are not allowed to first order (Koenig, 1968) and g_1 can therefore be assumed to be isotropic. It is assumed to be 2.019 in accord with the measurements of Title (1963). With this assumption, the g-values for the ferrous iron can be derived using Eq. 36 and the measured g-values for the proteins (Table 1). For spinach ferredoxin, these calculated values are g_{2x} = 2.12, g_{2y} = 2.07 and g_{2z} = 2.00.

In the high-spin ferrous ion, spin-orbit interactions mix the ground state wave functions with the excited states. If the ground state is assumed to have d_{z^2} symmetry, then the following expressions apply for an ion in a crystal field with both rhombic and axial distortions (Edwards et al., 1967):

$$g_{2x} = g_e + 6\lambda/\Delta_{yz} \tag{37}$$

$$g_{2y} = g_e + 6\lambda/\Delta_{xz} \tag{38}$$

$$g_{2z} = g_e \tag{39}$$

where λ is the spin-orbit coupling constant in the interaction $\lambda\tilde{L}\cdot\tilde{S}$ Δ_{xz} and Δ_{yz} are the energy gaps to the excited states having d_{xz} and d_{yz} symmetries, respectively. These expressions (37-39) are derived by assuming that the electronic ground state is equivalent to a hole with spin = 2 in a d_{z^2} orbital. λ can be estimated to be 80 cm^{-1} by taking into account the effects of covalency on other high-spin ferrous ions (Edwards et al., 1967). With the above assumptions, one can derive the following energy level scheme for the high-spin ferrous ion by combining Eq. 36 with Eqs. 37-39.

d_{yz}	———	
d_{xz}	———	6900 cm^{-1}
d_{yz}	———	4000 cm^{-1}
$d_{x^2-y^2}$	———	
d_{z^2}	———	0 cm^{-1}

FIGURE 26. ELECTRONIC ENERGY LEVELS FOR FERROUS SITE OF "SPIN-COUPLED" MODELS.

Both axial and rhombic distortions of a tetrahedral ligand field are necessary to cause the energy-level scheme shown above. Since this is the type of ligand field to be expected from compounds

analogous to that in Fig. 24, we are assured that this type of compound is consistent with the theoretical requirements of the "spin-coupled" model.

The energy levels shown in Fig. 26 for the ferrous-iron site of the reduced proteins is based on the assumption that the electron pair in the d-orbital system of this ion occupies a d_{z2} orbital. The proof of this assumption lies in the values of the derived parameters for the low-temperature spectra of the reduced proteins. Consider first the parameter, QS. The only d-orbitals which give negative values for QS are d_{z2}, d_{xz} and d_{yz} (Table 2). A large negative value -2.63 mm/S, for site #2 (Table 7) agrees well with that calculated for a single electron in a d_{z2} orbital. The experimental value of η is close to zero for the ferrous iron. This value is inconsistent with the theoretical values of η for d_{xz} and d_{yz} orbital density. In addition, the magnitude of the measured value of QS (-2.63 mm/S) is very close to that predicted for a d_{z2} electron: -3 mm/S (Lang and Oosterhuis, 1969).

Other Mossbauer data which indicate that the model is correct are the measured a-values for the low-temperature, reduced protein spectra. The measured a-values for the ferric iron (Table 7) are close to isotropic with an average value of -17 gauss. Remembering that this a-value is calculated for an electron spin = 1/2 situation, we now recalculate the a-value for the ferric site in terms of the 5/2 spin present at this site. For the ferric site in the spin-coupled model (Fig. 25),

$$\underline{a}_1 (S_1 = 5/2) = 7/15 \langle \underline{a}_1 \rangle_{\text{MEASURED}} = -8 \text{ gauss} \qquad (40)$$

In high-spin ferric iron this a-value is the result of the Fermi contact interaction alone (Section II-F). Hence, this a-value comprises an experimental determination of the Fermi contact interaction of the ferric iron in this protein.

The value of $-2g_N\beta\beta_N\langle r^{-3}\rangle$ in Eq. 22 is, by the above procedure, equal to -1.6 gauss. We now apply this constant to the calculation of the a-values for the ferrous iron. The Fermi contact interaction at the ferrous site is approximated by assuming that $-2g_N\beta\beta_N\langle r^{-3}\rangle$ for this site equals -1.6 gauss times 0.87 (Table 3). A value of 0.35 is assumed for κ (Section II-F), thus scaling the Fermi contact interaction to the dipolar interaction. These values are then entered into Eq. 23 using the data in Table 4 for the dipolar part of the hyperfine interaction. Using the orbital scheme in Fig. 26, the a-values for the ferrous iron are then:

A_x = -4.5 gauss

A_y = -4.5 gauss

A_z = -8 gauss

Following a procedure analogous to that in Eq. 40, a set of a-values are computed which correspond to those measured by Mossbauer spectroscopy for the ferrous iron. Table 8 shows these completed and measured a-values for the ferrous site.

TABLE 8

A-VALUES FOR FERROUS IRON

Computed	Measured
A_x = +6.6 gauss	A_x = +5.0 gauss
A_y = +6.6 gauss	A_y = +7.1 gauss
A_z = +11.8 gauss	A_z = +12.5 gauss

The agreement in the values of Table 8 not only indicates the validity of our assumptions regarding the hyperfine interaction of the ferrous iron, but also comprises a rigorous test for the model as a whole, since the presence of positive a-values for iron with magnitudes shown in Table 7 necessitates an exchange-coupling mechanism.

Presently, the most direct evidence for an exchange mechanism in the plant-type ferredoxins is contained in the applied magnetic field spectra of the oxidized proteins. As stated in Section V-B, these experimental spectra have been fitted with computed spectra from the time-independent program described in Chapter IV. The best fits to the experimental spectra give a measured effective magnetic field at the nucleus. In Fig. 27, this measured field is plotted against the applied field for the oxidized proteins. The straight line in Fig. 27 represents the expected plot of B vs. H if one assumes the Larmor precession time of the ^{57}Fe nucleus is zero. Since the Larmor precession time ($1/\omega_L$ for $^{57}Fe_{3/2}$) is about $2.1 \cdot 10^{-7}$S for the $^{57}Fe_{I = 3/2}$ nucleus at 10 kG magnetic field at the nucleus, the expected Zeeman splitting is not seen by Mossbauer spectroscopy because the mean lifetime (τ) of $^{57}Fe_{I=3/2}$ state is $1.4 \cdot 10^{-7}$S. Thus, at low applied field the Zeeman states in the excited nuclear state

FIGURE 27. THE MEASURED MAGNETIC FIELD AT THE NUCLEUS VS. THE APPLIED MAGNETIC FIELD FOR THE OXIDIZED PROTEIN MOSSBAUER SPECTRA.

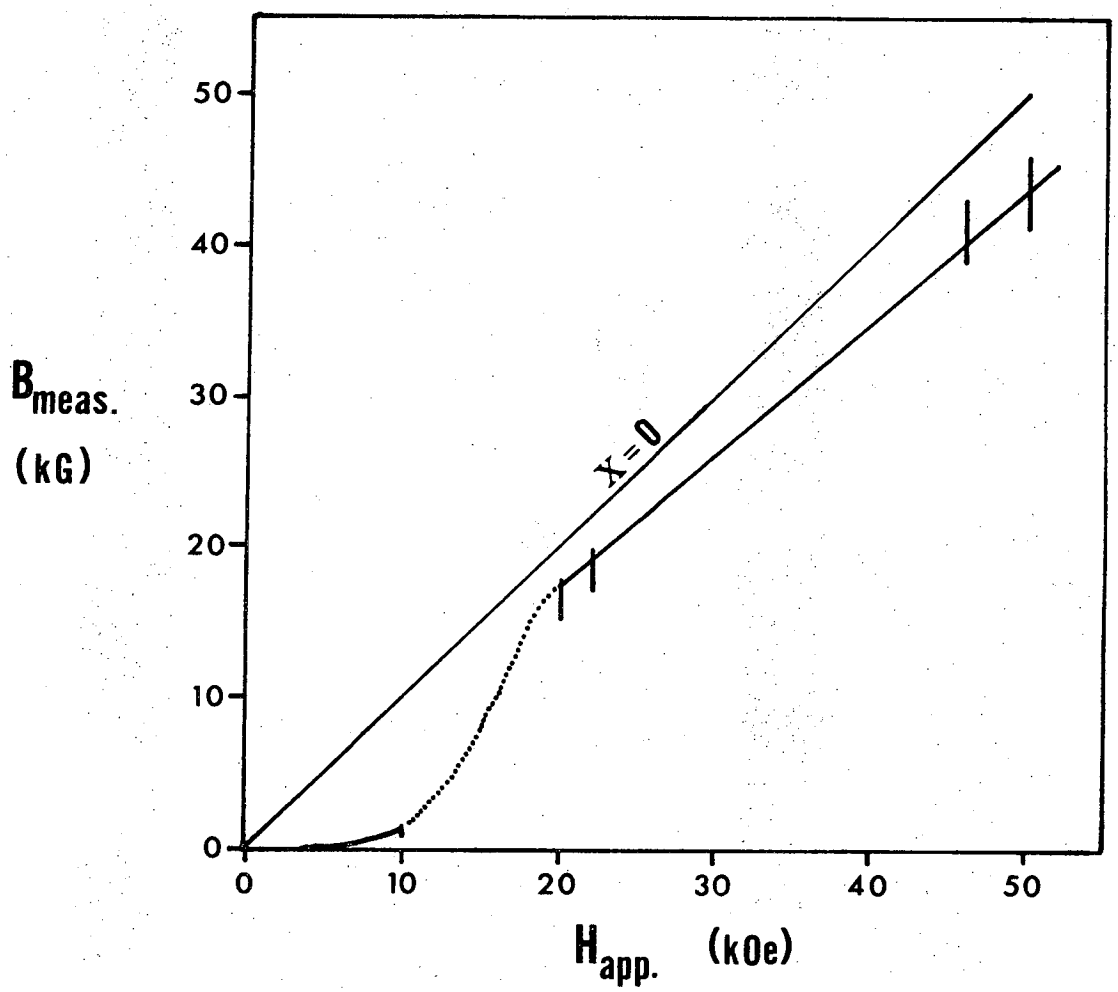
50
40
30
20
10
0
$B_{meas.}$
(kG)
X=0
0
10
20
30
40
50
$H_{app.}$ (kOe)

are not formed because the lifetime of this state is too short. At 30 kG magnetic field at the nucleus, $\tau\omega_L = 5$; so that the magnetic splittings in the excited nuclear state are treatable by time-independent perturbation calculations. Refering to Fig. 27, we see that the plot of B vs. H is linear in this region; however, B/H is less than one. We therefore observe a "diamagnetic" field in the oxidized protein spectra at high applied magnetic field of approximately one-tenth the applied field.

Since this "diamagnetic" field is far too large to attribute to a diamagnetic correction factor to the applied field (Evans, 1955, p. 188), it must result from magnetic mixing of the S = 1 state into the S = 0 ground state of the exchange-coupled, spin system for the oxidized proteins. This effect is called a "pseudo-nuclear Zeeman interaction" (Bleaney, 1967) and its matrix elements give an approximate value for J of 150 cm^{-1}. The Schiff-base compounds (Fig. 24) have J's of 100 cm^{-1}. Furthermore, the substitution of sulfur for the oxygen bridging atoms in Fig. 24 is expected to increase the magnitude of J, especially when the iron configuration is d^5 (Anderson, 1963). The value of J from the above Mossbauer spectra has not, as yet, been established to better than a range of 50 to 250 cm^{-1}; however, a value of J above 100 cm^{-1} would imply that sulfur is the bridging ligand in the iron-sulfur complex.

The existence of exchange-coupling between the iron atoms should also be detectable by magnetic susceptibility measurements (Section II-G). Ehrenberg (referenced in Thornley et al., 1966) made the first magnetic susceptibility measurements on these proteins

and detected a slight "excess" susceptibility for them at temperatures around 300°K. Moss et al. (1969) state that the oxidized protein is diamagnetic from 1.7°K to 201°K and that the reduced material is characteristic of an S = 1/2 material over this range. However, from the quoted precision of the measurements by Moss et al., the maximum value of J detectable in their experiments is about 40 cm^{-1}. Therefore, a more precise measurement of the value of J for these proteins must await the application of a specialized computer program to the oxidized protein Mossbauer spectra or more sensitive magnetic susceptibility measurements. In passing, one could also measure J by studying the reduced proteins. Considering that these proteins are paramagnetic with the splitting of 3J between the S = 1/2 and S = 3/2 states (Fig. 10), the exchange-coupling constant can be more easily obtained by studying the oxidized proteins.

F. MODEL OF THE ACTIVE CENTER OF THE PLANT-TYPE FERREDOXINS

In the preceding section we presented the experimental evidence in support of the "spin-coupled" model proposed by Gibson et al. (1966) and Thornley et al. (1966) for the plant-type ferredoxins. However, the "spin-coupled" model does not provide a spatial or configurational model for the active center. Therefore we proceed to a more detailed analysis with the goal of asserting a proper chemical and structural model of the active center. The following properties of the active site of these proteins are well substantiated experimentally by the present study:

1. The active center of the oxidized plant-type ferredoxins contains two iron atoms with identical electronic environments at the nuclei. These irons are high-spin ferric (S = 5/2), spin-coupled to give a resultant diamagnetism for the complex.

2. In the reduced state, the active center contains one high-spin ferric state spin-coupled to one high ferrous state (S = 2) to give a resultant S = 1/2 complex.

3. The ligand symmetry around both iron atoms is tetrahedral, but with both axial and rhombic distortions. This basic symmetry is not affected by reduction of the proteins.

4. The active center of the plant-type ferredoxins is nearly identical in every protein studied. The only differences in this active center are the presence and magnitude of the rhombic distortion of the symmetry for the ferrous iron in the reduced proteins.

In addition, the two-iron Schiff's-base compounds studied by Lewis et al. (Fig. 24) have magnetic properties which indicate a structure which may be similar to that in the active centers of the plant-type ferredoxins. The following arguments set forth criteria on which to base any model for the active site:

1. The iron atoms have been shown to be exchange-coupled through a superexchange mechanism. Thus, they are connected by a bridging ligand which, in view of the arguments in the previous section and the elemental composition of the holoprotein, is most likely a sulfur atom. This bridging ligand (sulfur) can, however, be either cysteine sulfur or "labile sulfur".

2. The ^{33}S EPR experiments (Section I-C) show that the "labile sulfur" atoms are in the active site. The magnitude of the sulfur hyperfine constants indicate that the "labile sulfur" is bonded to the iron. In view of the amino acid compositions of these proteins, the "labile sulfur" is either the bridging ligands for the iron atoms or part of a persulfide ligand to the iron atoms, as suggested by Beinert (1965).

Thus, the following persulfide structures are consistent with the above criteria:

A

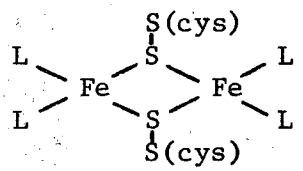

B

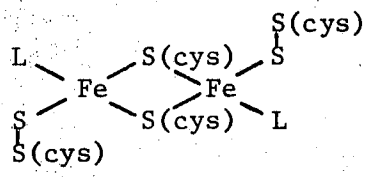

L = Ligand from amino acid side-chains.

FIGURE 28. PERSULFIDE STRUCTURES FOR ACTIVE SITE OF PLANT-TYPE FERREDOXINS.

Although no direct evidence has allowed a decision between these structures, we feel that the structures shown in Fig. 28 are doubtful because: 1) the persulfide bonds are higher energy than sulfur-iron bonds 2) these structures do not promote the similarities which are observed in the Mossbauer spectra of the seven proteins in this study, and 3) these structures do not explain the resistance of these proteins to two-electron reduction.

In contrast, we propose the following structure for the active site of the ferredoxins.

FIGURE 29. PROPOSED MODEL FOR THE ACTIVE CENTER OF THE PLANT-TYPE FERREDOXINS.

White = Cysteine sulfur

Black = Iron

Shaded = Labile sulfur

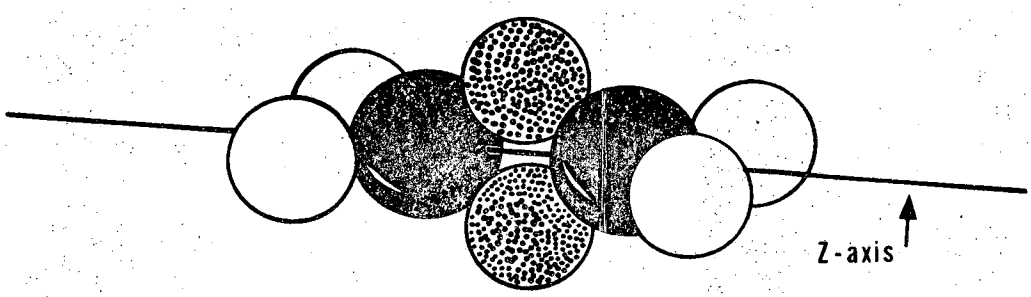
Z-axis

Note that in the structure in Fig. 29, there are six ligands: two "labile sulfur", iron-bridging ligands and four cysteinyl-sulfur ligands. The tetrahedral ligand symmetry of this model is dostorted by the difference in character between the "labile" and cysteinyl sulfur atoms and by the position of the iron atoms themselves.

In crystal field theory calculations the direction of the axial distortion is along the z-axis. Therefore, the d_{z2} orbitals in iron atoms in Fig. 29 are along the line joining the two iron atoms. Remembering that the d_{z2} orbital lies lowest in this symmetry, as shown in Fig. 26, the effect of reducing the complex is to add electron density to the d_{z2} orbitals of the iron atoms. Since the d_{z2} iron-orbitals in Fig. 29 overlap, this structure results in an electron repulsion term between the iron atoms which increases as the iron atoms in these proteins are reduced. Thus, the negative reduction potentials (Table 1) of the plant-type ferredoxins are accounted for by this model.

The protein sequence data in Table 4 show that the cysteine residues in all the proteins occur in identical positions (18, 39, 44, 47, 77) in the sequence. Thus, the ligand field produced by the cysteinyl sulfur atoms is not likely to be different among these proteins unless there is a difference in protein conformation which causes a displacement in one or more of the cysteinyl sulfur atoms. Note that a displacement of <u>any</u> cysteinyl sulfur atom in the model in Fig. 29 results in rhombic distortion at the iron to which it is ligated. Since, according to the "spin-coupled" model, this rhombic distortion will manifest itself in the difference

between g_x and g_y (Eqs. 37-39) for a particular protein, the EPR data in Table 1 provide a measure of the rhombic distortion around the ferrous iron in the reduced proteins. In particular, the g-values of adrenodoxin are axially symmetric while the g-values of spinach ferredoxin show a rhombic distortion. Thus, the observation of Kimura et al. (1969) that adrenodoxin and spinach ferredoxin have different protein conformations is consistent with the prediction of the above model.

The "spin-coupled" model also predicts a constant value of g_z, numerically 2.04. Inspection of Table 1 shows some deviation from $g_z = 2.04$ for the plant-type ferredoxins. With respect to the model shown in Fig. 29, we must invoke large strains on the cysteine sulfurs around the reduced protein ferric site in order to account for the deviations as the "spin-coupled" model attributes the value of g_z mainly to the g-value of the ferric site (Eq. 36).

Assuming that the structure shown in Fig. 29 is valid, one can draw some conclusions as to the characters of the iron d-orbitals in the "spin-coupled" model. Since the symmetry around the iron is tetrahedral, the d_{z^2} and $d_{x^2-y^2}$ orbital are more ionic than the t_g orbitals which must be covalent as the ligands are sulfur atoms. There are several important consequences of this conclusion: 1) The energy level scheme in Fig. 26 is based on crystal-field approximations and therefore can be considerably in error. 2) The reducing electrons will occupy an ionic orbital (d_{z^2}); thus, the reduction potential of the plant-type ferredoxins is justifiably attributed to electron repulsion between the d_{z^2} orbitals of the two iron atoms.

3) Covalency of the t_g iron orbitals with sulfur implies that the Mossbauer spectra of these proteins will be sensitive to ligand changes between the members of the plant-type ferredoxins. That is, the substitution of tyrosine or histidine for cysteine as a ligand is certain to cause a change in isomer shift which is not observed for these proteins (Fig. 16).

In fact, the similarities in the Mossbauer effect parameters impose tight constraints on the freedom to choose ligands for this complex. Thus, the suggestion by Yang and Huennekens (1969) that an iron-sulfur complex involves octahedral hydroxy ligands including tyrosine is not applicable on two counts: 1) the ligand symmetry is tetrahedral and 2) the positions of the tyrosine residues are not constant throughout the sequences of the plant-type ferredoxins.

The acidity of these proteins implies that the amino acids which occur in areas of the sequence with a preponderance of glutamic acid, aspartic acid and glutamine may not be free to ligate to the iron-sulfur complex, as they will be drawn out to the periphery of the protein conformation. Thus, consideration of the similarities in the Mossbauer spectra and inspection of the amino acid sequences (Fig. 4) and composition (Newman et al., 1969) imply that cysteine is the most probable ligand to the iron-sulfur complex, and that the structure shown in Fig. 29 is valid.

LIST OF REFERENCES

1. Abragam, A. and Pryce, M.H.L. (1951). Proc. Roy. Soc., A205:135.

2. Abragam, R.E. (1964). L'Effet Mossbauer et Ses Applications a D'Etude des Champs Internes. Gordon and Breach, New York.

3. Anderson, P.W. (1963) in Magnetism, edited by Rado, G.T. and Suhl, H. Academic Press, New York, p.70.

4. Arnon, D.I. (1965). Science, 149:1460.

5. Arnon, D.I., Tsujimoto, H.Y. and McSwain, B.D. (1964). Proc. Natl. Acad. Sci. U.S., 51:1274.

6. Ballhausen, K.J. (1962). Introduction to Ligand Field Theory. McGraw-Hill, New York, p.335.

7. Bearden, A.J. and Moss, T.H. (1967) in Magnetic Resonance in Biological Systems, edited by Ehrenberg, A., Malmstrom, B.J. and Vanngard, T. Pergamon Press, London, p.391.

8. Beinert, H. (1965) in Non-Heme Iron Proteins: Role in Energy Conversion, edited by San Pietro, A. Antioch Press, Yellow Springs, Ohio, p.23.

9. Beinert, H. (1969). Mossbauer Spectroscopy in Biological Systems, edited by Debrunner, P., Tsibris, J.C.M. and Munck, E. Univ. of Illinois Bull., 67:#41.

10. Beinert, H. and Palmer, G. (1965). Adv. Enzym., 27:105.

11. Beinert, H., DerVartanian, D.V., Hemmerich, P., Beeger, C. and VanVoorst, J.D.W. (1965). Biochim. Biophys. Acta, 96:530.

12. Bendall, D.S., Gregory, R.P.F. and Hill, R. (1963). Biol. J., 88:29p.

13. Benson, A.M. and Yasunobu, K.T. (1969). J. Biol. Chem., 244:955.

14. Bleaney, B. (1967). Hyperfine Interactions, edited by Freeman, A.J. and Frankel, R.B. New York, Academic Press, New York, p.33.

15. Blumberg, W.E. and Peisach, J. (1965) in Non-Heme Iron Proteins: Role in Energy Conversion, edited by San Pietro, A. Antioch Press, Yellow Springs, Ohio, p.101.

16. Boeri, E. and Magaldi, A.G. (1957). Biochim. Biophys. Acta, 23:489.

17. Brady, G.W., Kurkjian, C.R., Lyden, E.F.X., Robin, M.B., Saltman, P., Spiro, T. and Terzis, A. (1968). Biochemistry, 7:2185.

18. Brink, D.M. and Satchler, G.R. (1962). Angular Momentum. Oxford Press, London, p.21.

19. Brintzinger, H., Palmer, G. and Sands, R.H. (1966a). J. Am. Chem. Soc., 88:623.

20. Brintzinger, H., Palmer, G. and Sands, R.H. (1966b). Proc. Natl. Acad. Sci. U.S., 55:397.

21. Carrington, A. and McLachlan, A.D. (1967). Introduction to Magnetic Resonance. Harper and Row, New York.

22. Chance, B., Estabrook, R.W. and Yonetani, T. (1966). Heme Proteins and Hemoproteins, edited by Chance, B., Estabrook, R.W. and Yonetani, T. Academic Press, New York.

23. Collins, R.I. (1965). J. Chem. Phys., 42:1072.

24. Cooke, R., Tsibris, J.C.M., Debrunner, P.G., Tsai, R., Gunsalus, I.C. and Frauenfelder, H. (1968). Proc. Natl. Acad. Sci. U.S., 59:1045.

25. Cushman, D.W., Tsai, R.L. and Gunsalus, I.C. (1967). Biochem. Biophys. Res. Commun., 26:577.

26. Danon, J. (1968) in Chemical Applications of Mossbauer Spectroscopy, edited by Goldanskii, V.I. and Herber, R.H. Academic Press, New York, p.159.

27. DerVartanian, D.V., Orme-Johnson, W.H., Hansen, R.E., Beinert, H., Tsai, R.L., Tsibris, J.C.M., Bartholomaus, R.C. and Gunsalus, I.C. (1967). Biochem. Biophys. Res. Commun., 26:569.

28. Dunham, W.R., Bearden, A.J., Salmeen, I., Sands, R.H., Orme-Johnson, W.H. and Palmer, G. (1970). To be published in Proc. Natl. Acad. Sci. U.S.

29. Dus, K., DeKleck, H., Sletten, K. and Bartsch, R.G. (1967). Biochim. Biophys. Acta, 140:291.

30. Edwards, P.R., Johnson, C.E. and Williams, R.J.P. (1967). J. Chem. Phys., 47:2074.

31. Evans, M.C.W., Hall, D.O., Bothe, H. and Whatley, F.R. (1968). Biochem. J., 110:485.

32. Evans, R.D. (1955). The Atomic Nucleus. McGraw-Hill, York, Pennsylvania, p.167.

33. Falk, J.E. (1964). Porphyrins and Metalloporphyrins. (Vol.II of the BBA Library). Elsevier Publishing Company, Amsterdam.

34. Foust, G.P., Mayhew, S.G. and Massey, V. (1969). J. Biol. Chem., 244:964.

35. Frauenfelder, H. (1962). The Mossbauer Effect. W.A. Benjamin, Inc., New York.

36. Fry, K.T. and San Pietro, A. (1962). Biochem. Biophys. Res. Commun., 9:218.

37. Gabriel, J.R. and Olson, D. (1969). Nucl. Inst. Meth., 70:209.

38. Gabriel, J.R. and Ruby, S.L. (1965). Nucl. Inst. Meth., 36:23.

39. Gerloch, M., Lewis, J., Mabbs, F.E. and Richards, A. (1968). J. Chem. Soc. (A), 112.

40. Gibson, J.F., Hall, D.O., Thornley, J.H.M. and Whatley, F.R. (1966). Proc. Natl. Acad. Sci. U.S., 56:987.

41. Goldanskii, V.I. and Makarov, E.F. (1968) in Chemical Applications of Mossbauer Spectroscopy, edited by Goldanskii, V.I. and Herber, R.H. Academic Press, New York, p.1.

42. Grant, R.W. (1966) in Mossbauer Effect Methodology, v.2, edited by Gruverman, I.J. Plenum Press, New York, p.23.

43. Griffith, J.S. (1964). The Theory of Transition-Metal Ions. Cambridge University Press, London, p.325.

44. Hall, D.O. and Evans, M.C.W. (1969). Nature, 223:1342.

45. Hardy, R.W.F., Knight, E. Jr., McDonald, C.C. and Eustachio, A.J.D. (1965) in Non-Heme Iron Proteins: Role in Energy Conversion, edited by San Pietro, A. Antioch Press, Yellow Springs, Ohio, p.275.

46. Hecht, Harry G. (1967). Magnetic Resonance Spectroscopy. John Wiley and Sons, New York, p.134.

47. Herriott, J.R., Sieker, L.C., Jensen, R.H. and Lovenberg, W. (1970). To be published in Nature.

48. Hollocher, T.C., Solomon, F. and Ragland, T.E. (1966). J. Biol. Chem., 241:3452.

49. Hong, J. and Rabinowitz, J.C. (1967). Biochem. Biophys. Res. Commun., 29:246.

50. Ingalls, R. (1964). Phys. Rev., 133A:787.

51. Jørgensen, C.K. (1966) in Structure and Bonding, v.1, edited by Jørgensen, C.K., Neilands, J.B., Nyholm, R.S., Reinen, D. and Williams, R.J.P. Springer-Verlag, New York, p.3.

52. Johnson, C.E. and Hall, C.O. (1968). Nature, 217:446.

53. Johnson, C.E., Elstner, E., Gibson, J.F., Benfield, G., Evans, M.C.W. and Hall, D.O. (1968). Nature, 220:1291.

54. Johnson, C.E., Bray, R.C., Cammack, R. and Hall, D.O. (1969). Proc. Natl. Acad. Sci. U.S., 63:1234.

55. Keeson, P.H. and Pearlman, N. (1956) in Handbuch der Physik, v.14, edited by Fluegge, S. Springer-Verlag, Berlin, p.296.

56. Keresztes-Nagy, S. and Margoliash, E. (1966). J. Biol. Chem., 241:5955.

57. Keresztes-Nagy, S., Perini, F. and Margoliash, E. (1969). J. Biol. Chem., 244:981.

58. Keresztes-Nagy, S., Lager, L., Klapper, M. and Klotz, I.M. (1965). Science, 150:357.

59. Khedekar, A.V., Lewis, J., Mabbs, F.E. and Weigold, H. (1967). J. Chem. Soc. (A), 1561.

60. Kimura, T. (1968) in Structure and Bonding, v.5, edited by Jørgensen, C.K., Neilands, J.B., Nyholm, R.S., Reinen, D. and Williams, R.J.P. Springer-Verlag, New York, p.1.

61. Kimura, T. and Suzuki, K. (1967). J. Biol. Chem., 242:485.

62. Kimura, T., Suzuki, K., Padmaabhan, R., Samejima, T., Tarutani, O. and Vi, N. (1969). Biochemistry 8:4027.

63. Kistner, O.C. and Sunyar, A.W. (1965). Phys. Rev., 139:B295.

64. Koenig, E. in Physical Methods in Organic Chemistry (1968), edited by Hill, H.A.O. and Day, P. Interscience Publishers, London.

65. Kundig, W. (1967). Nucl. Instr. Meth., 48:219.

66. Lewis, J., Mabbs, F.E. and Richards, A. (1967). J. Chem. Soc. (A), 1014.

67. Locher, P.R. and Geschwind, S. (1965). Phys. Rev., 139:A991.

68. Love, W.E. (1957). Biochim. Biophys. Acta, 23:465.

69. Lovenberg, W. and Sobel, B.E. (1965). Proc. Natl. Acad. Sci. U.S., 54:193.

70. Mahler, H.R. and Cordes, E.H. (1966) in Biological Chemistry. Harper and Row, New York, p.207.

71. Malkin, R. and Rabinowitz, J.C. (1966). Biochem. Biophys. Res. Commun., 23:822.

72. Matsubara, H. and Sasaki, R.M. (1967). J. Biol. Chem., 243:1732.

73. Matsubara, H., Jukes, P.H. and Cantor, C.R. (1968a). Brookhaven Symp. Biol., 21:201.

74. Matsubara, H., Sasaki, R.M. and Chain, R.K. (1968b). J. Biol. Chem., 243:1725.

75. Mayhew, S.G., Petering, D., Palmer, G. and Foust, G.P. (1969). J. Biol. Chem., 244:2830.

76. Mortenson, I.E., Valentine, R.C. and Carnahan, J.E. (1962). Biochem. Biophys. Res. Commun., 1:448.

77. Moss, T.H. (1965). Ph.D. Thesis, Cornell University.

78. Moss, T.H., Petering, D. and Palmer, G. (1969). J. Biol. Chem., 244:2275.

79. Moss, T.H., Bearden, A.J., Bartsch, R.G., Cusanovich, M.A. and San Pietro, A. (1968). Biochemistry 7:159.

80. Neuringer, L.J. and Shapira, Y. (1969). Rev. Sci. Instr., 40: 1314.

81. Newman, D.J. and Postgate, J.R. (1968). Eur. J. Biochem., 7:45.

82. Newman, D.J., Ihle, J.N., Dure, L. III (1969). Biochem. Biophys. Res. Commun., 36:947.

83. Novikov, G.V., Syrtsova, L.A., Likhtenshtein, G.I., Trukhtanov, V.A., Rachek, V.F. and Goldanskii, V.I. (1968). Dokl. Akad. Nauk SSSR, 181:1170.

84. Oosterhuis, W.T. and Lang, G. (1969). Phys. Rev., 178:439.

85. Orbach, R. (1961). Proc. Roy. Soc., A264:458.

86. Orme-Johnson, W.H. and Beinert, H. (1969). Biochem. Biophys. Res. Commun., 36:337.

87. Orme-Johnson, W.H., Hansen, R.E., Beinert, H., Tsibris, J.C.M., Bartholomaus, R.C. and Gunsalus, I.C. (1968). Proc. Natl. Acad. Sci. U.S., 60:368.

88. Owen, J. (1961). J. Appl. Phys., 32:213 (Suppl.).

89. Palmer, G. (1967). Biochem. Biophys. Res. Commun., 27:315.

90. Palmer, G. and Brintzinger, H. (1966). Nature, 212:189.

91. Palmer, G. and Sands, R.H. (1966). J. Biol. Chem., 241:253.

92. Palmer, G., Brintzinger, H. and Estabrook, R.W. (1967a). Biochemistry, 6:1658.

93. Palmer, G., Brintzinger, H., Estabrook, R.W. and Sands, R.H. (1967b) in Magnetic Resonance in Biological Systems, edited by Ehrenberg, A., Malmstrom, B.G. and Vanngard, T. Pergamon Press, London, p.159.

94. Pitzer, K.S. (1953). Quantum Chemistry. Prentice-Hall, Englewood Cliffs, N.J., p.55.

95. Preston, R.S., Hanna, S.S. and Heberle, J. (1962). Phys. Rev., 128:2207.

96. Rinzel, John and Funderlic, R.E. (1968). Programmer's Handbook (AEC Research and Development Report K-1729).

97. Sasaki, R.M. and Matsubara, H. (1967). Biochem. Biophys. Res. Commun., 28:467.

98. Shethna, Y.I., Wilson, P.W., Hansen, R.E. and Beinert, H. (1964). Proc. Natl. Acad. Sci. U.S., 52:1263.

99. Shethna, Y.I., DerVartanian, D.V. and Beinert, H. (1968). Biochem. Biophys. Res. Commun., 31:862.

100. Shulman, R.G. and Sugano, S. (1965). J. Chem. Phys., 42:39.

101. Sugeno, K. and Matsubara, H. (1968). Biochem. Biophys. Res. Commun., 32:951.

102. Tagawa, K. and Arnon, D.I. (1962). Nature, 195:537.

103. Tagawa, K. and Arnon, D.I. (1968). Biochim. Biophys. Acta, 153:602.

104. Thornley, J.H.M., Gibson, J.F., Whatley, F.R. and Hall, D.O. (1966). Biochem. Biophys. Res. Commun., 24:877.

105. Tsai, R.L. and Gunsalus, I.C. (1969). Univ. of Illinois Bull., 67:64.

106. Tsibris, J.C.M., Tsai, R.L., Gunsalus, I.C., Orme-Johnson, W.H., Hansen, R.E. and Beinert, H. (1968). Proc. Natl. Acad. Sci. U.S., 59:959.

107. VanVoorst, J.D.W. and Hemmerich, P. (1967) in Magnetic Resonance in Biological Systems, edited by Ehrenberg, A., Malmstrom, B.G. and Vanngard, T. Pergamon Press, Belfast, Ireland, p.183.

108. Walker, L.R., Wertheim, G.K. and Jaccarino, V. (1961). Phys. Rev. Letters, 6:98.

109. Watari, H. and Kimura, T. (1966). Biochem. Biophys. Res. Commun., 24:106.

110. Watson, R.E. and Freeman, A.J. (1961). Phys. Rev., 123:2027.

111. Watson, R.E. and Freeman, A.J. (1967) in Hyperfine Interactions, edited by Freeman, A.J. and Frankel, R.B. Academic Press, New York, p.59.

112. Wertheim, G.K. (1964). Mossbauer Effect: Principles and Applications. Academic Press, New York.

113. Wickman, H. (1965). Nuclear and Magnetic Resonance Studies in S-State Ions. Ph.D. Thesis, University of California at Berkeley.

114. Yang, C.S. and Huennekens, F.M. (1969). Biochem. Biophys. Res. Commun., 35:634.

115. Yocum, C.F. and San Pietro, A. (1969). Biochem. Biophys. Res. Commun., 36:614.

116. Zener, C. (1951). Phys. Rev., 88:403.

BIBLIOGRAPHY

1. Abragam, R.E. L'Effet Mossbauer et Ses Applications a l'Etude des Champs Internes. Gordon and Breach, New York, 1964.

2. Debrunner, P., Munck, E. and Tsibris, J.C.M. Mossbauer Spectroscopy in Biological Systems, edited by P. Debrunner. University of Illinois, Urbana, Illinois, 1969.

3. Frauenfelder, Hans. The Mossbauer Effect. W.A. Benjamin, Inc., New York, 1962.

4. Goldanskii, V.I. and Herber, R.H. Chemical Applications of Mossbauer Spectroscopy, edited by V.I. Goldanskii. Academic Press, New York, 1968.

5. Gruverman, Irwin J. Mossbauer Effect Methodology, v.1-2, edited by Irwin J. Gruverman. Plenum Press, New York, 1965-1966.

6. Herber, R.H. "Chemical Applications of Mossbauer Spectroscopy" in Annual Reviews of Physical Chemistry, 17:261 (1966).

7. Hill, H.A.O. and Day, P. Physical Methods in Advanced Inorganic Chemistry, edited by H.A.O. Hill. Interscience Publishers, London, 1968.

8. Muir, Arthur H. Jr., Ando, K.J. and Coogan, H.M. Mossbauer Effect Data Index 1958-1965. Interscience Publishers, New York, 1966.

9. Shirley, D.A. "Topics in Mossbauer Spectroscopy" in Annual Reviews of Physical Chemistry, 20:25 (1969).

10. Wertheim, Gunther K. Mossbauer Effect: Principles and Applications. Academic Press, New York, 1964.

APPENDIX I

PROGRAM ANIMO

A. Purpose

1. Refer to Chapter IV

B. Usage

1. Control cards
2. End of record card
3. Source deck
4. End of record card
5. Data cards (4 cards/RUN)
6. End of file cards

C. Input and Output Formats

1. Input formats

a. READ 200, INCH, IRUN, PUN, RATIO, SHIFT

200 FORMAT (2I10, 3E10)

INCH - The height of the plot output in tenths of inches

IRUN - Identification number for job; appears on plots and printed output; $1 \leq$ IRUN ≤ 99

PUN - If PUN $\neq 0$, then the ordinates of the plot points will be punched on cards for <u>special output</u> jobs

RATIO - If RATIO $\neq 0$, then the output of this run will be placed in a common block which will be the sum of the intensities of consecutive runs. This sum is defined as follows, where I is the intensity of the output Mossbauer spectrum:

$$\text{Sum} = \sum_{\text{RUNS}} |\text{RATIO}_{\text{RUN}}| \cdot I_{\text{RUN}}$$

If RATIO is less than zero, then this sum is terminated at the end of the run and the absorption spectrum of the SUM is plotted in addition to the RUN spectrum. This option allows one to generate Mossbauer spectra which are the sums of the computed spectra for different environment, electronic spin states, etc.

SHIFT - Shifts the computed spectrum an integer number of points along the incremented velocity axis before this spectrum is entered into the special output common block. The shift velocity in mm/S corresponding to SHIFT is:

$$\frac{(XF - XI)}{398} \times SHIFT$$

b. READ 101, TITLE

101 FORMAT (10A8)

This title will appear on the printed output.

c. READ 400, HAPP, QS, ETA, XI, XF, BEI, GMI, PUN, NOGRPH, NID

400 FORMAT (7E10, E7, I1, I2)

HAPP - Applied magnetic field in kG (parallel to gamma ray direction)

QS - Refer to Eq. 7-8 (units: mm/S)

ETA - η

XI - Velocity of left-hand boundary of plot in mm/S

XF - Velocity of right-hand boundary of plot in mm/S

BEI, GMI - Initial Euler angles in powder integration (refer to Eq. 31). This option is useful only for single crystal spectra (NID = 1). If both BEI and GMI = 0, the program will choose values for these parameters which optimize the powder integration.

PUN - If PUN $\neq$ 0, then card output will be generated for this run in units of per cent absorption (399 points).

NOGRPH - If NOGRPH $\neq$ 0, then no plot output will be generated for this run. This option allows one to dispense with the intermediate plots when special output is desired.

NID - The number of powder integration steps equals NID^2. NID = 11 is the optimum value for good plots.

d. READ 401, AX, AY, AZ, GX, GY, GZ, ALIGN

401 FORMAT (7E10)

AX, AY, AZ - Three principle components of the A tensor in electron gauss for S = 1/2 systems. When S ≠ 1/2, refer to Eq. 34.

GX, GY, GZ - Three principle components of the G tensor.

ALIGN - Is the flag which chooses whether the internal magnetic field is added or subtracted from the applied magnetic field. ALIGN = 1. or 2. Use of this parameter requires a detailed understanding of the calculation in SUBROUTINE ANI; however, if the A tensor has positive components and S = 1/2, then ALIGN = 1. corresponds to electronic ground state and ALIGN = 2. corresponds to the electronic excited state. If HAPP is less than 3., then the value of ALIGN has no measurable effect on the computed spectrum.

2. Output formats

a. The following material is printed:

1. A list of the input parameters

2. The P tensor in mm/S

3. The RUN number

4. The sum of the intensities for the plot points

5. The maximum and minimum of the computed spectrum

b. The following material is plotted:

1. A square with the computed spectrum

2. An identification number of the plot.

c. The mathematical method is given in Section IV.

d. EXECUTION TIME = 10 x NID^2 milliseconds per RUN on a Control Data Corporation computer, Model 6600.

```
      PROGRAM ANIMOSS(INPUT=101,OUTPUT=101,PUNCH=640,PLOT=1001,TAPE5=INP
     1UT,TAPE6=OUTPUT,TAPE99=PLOT)
C     THIS ROUTINE ASSEMBLES THE DATA FOR SPECIAL PLOT OUTPUT
      COMMON/1/X(402),HOD(419),YDMY(401),LGND(15,5)
      DIMENSION BOLZ(401),LMNT(15,5)
      DATA (J2=0)
      LMNT(1,1)=3HSPL
      DO 2 I=1,399
 2    BOLZ(I)=0.
 110  J2=J2+1
 121  FORMAT(1H1,*RUN*,I3,*   (NOT NECESSARILY EQUAL TO PLOT NUMBER)*)
      READ 200,INCH,IRUN,PUN,RATIO,SHIFT
 200  FORMAT(2I10,3E10)
      IF(EOF,5) 12,109
 109  LMNT(2,1)=IRUN
      LGND(2,1)=IRUN
      PRINT 121,J2
      CALL PDRANI(INCH)
 120  J1=RATIO*1000.
      PRINT 201,INCH,IRUN,PUN,RATIO,SHIFT
 201  FORMAT(1X*INCH=*,I2/1X,*IRUN=*,I2/1X,*PUN=*,F2.0/1X,*RATIO=*,F10.5
     1/1X,*SHIFT=*,F3.0)
      IF(J1) 4,110,5
 4    RATIO=-RATIO
 5    NPTS=399
      M=NPTS
      MM=SHIFT
      N=1+MM
      IF(MM)11,10,10
 11   N=1
      M=NPTS + MM
 10   DO 1 J=N,M
 1    BOLZ(J)=BOLZ(J) + RATIO*YDMY(J-MM)
      IF(J1)6,110,110
 6    CALL GRPLTR(X,BOLZ,NPTS,LMNT,PUN  ,INCH)
      DO 7 J=1,399
 7    BOLZ(J)=0.
      GO TO 110
 12   CALL CCEND
      END

      SUBROUTINE GRPLTR(X,Z,NPAR,LGND,XPUN,INCH)
C     THIS SUBROUTINE GENERATES THE PLOT OUTPUT
C     THE CC--- ROUTINES ARE CALCOMP LIBRARY ROUTINES
      DIMENSION X(402),Y(401),LGND(15,5),Z(401),ILET(12)
      COMMON/CCPOOL/XMIN,XMAX,YMIN,YMAX,CCXMIN,CCXMAX,CCYMIN,CCYMAX
      COMMON/CCFACT/FACTOR
      DATA (K=0)
      K=K+1
      FACTOR=100.
      CCXMIN=1.3
      CCXMAX=10.9
      CCYMIN=1.
      CCYMAX=7.
      N=NPAR
      XMIN=X(1)
      XMAX=X(N)
      FINCH=INCH
      FINCH=FINCH/10.
      DO1I=1,399
 1    Y(I)=100.-Z(I)
      IF(INCH.EQ.0)FINCH=5.
      PMIN=XMINI(Y,N)
```

```
      A=(Y(1) + PMIN)/2.
      B=(Y(1) - PMIN)*3./FINCH
      YMAX=A+B
      YMIN=A-B
      CALL CCGRID(1,6HNOLBLS,1)
 3    FORMAT(F6.3,* TO *,F6.3,* MM/SEC*/F5.1,* TO *,F4.1,* PCA*)
      ENCODE(40,3,ILET(1))X(1),X(N),Y(1),PMIN
      ENCODE(40,10,ILET(9))LGND(1,1),LGND(2,1),K
 10   FORMAT(A3,I2,*-*,I2)
      CALL CCLTR(1.4,6.9,0,1,ILET(9),8)
      CALLCCPLOT(X,Y,N)
      CALL CCNEXT
      PRINT 2,(ILET(I),I=1,8)
 2    FORMAT(1X,4A10)
      IF(XPUN.EQ.0.) GO TO 7
      PUNCH 9,(ILET(I),I=9,12)
 9    FORMAT(4A10)
      PUNCH 8,(Y(I),I=1,N)
 8    FORMAT(10F8.4)
 7    RETURN
      END


      SUBROUTINE PDRANI(INCH)
C     THIS SUBROUTINE PERFORMS THE MAIN CALCULATION FOR A SINGLE IRON
C     ENVIRONMENT MOSSBAUER SPECTRUM IN APPLIED FIELD.  THE SAMPLE MAY
C     BE A SINGLE CRYSTAL OR A POWDER.
      DIMENSION LGND(15,5),TITLE(8)
      DIMENSION NXS(2),GB(3),D(2),E(2),B(2),S(8,4,6),HY2(8,4,2), DJB(8,4
     1,2),DJA(8,4,2),DJT(8,4,2),H(8,4,2),DJ1(8,4),DJ2(8,4), VAL(4,2),
     2XINT(4,2),DJ3(8,4),L(3),FLOR(401),XS(2),EI2(4,2)
      EQUIVALENCE (N1,NXS(1)),(N2,NXS(2)),(L(1),LX),(L(2),LY),(L(3),LZ)
      COMMON/1/X(402),Y(401),  NAL,NBE,AL,BE,CBE,
     1DAL,DCBE,       EI2,IEI2,EIEI2,DX
     2,YDMY(401),LGND
      COMMON/TEN/GX,GY,GZ,AX,AY,AZ,ALIGN
      DATA (GMMA=.15)
      REAL L,LX,LY,LZ
 101  FORMAT(8A10)
 102  FORMAT(1X,8A10)
C     INITIALISE PARAMETERS.
      PI=4.0*ATAN(1.0)
      NPTS=399
      READ 101,TITLE
      READ 400,HAPP,QS,ETA,XI,XF,BEI,GMI,    PUN,NOGRPH,NID
 400  FORMAT(7E10,E7,I1,I2)
      READ 401,            AX,AY,AZ,GX,GY,GZ,ALIGN
 401  FORMAT(7E10)
      XS(1)=1.5
      XS(2)=.5
      E(2)=0.
      D(2)=0.
      D(1)=QS/(6.*SQRTF(1.+(ETA*ETA)/3.))
      B(2)=-0.01189
      B(1)=0.0068
      E(1)= ETA*D(1)
      NINT=0
      ENPT=NPTS-1
      DX=(XF-XI)/ENPT
C     CLEAR CHANNELS Y FOR ACCUMULATING INTENSITIES.
      DO1045IPT=1,NPTS
 1045 Y(IPT)=0.
```

```
C     SET UP INITIAL E2QQ HAMILTONIAN INN CRYSTAL FRAME
      DO1050IL=1,2
      NXS(IL)=2.0*XS(IL)+1.01
      CALL FRMS(S(1,1,3*IL-2),NXS(IL))
      CALLCOCLR(HY2(1,1,IL),NXS(IL))
      CALL Y2OP(S(1,1,3*IL-2),D(IL),E(IL),HY2(1,1,IL),NXS(IL))
 1050 CONTINUE
C     CHECK TO SEE IF SINGLE CRYSTAL SPECTRUM, IF NOT, THEN GENERATE
C     BEI, GMI WHICH LEAD TO MOST EFFICIENT INTEGRATION STEPS
      IF(NID.EQ.1) GO TO 4040
      GMI=PI/(4.*NID)
      BEI=ACOS(1.-.5/NID)
 4040 CONTINUE
C     START BETA LOOP
      DCBE=1./NID
      CBE=DCBE +  COS(BEI)
      DO 1063 IB=1,NID
      CBE=CBE-DCBE
      BE=ACOS(CBE)
      DO 4001 IL=1,2
 4001 CALL FRMDJB(DJB(1,1,IL),BE,NXS(IL))
C     START GAMMA LOOP
      DGM=PI/(2.*NID)
      GM=GMI-DGM
      DO 1064 IG=1,NID
      GM=GM+DGM
C     CALCULATE THE EFFECTIVE MAGNETIC FIELD AT THE NUCLEUS FOR THIS
C     CRYSTAL ORIENTATION
      CALL ANI(BE,GM,HAPP,LX,LY,LZ,HEFF)
C     START LEVEL LOOP
      DO 1061 IL=1,2
C     ROTATE THE QUADRUPOLE HAMILTONIAN INTO CRYSTAL FRAME
      CALL FRMDJZ(DJ2,GM,NXS(IL))
      CALL COMPY(DJ2,DJB(1,1,IL),DJ1,NXS(IL))
      CALL COROT(HY2(1,1,IL),DJ1,DJ2,NXS(IL))
      DO 1049 K=1,3
 1049 GB(K)=L(K)*B(IL)*HEFF
C     ADD QUADRUPOLE AND MAGNETIC HAMILTONIANS
      CALL ZEEMAN(S(1,1,3*IL-2),GB,DJ1,NXS(IL))
      CALL COMAD(DJ1,DJ2,H(1,1,IL),NXS(IL))
C     DIAGONALISE
 1061 CALL ALLMAT(H(1,1,IL),VAL(1,IL),NXS(IL),4,NXS(IL))
C     AT THIS STAGE H IS IN A BASIS WHERE THE AMPLITUDES OF
C     RIGHT AND LEFT POLARISED PHOTONS ARE GIVEN BY MATRIX ELEMENTS
C     OF UNIT TENSORS BETWEEN EIGENVECTORS
      CALL PDRHIN(N1,N2,H,XINT,TOTX)
      DO 2014 J1=1,N1
      DO 2014 J2=1,N2
      E12(J1,J2)=VAL(J1,1)-VAL(J2,2)
      EIE12=(E12(J1,J2)-XI)/DX+1.
      IE12=EIE12
      IF(IE12.GT.NPTS)GO TO 2014
      IF(IE12.LT.1) GO TO 2014
      Y(IE12)=Y(IE12) + XINT(J1,J2)
 2014 CONTINUE
      NINT=NINT+1
C     END OF GAMMA LOOP FOLLOWS
 1064 CONTINUE
C     END OF BETA LOOP FOLLOWS
 1063 CONTINUE
C     AT THIS STAGE THE LINE SPECTRA ARE IN Y
```

```
C       FCRM BREIT-WIGNER LINESHAPE MCSSBAUER INTENSITY SPECTRUM
        X(1)=XI
        DC3000IPT=1,NPTS
 3000   X(IPT+1)=X(IPT)+DX
        PRINT 102,TITLE
        PRINT 402,HAPP,QS,ETA,PUN,NOGRPH,BEI,GMI
 402    FCRMAT(1X,*HAPP=*,F6.1/1X,*QS=*,F8.3/1X,*ETA=*,F8.3/1X,*PUN=*,F2.0
       1/1X,*NOGRPH=*,I2/1X,*BEI=*,F6.3/1X,*GMI=*,F6.3)
        PRINT 403,            AX,AY,AZ,GX,GY,GZ,ALIGN
 403    FCRMAT(1X,                                    *AX=*,F7.3/1X,*AY=*,F7.
       23/1X,*AZ=*,F7.3/1X,*GX=*,F5.3/1X,*GY=*,F5.3/1X,*GZ=*,F5.3/1X,*ALIG
       3N=*,F2.0)
        ENINT=NINT$GMALOR=GMMA*8.      /(ENINT*TOTX)
        DX2=DX*DX$G2=GMMA*GMMA
        DC3010K=1,NPTS
        ENK1=K-1$FLOR(K)=GMALOR/(G2+DX2*ENK1*ENK1)
 3010   CCNTINUE
        DC3012K=1,NPTS
        YDMY(K)=0.0
 3012   CCNTINUE
        DC3014ILIN=1,NPTS
        IF(Y(ILIN).EQ.0.) GC TO 3014
        DC3013IFOLD=1,NPTS
        ICELT=ILIN-IFOLD
        IF(IDELT.LT.0)IDELT=-IDELT
        KC=IDELT+1
        YDMY(IFOLD)=YDMY(IFOLD)+Y(ILIN)*FLOR(KD)
 3013   CCNTINUE
 3014   CONTINUE
        TCTI=0.
        DC 10 IN=1,NPTS
 10     TCTI=TOTI+YDMY(IN)
        PRINT 11,TOTI
 11     FCRMAT(1X,*THE SUM OF THE INTENSITIES IS*,E12.2/1X,*(NOTE ... ABSO
       1RPTICN AT CHANNEL(I) = 100 MINUS INTENSITY AT CHANNEL(I).)*)
        IF(NCGRPH.NE.0) GO TO 35
        LGND(1,1)=10HC
        CALL GRPLTR(X,YDMY,NPTS,LGND,PUN  ,INCH)
 35     RETURN
        END

        FUNCTION XMINI(X,N)
C       FIND THE MINUMUM OF X
        DIMENSION X(399)
        XMINI=X(1)
        DC 20 J=2,N
        IF(X(J).LT.XMINI)  XMINI=X(J)
 20     CCNTINUE
        RETURN
        END

        SUBRCUTINE FRMDJB(A,BETA,N)
C       FCRMS A ROTATION MATRIX AROUNC AXIS Y, FCR EULER ANGLE BETA
C       SEE BRINK AND SATCHLER
        DIMENSION A(8,4)
        DC 3 I=1,4
        DC 3 J=1,4
        A(2*I-1,J)=A(2*I,J)=0.0
 3      CCNTINUE
        C=COSF(BETA/2.0)
        S=SINF(BETA/2.)
```

```
      IF(N.EQ.2) GO TO 1
      IF(N.EQ.4) GO TO 2
      IF(N.NE.4) STOP
 1    A(1,1)=A(3,2)=C
      A(3,1)=-S
      A(1,2)=-A(3,1)
      GO TO 4
 2    A(1,1)=A(7,4)=(COSF(BETA/2.0))**3
      A(7,3)=A(3,1)=-SQRTF(3.)*(C**2)*(S)
      A(5,4)=A(1,2)=+SQRTF (3.)*(C**2)*(S)
      A(7,2)=A(3,4)=A(5,1)=A(1,3)=SQRTF(3.)*C*(S**2)
      A(1,4)=+S**3$A(7,1)=-A(1,4)
      A(5,3)=A(3,2)=C*(3.*C**2-2.)
      A(3,3)=-S*(3.*S**2-2.)$A(5,2)=-A(3,3)
 4    RETURN
      END

      SUBROUTINE ALLMAT(A,XLAM,M,IA,NCAL)
C     DIAGONALIZES ANY 5X5 ARRAY OF COMPLEX NUMBERS
C     CALCULATES EIGENVECTORS AND EIGENVALUES
C
C     PROG.AUTHORS JOHN RINZEL,R.E.FUNDERLIC,UNION CARBIDE CORP.
C     NUCLEAR DIVISION,CENTRAL DATA PROCESSING FACILITY,
C     OAK RIDGE TENNESSEE
C
      DIMENSION A(IA,1),H(5,5),HL(5,5),LAMBDA(5),VECT(5),MULT(5),
     1SHIFT(3),INTH(5),INT(5),XLAM(5),KEY(5),XLAMA(5),B(5,5)
      COMPLEX A , H , HL , LAMBDA , VECT , MULT , SHIFT , TEMP , SIN ,
     1 COS , TEMP1 , TEMP2  , B
      LOGICAL INTH , TWICE
      INTEGER  INT , R , RP1 , RP2
      DO 60 I6=1,M
 60   LAMBDA(I6)=(0.,0.)
      N=M
      NCAL=N
      IF(N.NE.1)GO TO 1
      LAMBDA(1)=A(1,1)
      A(1,1)=1.
      GO TO 57
  1   ICOUNT=0
      SHIFT(1) = 0.
      IF(N.NE.2)GO TO 4
    2 TEMP=(A(1,1)+A(2,2)+CSQRT((A(1,1)+A(2,2))**2-
     14.*(A(2,2)*A(1,1)-A(2,1)*A(1,2))))/2.
      IF(REAL(TEMP).NE.0..OR.AIMAG(TEMP).NE.0.)GO TO 3
      LAMBDA(M) = SHIFT(1)
      LAMBDA(M-1) = A(1,1) + A(2,2) + SHIFT(1)
      GO TO 37
    3 LAMBDA(M) = TEMP + SHIFT(1)
      LAMBDA(M-1)=(A(2,2)*A(1,1)-A(2,1)*A(1,2))/(LAMBDA(M)-SHIFT(1))+
     1SHIFT(1)
      GO TO 37
C
C     REDUCE MATRIX A TO HESSENBERG FORM
C
    4 NM2=N-2
      DO 15 R=1,NM2
      RP1=R+1
      RP2=R+2
      ABIG=0.
      INT(R)=RP1
```

```
      DO 5 I=RP1,N
      ABSSQ=REAL(A(I,R))**2+AIMAG(A(I,R))**2
      IF(ABSSQ.LE.ABIG)GO TO 5
      INT(R)=I
      ABIG=ABSSQ
    5 CONTINUE
      INTER=INT(R)
      IF(INTER.EQ.RP1)GO TO 8
      IF(ABIG.EQ.0.)GO TO 15
      DO 6 I=R,N
      TEMP=A(RP1,I)
      A(RP1,I)=A(INTER,I)
    6 A(INTER,I)=TEMP
      DO 7 I=1,N
      TEMP=A(I,RP1)
      A(I,RP1)=A(I,INTER)
    7 A(I,INTER)=TEMP
    8 DO 9 I=RP2,N
      MULT(I)=A(I,R)/A(RP1,R)
    9 A(I,R)=MULT(I)
      DO 11 I=1,RP1
      TEMP=0.
      DO 10 J=RP2,N
   10 TEMP=TEMP+A(I,J)*MULT(J)
   11 A(I,RP1)=A(I,RP1)+TEMP
      DO 13 I=RP2,N
      TEMP=0.
      DO 12 J=RP2,N
   12 TEMP=TEMP+A(I,J)*MULT(J)
   13 A(I,RP1)=A(I,RP1)+TEMP-MULT(I)*A(RP1,RP1)
      DO 14 I=RP2,N
      DO 14 J=RP2,N
   14 A(I,J)=A(I,J)-MULT(I)*A(RP1,J)
   15 CONTINUE
C
C     CALCULATE EPSILON
C
      EPS=0.
      DO 16 I=1,N
   16 EPS=EPS+CABS(A(1,I))
      DO 18 I=2,N
      SUM=0.
      IM1=I-1
      DO 17 J=IM1,N
   17 SUM=SUM+CABS(A(I,J))
      IF(SUM.GT.EPS)EPS=SUM
   18 CONTINUE
      EPS=SQRT(FLOAT(N))*EPS*1.E-12
      IF(EPS.EQ.0.)EPS=1.E-12
      DO 19 I=1,N
      DO 19 J=1,N
   19 H(I,J)=A(I,J)
   20 IF(N.NE.1)GO TO 21
      LAMBDA(M) = A(1,1) + SHIFT(1)
      GO TO 37
   21 IF(N.EQ.2)GO TO 2
   22 MN1=M-N+1
      IF(REAL(A(N,N)).NE.0..OR.AIMAG(A(N,N)).NE.0.)
     1 IF(ABS(REAL(A(N,N-1)/A(N,N)))+ABS(AIMAG(A(N,N-1)/A(N,N)))-1.E-9)
     2 24,24,23
   23 IF(ABS(REAL(A(N,N-1)))+ABS(AIMAG(A(N,N-1))).GE.EPS)GO TO 25
   24 LAMBDA(MN1) = A(N,N) + SHIFT(1)
```

```
      ICOUNT=0
      N=N-1
      GO TO 21
C
C     DETERMINE SHIFT
C
   25 SHIFT(2)=(A(N-1,N-1)+A(N,N)+CSQRT((A(N-1,N-1)+A(N,N))**2
     1 -4.*(A(N,N)*A(N-1,N-1)-A(N,N-1)*A(N-1,N))))/2.
      IF(REAL(SHIFT(2)).NE.0..OR.AIMAG(SHIFT(2)).NE.0.)GO TO 26
      SHIFT(3)=A(N-1,N-1)+A(N,N)
      GO TO 27
   26 SHIFT(3)=(A(N,N)*A(N-1,N-1)-A(N,N-1)*A(N-1,N))/SHIFT(2)
   27 IF(CABS(SHIFT(2)-A(N,N)).LT.CABS(SHIFT(3)-A(N,N)))GO TO 28
      INDEX=3
      GO TO 29
   28 INDEX=2
   29 IF(CABS(A(N-1,N-2)).GE.EPS)GO TO 30
      LAMBDA(MN1) = SHIFT(2) + SHIFT(1)
      LAMBDA(MN1+1) = SHIFT(3) + SHIFT(1)
      ICOUNT=0
      N=N-2
      GO TO 20
   30 SHIFT(1) = SHIFT(1) + SHIFT(INDEX)
      DO 31 I=1,N
   31 A(I,I)=A(I,I)-SHIFT(INDEX)
C
C     PERFORM GIVENS ROTATIONS, QR ITERATES
C
      IF(ICOUNT.LE.10)GO TO 32
      NCAL=M-N
      GO TO 37
   32 NM1=N-1
      TEMP1=A(1,1)
      TEMP2=A(2,1)
      DO 36 R=1,NM1
      RP1=R+1
      RHO=SQRT(REAL(TEMP1)**2+AIMAG(TEMP1)**2+
     1 REAL(TEMP2)**2+AIMAG(TEMP2)**2)
      IF(RHO.EQ.0.)GO TO 36
      COS=TEMP1/RHO
      SIN=TEMP2/RHO
      INDEX=MAX0(R-1,1)
      DO 33 I=INDEX,N
      TEMP=CONJG(COS)*A(R,I)+CONJG(SIN)*A(RP1,I)
      A(RP1,I)=-SIN*A(R,I)+COS*A(RP1,I)
   33 A(R,I)=TEMP
      TEMP1=A(RP1,RP1)
      TEMP2=A(R+2,R+1)
      DO 34 I=1,R
      TEMP=COS*A(I,R)+SIN*A(I,RP1)
      A(I,RP1)=-CONJG(SIN)*A(I,R)+CONJG(COS)*A(I,RP1)
   34 A(I,R)=TEMP
      INDEX=MIN0(R+2,N)
      DO 35 I=RP1,INDEX
      A(I,R)=SIN*A(I,RP1)
   35 A(I,RP1)=CONJG(COS)*A(I,RP1)
   36 CONTINUE
      ICOUNT=ICOUNT+1
      GO TO 22
C
C     CALCULATE VECTORS
```

```
C
   37 IF(NCAL.EQ.0)GO TO 57
      N=M
      NM1=N-1
      IF(N.NE.2)GO TO 38
      EPS=AMAX1(CABS(LAMBDA(1)),CABS(LAMBDA(2)))*1.E-8
      IF(EPS.EQ.0.)EPS=1.E-12
      H(1,1)=A(1,1)
      H(1,2)=A(1,2)
      H(2,1)=A(2,1)
      H(2,2)=A(2,2)
   38 DO 56 L=1,NCAL
      DO 40 I=1,N
      DO 39 J=1,N
   39 HL(I,J)=H(I,J)
   40 HL(I,I)=HL(I,I)-LAMBDA(L)
      DO 44 I=1,NM1
      MULT(I)=0.
      INTH(I) = 0
      IP1=I+1
      IF(CABS(HL(I+1,I)).LE.CABS(HL(I,I)))GO TO 42
      INTH(I) = 1
      DO 41 J=I,N
      TEMP=HL(I+1,J)
      HL(I+1,J)=HL(I,J)
   41 HL(I,J)=TEMP
   42 IF(REAL(HL(I,I)).EQ.0..AND.AIMAG(HL(I,I)).EQ.0.)GO TO 44
      MULT(I)=-HL(I+1,I)/HL(I,I)
      DO 43 J=IP1,N
   43 HL(I+1,J)=HL(I+1,J)+MULT(I)*HL(I,J)
   44 CONTINUE
      DO 45 I=1,N
   45 VECT(I)=1.
      TWICE = 0
   46 IF(REAL(HL(N,N)).EQ.0..AND.AIMAG(HL(N,N)).EQ.0.)HL(N,N)=EPS
      VECT(N)=VECT(N)/HL(N,N)
      DO 48 I=1,NM1
      K=N-I
      DO 47 J=K,NM1
   47 VECT(K)=VECT(K)-HL(K,J+1)*VECT(J+1)
      IF(REAL(HL(K,K)).EQ.0..AND.AIMAG(HL(K,K)).EQ.0.)HL(K,K)=EPS
   48 VECT(K)=VECT(K)/HL(K,K)
      BIG=0.
      DO 49 I=1,N
      SUM=ABS(REAL(VECT(I)))+ABS(AIMAG(VECT(I)))
      IF(SUM.GT.BIG)BIG=SUM
   49 CONTINUE
      DO 50 I=1,N
   50 VECT(I)=VECT(I)/BIG
      IF(TWICE)GO TO 52
      DO 51 I=1,NM1
      IF(.NOT.INTH(I))GO TO 51
      TEMP=VECT(I)
      VECT(I)=VECT(I+1)
      VECT(I+1)=TEMP
   51 VECT(I+1)=VECT(I+1)+MULT(I)*VECT(I)
      TWICE = 1
      GO TO 46
   52 IF(N.EQ.2)GO TO 55
      NM2=N-2
      DO 54 I=1,NM2
      N1I=N-1-I
```

```
      NI1=N-I+1
      DO 53 J=NI1,N
   53 VECT(J)=H(J,N1I)*VECT(N1I+1)+VECT(J)
      INDEX=INT(N1I)
      TEMP=VECT(N1I+1)
      VECT(N1I+1)=VECT(INDEX)
   54 VECT(INDEX)=TEMP
   55 DO 56 I=1,N
   56 A(I,L)=VECT(I)
 57   CONTINUE
      DO 61 I6=1,N
  61  XLAMA(I6)=LAMBDA(I6)
      CALL SORT(XLAMA,KEY,N)
      DO 63 I5=1,N
      XLAM(I5)=XLAMA(N-I5+1)
      DO 63 I4=1,N
      IT=KEY(N-I5+1)
 63   B(I4,I5)=A(I4,IT)
      DO 64  I2=1,N
      DO 64  I3=1,N
 64   A(I3,I2)=B(I3,I2)
      DO 67 I7=1,N
      SNORM=0.
      DO 66 I8=1,N
 66   SNORM=SNORM+C2MAG(A(I8,I7))
      IF(SNORM.GT.9999.AND.SNORM.LT.1.0001) GO TO 67
      SCALE=SQRTF(1./SNORM)
      DO 68 I9=1,N
 68   A(I9,I7)=SCALE*A(I9,I7)
 67   CONTINUE
      RETURN
      END

      SUBROUTINEFRMS(S,N)
C     FRMS GENERATES PAULI SPIN MATRICES
      DIMENSION S(8,4,3)
 100  XS=(FLOATF(N-1))/2.0
 105  DO125I=1,N
 110  DO125J=1,N
 115  DO125K=1,3
 120  S(2*I-1,J,K)=0.0
 125  S(2*I,J,K)=0.0
 130  DO185I=1,N
 135  XI=I
 140  XM=XS-XI+1.0
 145  S(2*I-1,I,3)=XM
 155  IF(I-N)160,185,185
 160  XP=0.5*SQRTF(XS*(XS+1.0)-XM*(XM-1.0))
 165  S(2*I-1,I+1,1)=XP
 170  S(2*I,I+1,2)= XP
 175  S(2*I+1,I,1)=XP
 180  S(2*I+2,I,2)=-XP
 185  CONTINUE
 190  RETURN
      END

      SUBROUTINE FRMDJZ(DJ,THETA,NJ)
C     FORMS A ROTATION MATRIX FOR ANGLE THETA ABOUT Z AXIS
C     SEE BRINK AND SATCHLER
      DIMENSION DJ(8,4)
      CALL COCLR(DJ,NJ)
```

```
      IF(NJ.EQ.4) GO TO 1
      C=COS(THETA/2.)
      S=SIN(THETA/2.)
      DJ(1,1)=DJ(3,2)=C
      DJ(2,1)=-S
      DJ(4,2)=S
      GO TO 2
 1    C1=COS(THETA/2.)
      C3=COS(THETA*3./2.)
      S1=SIN(THETA/2.)
      S3=SIN(THETA*3./2.)
      DJ(1,1)=DJ(7,4)=C3
      DJ(3,2)=DJ(5,3)=C1
      DJ(2,1)=-S3
      DJ(4,2)=-S1
      DJ(6,3)=S1
      DJ(8,4)=S3
 2    RETURN
      END

      SUBROUTINE Y2OP (S,D,E,H,N)
C     CALCULATES Y2OP MATRIX AND ADDS IT TO H
C     EQUIVALENT OPERATOR FOR D(3SZ**2+S(S+1))+E(SX**2-SY**2)
      DIMENSION S(8,4,3),H(8,4),DK(3),DMY(8,4)
      DK(1)=E-D
      DK(2)=-E-D
      DK(3)=2.0*D
      N2=2*N
      DO 1 K=1,3
      CALL COMPY(S(1,1,K),S(1,1,K),DMY,N)
      DO 1 I=1,N2
      DO 1 J=1,N
 1    H(I,J)=H(I,J)+DMY(I,J)*DK(K)
      PRINT 2,DK(1),DK(2),DK(3)
 2    FORMAT(1X,*HQ=*,F8.3,5HIX**2,F8.3,5HIY**2,F8.3,5HIZ**2)
      RETURN
      END

      SUBROUTINEZEEMAN(S,GB,H,N)
C     COMPUTES ZEEMAN HAMILTONIAN
      DIMENSION S(8,4,3),GB(3),H(8,4)
      N2=N+N
      DO1J=1,N
      DO1I=1,N2
 1    H(I,J)=GB(1)*S(I,J,1)+GB(2)*S(I,J,2)+GB(3)*S(I,J,3)
      RETURN
      END

      SUBROUTINE ANI(BE,GM,HAPP,DX,DY,DZ,HEFF)
C     GIVEN THE MAJOR COMPONENTS OF THE G AND A TENSORS AND THE
C     DIRECTION AND MAGNITUDE OF H(APPLIED, THIS SUBROUTINE RETURNS THE
C     DIRECTION AND MAGNITUDE OF H(EFFECTIVE FOR S=1/2 SPIN SYSTEMS WHEN
C     S(EFF) AT THE NUCLEUS EITHER ADDS OR SUBTRACTS FROM THE APPLIED
C     FIELD, DEPENDING ON THE VALUE OF ALIGN
      COMMON/TEN/GX,GY,GZ,AX,AY,AZ,ALIGN
      REAL LX,LY,LZ
      DATA  (H=10.174)
      ST=SIN(BE)
      CT=COS(BE)
      SP=SIN(GM)
      CP=COS(GM)
```

```
C     DIRECTION COSINES OF H(APPLIED)
      LX= ST*CP
      HLX=HAPP*LX
      LY=ST*SP
      HLY=HAPP*LY
      LZ=CT
      HLZ=HAPP*LZ
C     SPIN EXPECTATION VALUES
      Z=SQRT((LX*GX)**2+(LY*GY)**2+(LZ*GZ)**2)/H
      HSX=LX*GX*AX/Z
      HSY=LY*GY*AY/Z
      HSZ=LZ*GZ*AZ/Z
C     CHOOSE COUPLING OF FIELDS
      IF(ALIGN-2.) 1,2,2
 1    HEX=HLX-HSX
      HEY=HLY-HSY
      HEZ=HLZ-HSZ
      GO TO 3
 2    HEX=HSX+HLX
      HEY=HSY+HLY
      HEZ=HSZ+HLZ
 3    HEFF=SQRT(HEX**2+HEY**2+HEZ**2)
      BX=HEX/HEFF
      BY=HEY/HEFF
      BZ=HEZ/HEFF
      DX=CP*CT*BX+SP*CT*BY-BZ*ST
      DY=-SP*BX+CP*BY
      DZ=BX*LX+BY*LY+BZ*LZ
      RETURN
      END


      SUBROUTINE PDRHIN(N1,N2,H,XINT,TOTX)
C     CALCULATES THE INTENSITY OF A TRANSITION FOR STATES N1, N2 WHERE
C     RADIATION IS PROPAGATED ALONG Z-AXIS OF BASIS SET COORDINATES
      DIMENSION H(4,4,2),XINT(4,2)
      COMPLEX H,C1,C3,C4,C6
      TOTX=0.
      DO 1 J1=1,N1
      DO 1 J2=1,N2
      C1=H(1,J1,1)*CONJG(H(1,J2,2))
      C3=H(3,J1,1)*CONJG(H(1,J2,2))
      C4=H(2,J1,1)*CONJG(H(2,J2,2))
      C6=H(4,J1,1)*CONJG(H(2,J2,2))
      XINT(J1,J2)=C2MAG(C1)+C2MAG(C6)+(C2MAG(C3)+C2MAG(C4)+REAL(C4*CONJG
     1(C1)+C6*CONJG(C3)+C1*CONJG(C4)+C3*CONJG(C6)))/3.
 1    TOTX=TOTX+XINT(J1,J2)
      RETURN
      END PDRHIN


      SUBROUTINE COCLR(A,N)
C     THIS SUBROUTINE SETS COMPLEX MATRIX 'A' TO ZERO
      DIMENSION A(8,4)
      DO 2 I=1,N
      DO 2 J=1,N
      A(2*I-1,J)=0.0
 2    A(2*I,J)=0.0
      RETURN
      END
```

```
      SUBROUTINECOTRAN(A,B,N)
C     THIS SUBROUTINE FORMS THE ADJOINT OF COMPLEX MATRIX 'A' AND
C     STORES IN -B-
      DIMENSION A(8,4),B(8,4)
      DO115J=1,N
      DO115I=1,N
      B(2*I-1,J)=A(2*J-1,I)
 115  B(2*I,J)=-A(2*J,I)
      RETURN
      END


 1    SUBROUTINECOMAD(A,B,C,N)
C     THIS SUBROUTINE PERFORMS THE COMPLEX MATRIX ADDITION (A + B = C)
      DIMENSION A(8,4),B(8,4),C(8,4)
      M=2*N
      DO2I=1,M
      DO2J=1,N
 2    C(I,J)=A(I,J)+B(I,J)
      RETURN
      END


      SUBROUTINECOMPY(A,B,C,N)
C     THIS SUBROUTINE PERFORMS MATRIX MULTIPLICATION--(A X B = C) FOR
C     COMPLEX MATRICES
      DIMENSION A(8,4),B(8,4),C(8,4)
      DO2I=1,N
      DO2J=1,N
      C(2*I-1,J)=0
      C(2*I,J)=0
      DO2K=1,N
      C(2*I-1,J)=C(2*I-1,J)+B(2*I-1,K)*A(2*K-1,J)-
     1B(2*I,K)*A(2*K,J)
 2    C(2*I,J)=C(2*I,J)+B(2*I-1,K)*A(2*K,J)+B(2*I,K)*
     1A(2*K-1,J)
      RETURN
      END


      SUBRCUTINE COROT(A,P,B,N)
C     PERFORMS THE COMPLEX ROTATION (P*XAXP=B)
      DIMENSION A(8,4),B(8,4),P(8,4),DMY(8,4)
      CALL COTRAN(P,B,N)
      CALL COMPY(B,A,DMY,N)
      CALL COMPY(DMY,P,B,N)
      RETURN
      END COROT


      FUNCTION C2MAG(C)
C     FORMS THE SQUARED ABSOLUTE VALUE OF A COMPLEX NUMBER
      TYPE COMPLEX C
      TYPE REAL IM
      RE=C
      IM=(0.0,-1.0)*C
      C2MAG=(RE*RE+IM*IM)
      RETURN
      END
```

```
      SUBROUTINE SORT(X,KEY,NO)
C     ORDERS THE ARRAY X
C     M1 UCSD SORT
      DIMENSION X( 2),KEY( 2)
      DO 1 I=1,NO
 1    KEY(I)=I
      MO=NO
 2    IF(MO-15)21,21,23
 21   IF(MO-1)9,9,22
 22   MO=2*(MO/4)+1
      GO TO 24
 23   MO=2*(MO/8)+1
 24   KO=NO-MO
      JO=1
 25   I=JO
 26   IF(X(I)-X(I+MO))28,28,27
 27   TEMP=X(I)
 2701 X(I)=X(I+MO)
 2702 X(I+MO)=TEMP
 2703 KEMP=KEY(I)
 2704 KEY(I)=KEY(I+MO)
 2705 KEY(I+MO)=KEMP
      I=I-MO
      IF(I-1)28,26,26
 28   JO=JO+1
      IF(JO-KO)25,25,2
 9    RETURN
      END
```

APPENDIX II

ENERGY CONVERSION TABLE

The following formulae and constants were used to form this table:

a. $E = kT$

$E = hc/\lambda$

$\Delta E = E\gamma\frac{v}{c}$

$E = h\nu$

$E = g_e\beta_e H$

$E = g\ (^{57}Fe_{I = 1/2})\ \beta_n H$

$E = Jq$

b. $k = 1.38053 \times 10^{-16}$ erg/°K

$h = 6.62554 \times 10^{-27}$ erg · S

$c = 2.997925 \times 10^{10}$ cm/S

$E = 14.4125$ keV

$g_e = 2.00229$

$\beta_e = 9.27314 \times 10^{-21}$ erg/gauss

$g\ (^{57}Fe_{I = 1/2}) = 0.18048$

$\beta_n = 5.05048 \times 10^{-24}$ erg/gauss

$J = 4.18400$ joule/cal

$L = 6.0226 \times 10^{23}$/mole

$1eV = 1.60209 \times 10^{-12}$ erg

1 erg $= 10^{-7}$ joule

c. Read chart: $A = XB$

A \ B	erg	eV	mm/S	^{o}K	cm^{-1}	Hz	electron gauss	$^{57}Fe_{1:1/2}$ gauss	kcal/ mole
erg	1	6.2418×10^{11}	1.2984×10^{19}	7.2438×10^{15}	5.0345×10^{15}	1.5093×10^{26}	5.3856×10^{19}	1.0971×10^{24}	1.4394×10^{13}
eV	1.60209×10^{-12}	1	2.0801×10^{7}	1.1605×10^{4}	8.0658×10^{3}	2.4181×10^{14}	8.6281×10^{7}	1.7576×10^{12}	2.3061×10^{1}
mm/S	7.7020×10^{-20}	4.8075×10^{-8}	1	5.5791×10^{-4}	3.8778×10^{-4}	1.1625×10^{7}	4.1480	8.4495×10^{4}	1.1086×10^{-6}
^{o}K	1.3805×10^{-16}	8.6168×10^{-5}	1.7924×10^{3}	1	6.9507×10^{-1}	2.0837×10^{10}	7.4349×10^{3}	1.5145×10^{8}	1.9872×10^{-3}
cm^{-1}	1.9863×10^{-16}	1.2398×10^{-4}	2.5788×10^{3}	1.4387	1	2.9978×10^{10}	1.0697×10^{4}	2.1789×10^{8}	2.8589×10^{-3}
Hz	6.6255×10^{-27}	4.1355×10^{-15}	8.6021×10^{-8}	4.7992×10^{-11}	3.3358×10^{-11}	1	3.5682×10^{-7}	7.2685×10^{-3}	9.5368×10^{-14}
electron gauss	1.8568×10^{-20}	1.1590×10^{-8}	2.4108×10^{-1}	1.3450×10^{-4}	9.3487×10^{-5}	2.8025×10^{6}	1	2.0370×10^{4}	2.6726×10^{-7}
$^{57}Fe_{1:1/2}$ gauss	9.1151×10^{-25}	5.6895×10^{-13}	1.1835×10^{-5}	6.6028×10^{-9}	4.5894×10^{-9}	1.3758×10^{2}	4.9091×10^{-5}	1	1.3121×10^{-11}
kcal/ mole	6.9473×10^{-14}	4.3363×10^{-2}	9.0204×10^{5}	5.0322×10^{2}	3.4978×10^{2}	1.0486×10^{13}	3.7417×10^{6}	7.6214×10^{10}	1

LEGAL NOTICE

This report was prepared as an account of Government sponsored work. Neither the United States, nor the Commission, nor any person acting on behalf of the Commission:

A. Makes any warranty or representation, expressed or implied, with respect to the accuracy, completeness, or usefulness of the information contained in this report, or that the use of any information, apparatus, method, or process disclosed in this report may not infringe privately owned rights; or

B. Assumes any liabilities with respect to the use of, or for damages resulting from the use of any information, apparatus, method, or process disclosed in this report.

As used in the above, "person acting on behalf of the Commission" includes any employee or contractor of the Commission, or employee of such contractor, to the extent that such employee or contractor of the Commission, or employee of such contractor prepares, disseminates, or provides access to, any information pursuant to his employment or contract with the Commission, or his employment with such contractor.

TECHNICAL INFORMATION DIVISION
LAWRENCE RADIATION LABORATORY
UNIVERSITY OF CALIFORNIA
BERKELEY, CALIFORNIA 94720